Title
Development and Characterization of Novel Rhodol Calcium Sensors for Investigating Neuronal Activity

Author
Contractor, Alisha Anwer

Publication Date
2018

Peer reviewed|Thesis/dissertation

Development and Characterization of Novel Rhodol Calcium Sensors for Investigating Neuronal Activity

By

Alisha Contractor

A dissertation submitted in partial fulfillment of the

requirements for the degree of

Doctor of Philosophy

in

Chemical Biology

in the

College of Chemistry

of the

University of California, Berkeley

Dissertation Committee:

Professor Evan W. Miller (Chair)
Professor Ke Xu
Professor Marla Feller

Summer 2018

Development and Characterization of Novel Rhodol Calcium Sensors for Investigating Neuronal Activity

Abstract

Development and Characterization of Novel Rhodol Calcium Sensors for Investigating Neuronal Activity

by

Alisha Anwer Contractor

Doctor of Philosophy in Chemistry

University of California, Berkeley

Professor Evan W. Miller, Chair

Calcium ions mediate a multitude of biochemical and biophysical signaling processes in cells. Calcium imaging is the use of fluorescent probes and microscopy to monitor changes in intracellular calcium concentration, [Ca^{2+}], to track calcium associated cellular processes. The development of fluorescent reporters of [Ca^{2+}], genetically-encoded calcium indicators and chemical calcium indicators, has been paramount in increasing our understanding of the temporal and spatial dynamics of Ca^{2+} signaling. Coupling Ca^{2+}-selective ligands to fluorescent reporters has provided a wealth of excellent indicators that span the visible excitation and emission spectrum and possess Ca^{2+} affinities suited to a variety of cellular contexts. One underdeveloped area is the use of rhodamine/fluorescein fluorophores, or rhodols, in the context of Ca^{2+} sensing. Rhodols are bright and photostable and have good two-photon absorption cross sections (σ_{TPA}), making them excellent candidates for incorporation into Ca^{2+}-sensing scaffolds.

In Chapter 1 of this dissertation, I provide an overview of calcium imaging including the commonly used calcium indicators and imaging techniques. In Chapter 2, I describe the design, synthesis, and application of a previously-published rhodol-based Ca^{2+} sensor RCS-1, a chlorinated pyrrolidinyl-rhodol calcium sensor. RCS-1 possesses a Ca^{2+} binding constant of 240 nM and a 10-fold turn-on response to Ca^{2+} ion binding. RCS-1 effectively absorbs infrared light and has a σ_{TPA} of 76 GM at 840 nm, 3-fold greater than that of its fluorescein-based counterpart. The acetoxy-methyl ester of RCS-1 stains the cytosol of live cells, enabling observation of Ca^{2+} fluctuations and cultured neurons using both one- and two-photon illumination. In Chapter 3, I present the design, synthesis, and application of four rhodol-based Ca^{2+} sensors: 5'- and 6'-isomers of a chlorinated pyrrolidine-based rhodol (RCS 1a and 1b, respectively) and a chlorinated azetidine-based rhodol (RCS 2a and 2b, respectively). The RCSs possess Ca^{2+} binding constants of 215 – 240 nM and 10-fold turn-on responses to Ca^{2+} ion binding. The pyrrolidinyl-rhodol Ca^{2+} sensors effectively absorb infrared light and have σ_{TPA}s of ~76 GM at 840 nm, 3-fold greater than that of its fluorescein-based counterpart. The azetidinyl-rhodol Ca^{2+} sensors also absorb infrared light and have σ_{TPA}s of ~44 GM at 840 nm, 2-fold greater than that of its fluorescein-based counterpart. The tetra-acetoxymethyl esters of RCS 1a, 1b, 2a, and 2b label the cytosol of live cells, enabling observation of histamine-induced Ca^{2+} fluctuations

in HeLa cells, spontaneous activity in cultured hippocampal neurons, and retinal waves in developing retinal ganglion cells using both one- and two-photon illumination. Together, these results demonstrate the utility of rhodol-based scaffolds for Ca^{2+} sensing using two-photon illumination in neurons. In Chapter 4, I describe our attempt to utilize amino acid acyl ester salts to deliver negatively charged fluorescent probes to cells using carboxyfluorescein as a test probe. Using carboxyfluorescein as a test fluorophore, we were able to show that amino acyl esters of proline and beta-alanine increase cell permeability of negatively charged carboxyfluorescein, while the salts of the amino acyl esters retain solubility of the capped dye in aqueous solutions.

Dedicated To:

Mia Familia: Mom, Dad, Aziz, Sanah, and Sofia – without them and their unwavering love and support, I wouldn't have made it this far.

You're the wind beneath my wings, my loves.

Thank you for helping me soar.

Development and Characterization of Novel Rhodol Calcium Sensors for Investigating Neuronal Activity

Table of Contents

List of Figures

List of Tables

List of Schemes

Acknowledgements

I would like to start by thanking Evan, for allowing me to be a part of his new laboratory at UC Berkeley. I would also like to thank him for believing in me and my capabilities as a scientist, and for allowing me the space to grow at my own pace. For your helpful mentorship, understanding, and encouragement, I will forever be indebted to you, Evan. Thank you for all the guidance; with your help I have grown into a more independent researcher, and I feel well-prepared to leave UC Berkeley to start a post-doctoral chemical biology synthetic project in a largely bio-heavy lab! And, of course, thank you for all the pre-21 juice boxes and post-21 champagne toasts!

Secondly, I would like to thank my OG lab buddies: Parker Deal, Rishi Kulkarni, and Vincent Grenier. We started out with shared hoods, and group meetings in Evan's office with homemade dinners and grew into two floors of lab space and undergrads pouring out of our ears. We've watched each other grow as scientists, and, together, we've had the opportunity to build a nurturing, fun, and relaxed culture for the Miller Lab of the future. I am incredibly grateful for the camaraderie and helpful chemistry/life tips I've gotten from each one of you. I got to discover science and California with you guys; from picnics with cows to camping in Big Sur, to neuroscience conferences, and the Santa Cruz Boardwalk, it has been a fantastic five years, and I am glad I got to spend it with you.

I would also like to thank the rest of the Miller Lab: Julia Lazzari-Dean, Pei Liu, Gloria Ortiz, Steven Boggess, Jenna Franke, Monica Gonzalez, Benjamin Raliski, Molly Kirk, Brittany Daws, and Pavel Klier. Julia and Pei thank you for your sense of humor and biochemistry expertise. I've learned so much from both of you. Steven and Gloria, my 215 Hildebrand buddies, I had so much fun doing chemistry beside the two of you. From unexpected sassy comebacks (Gloria) to making fun of undergrads (poor WooTack), 215 Hildebrand was always full of laughter and chemical fumes! After the lab expansion, I got to know Ben and Monica really well in 215 Hildebrand as well, but this time I didn't have to share a hood. Brittany and Pavel, thanks for making my last year at Berkeley an easy transition. We've had some good times setting up QR codes for the inventory. Pavel, thank you, thank you, thank you for taking over the ordering job! You've been doing a great job, and I wish you continued good luck with it in the future! Jenna, thank you for keeping me motivated, and always being excited about my interviews and future plans! Molly, without our conversations and jokes these last two years, I wouldn't have gotten through Berkeley. Thank you for always being kind, and sassy, and hilarious!

To the new members of Miller Lab, I'm sorry I haven't gotten to know you guys well, but I wish you all the best in your doctoral journeys! Thank you for choosing the best lab on campus.

I would, particularly, like to thank Dr. Alison Evans (née Walker) and Dr. Yi-Lin Huang. I learned what kind of scientist I wanted to be from both of these young ladies. Dr. Evans was instrumental in enabling the Miller Lab to be set up as a chemical biology lab. She helped us establish all the biological protocols like cell culture, and cellular imaging. Moreover, she has an inquisitive, creative mind that made her indubitably the best

scientist to run new ideas by, because she would help you realize those ideas into actual scientific experiment. She is also a genuinely kind, encouraging, and hilarious person that made her a great lab companion and friend. Dr. Yi-Lin Huang is an incredible research chemist, and a quietly hilarious person. She routinely had the best recommendations for failed experiments, but also always had a sassy quip to accompany them. She added to the caliber of chemistry and the quality of life in the Miller Lab! I am honored to have had the chance to work with, and laugh with both these amazing ladies.

How could I have gotten through graduate school without Samantha Keyser and Jackie Blake-Hedges? My two best Berkeley friends. We've gone through so much together: from serious injuries to moving to a different school and from moving to new apartments to convincing Sam to buy kitties on a whim. Whatever I've needed – whether it be multiple trips to move my stuff into a new apartment or a wine and whine night – these two have been there to help me get through graduate school and all its ups and downs. We may not brunch together often anymore, but I am grateful for your friendship, your kindness, and your willingness to show up whenever, wherever, I've needed you. Sam, thank you for driving me to jamatkhana for two years; those short drives with you brought us closer together and I am forever indebted to you for taking me with you to Alameda so that I could go to khane daily. Jackie, thank you for facilitating my painting addiction. Our wine-and-paint nights are some of my favorite memories of graduate school! Here's to more thanksgiving dinners together in the future ladies! I love you both! Thank you!

Jessica Ziegler, thank you for agreeing to be my roommate after first year! Living with you these last four years has been an amazing experience. I'm sorry I'm a messy roommate, but thank you for never saying it to my face! Thank you for always letting my friends crash on the couch or take over the living room! Thanks for always lending an ear when I was stressed out about graduate school. Rooming with someone who truly understood the struggle was a huge asset, and that I was rooming with you was a blessing.

I'd like to thank my high school AP Chemistry teacher, Mr. Kuykendall for introducing me to this fascinating science and helping me – through his passion for the subject – fall in love with science. Thank you for me an amazing teacher and taking the time to really teach young teenagers who didn't want to be stuck in chemistry class. You showed me that science could be fun.

I'd also like to thank my undergraduate mentors that guided me to research and fostered my love for research: Drs. Megumi Fujita, Farooq Khan, Spencer Slattery, and John Hansen. Drs. Fujita and Khan, thank you for giving me my first research opportunity, and introducing me to the world of science conferences and scientific presentations. Drs. Slattery and Hansen, thank you for challenging me always. Learning science from the two of you was always challenging but also always enjoyable! Dr. Slattery, thank you for all the hours of conversations in your office. Thank you for letting me see that brilliance is humbling. To everyone at the University of West Georgia, thank you for your unquestionable faith in me, letting me bend the rules and earn a B.S. in chemistry on my own terms. Without the opportunities I had at UWG, I would've never made it to and through graduate school at University of California, Berkeley.

Thank you to my committee: Professor Marla Feller and Dr. Ke Xu for taking the time to read this work.

Additionally, I'd like to thank the slew of intellectuals I met at Alameda Jamatkhana. Everyone who took me in, and made feel like a part of their family – no expectations, no questions, just love.

Firstly, thank you, Shamsah Ebrahim – you believe in me always, and you inspire me always. Without your advice and mentorship, I wouldn't have gotten here. Thank you, Saira Shamji – your love for me is awesome. Thank you for being my big sisters at Berkeley. Thank you for always showing up for me – whether it's Graduate Research Seminar or my graduation! I love and appreciate the both you so much.

To Naseem and Shiraz Jaffer, thank you for taking me in and opening your arms and home for me. You guys invited me not only into your home but into your family, and love me as if I am blood. For that, I am eternally grateful! Naseem aunty, thank you for always being ready to listen and advise. Thank you also for all the cooking lessons, and the delicious yummy foods. Shiraz Uncle, thank you for being my cricket, soccer, NBA, really any sport buddy! Thank you for always, always listening and mentoring, and sharing your own experiences with me. I treasure the time I've spent with the two of you. I love you. Thank you. For everything.

To Banaa, Shazma, and Asim: "Aaja!" My dot family + banker crew. Thank you for making my years in California unforgettable. Thank you for keeping me grounded. Thank you for the encouragement and the love. Thank you for the laughs! I'm sitting in Banaa's AZ apartment and looking back on our time together with tears in my eyes. How much we've all grown and accomplished in the last three years! I'm proud to be a part of your lives, and I can't wait to see how far we go! Cheers to us!

To Aadil Sarfani, you're too far away. You don't answer my messages all the time, but you were an important part of my graduate school years. Thank you for always listening to my graduate school woes. Thank you for always being on my side. I'm glad to have met you, and I hope we end up in the same place again soon.

To my girls, Sanah Bhimani and Sofia Dhanani, I don't have words that can describe my gratitude, my love, and my indebtedness to you two for…everything. What adventures we've had together these last three years! I'm humbled by you both. I'm grateful to have you guys in my life. I honestly can't thank you guys enough for your love, faith, and encouragement through life in general but especially through graduate school. I won't take up more space because I could wax on forever.

Who knew that I'd go move across the country for graduate school and end up building so much family here.

But of course, I need thank the three people that made all of this possible: my parents, Anwer and Nevina, and brother, Aziz. Without the constant support and backing of these

three, none of this would've been possible. Never once did they "No you can't do that" to me. They've always supported my dreams, no matter what they have entailed. Thank you so much for giving me roots, but allowing me to fly unencumbered.

As a wise woman told Hodding Carter, "There are only two lasting bequests we can hope to give our children. One of these is roots, the other wings."

Mom and Dad, mission accomplished!

Chapter One: Calcium Imaging Probes and Techniques

1. Calcium and neuronal function

Calcium ions (Ca^{2+}) are involved in various regulatory processes of all mammalian cells, and are especially important in neurons. Extracellular calcium affects neuronal excitability, and is needed for neurotransmitter release. Calcium ions also function as secondary messengers regulating various cellular processes like plasticity, cell growth and death, neurogenesis, enzymatic activity, etc. Therefore, intracellular calcium concentration is tightly regulated (Figure 1A); typical resting intracellular concentration Ca^{2+} is 100s of nanomolar (nM), while, extracellularly, calcium is present in millimolar (mM) quantities. Changes in cytosolic calcium concentration are caused by cellular activity – like action potentials – and are intimately involved in generation of various cellular responses. Therefore, calcium concentrations are monitored to study various cellular processes.[1,2]

In neurons, specifically, changes in calcium concentrations can be used to track neuronal activity. Immediately following an action potential, there is an influx of calcium ions into the cytoplasm by traveling down the calcium concentration gradient through the opening of voltage-gated Ca^{2+} channels. This influx of calcium ions lasts on the order of 100s of milliseconds (Figure 1B). Calcium imaging is utilized to track neuronal activity and record changes in neuronal activity. Calcium imaging reports the current calcium status of cells or tissues. Techniques take advantage of calcium indicators: fluorescent molecules that respond to the binding of Ca^{2+} ions by changing their fluorescence properties. This method is used to probe intracellular calcium in living animals.[2]

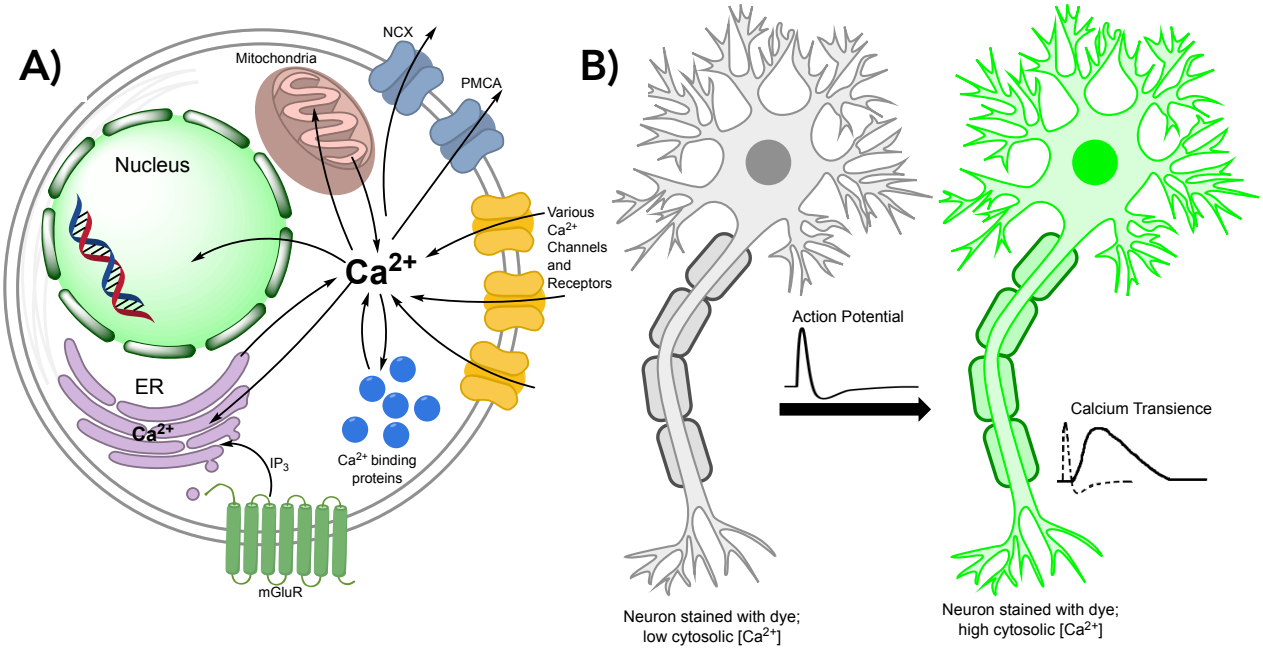

Figure 1. A) Regulation of cytoplasmic Ca^{2+}: influx of ions through the plasma membrane (Ca^{2+}channels), efflux across the membrane, and intracellular buffering systems (release and reuptake by internal stores). **B)** Neurons are loaded with dye prior to stimulation. Immediately following action potential, Ca^{2+} flood the cytoplasm and saturate indicator's binding sites causes a fluorescent response

2. Calcium Imaging

There are two types of fluorescent calcium indicators: genetically-encoded calcium indicators (GECIs) and small-molecule chemical calcium indicators. Genetically-encoded calcium indicators are fluorescent-protein based calcium indicators, while chemical calcium indicators are small-molecule fluorescent dye-based calcium indicators.[1]

2.1 Genetically-Encoded Calcium Indicators (GECIs)

Protein-based calcium indicators are comprised of three parts: fluorescent proteins, calmodulin, and the M13 peptide. Calmodulin (CaM) is a calcium binding protein, and M13 is a calmodulin-binding peptide. Upon the binding of four Ca^{2+} ions to calmodulin, the M13 peptide binds to calmodulin and causes a conformational change in the protein. GECIs take advantage of this binding by using calmodulin and the M13 peptide to cause changes to a fluorescent protein structure and induce fluorescence changes that relies on the binding of Ca^{2+} ions. There are two types of GECIs: FRET-based GECIs and single-fluorophore GECIs.[3–8]

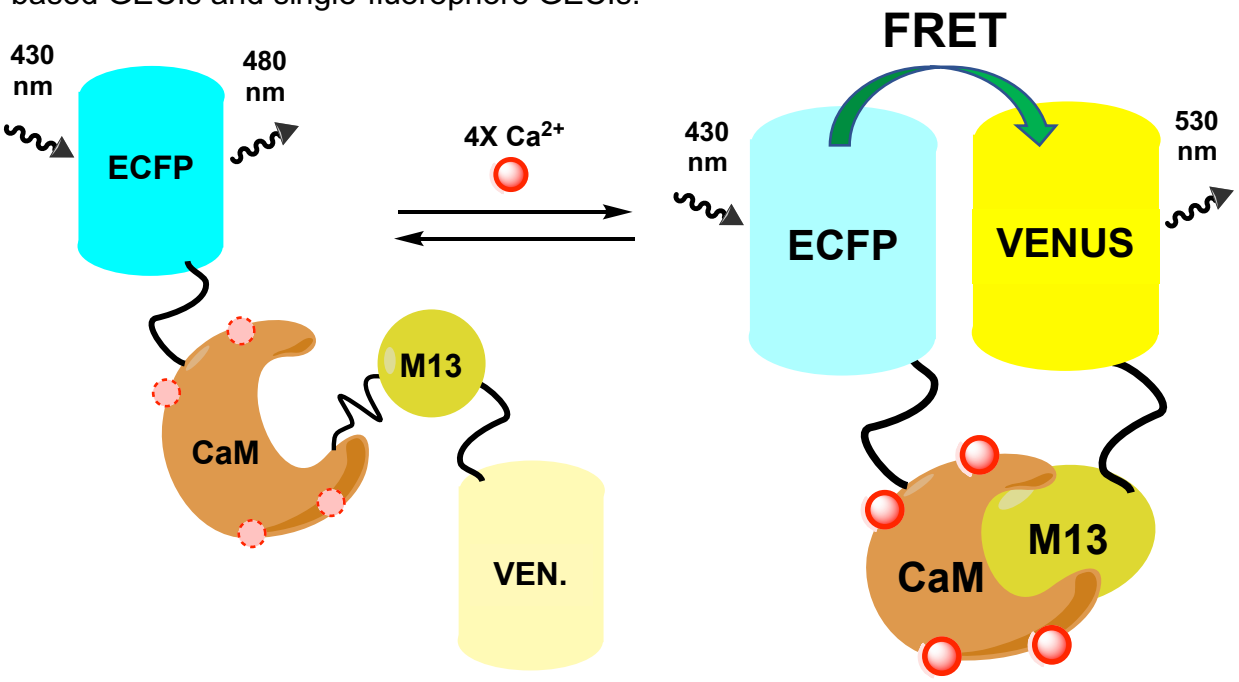

Figure 2. YC 3.60 Structure and mechanism of action of FRET-based genetically-encoded calcium Indicator (GECI): Yellow Chameleon. Calmodulin (CaM) binds four Ca^{2+} ions, and the M13 peptide binds to calmodulin.

FRET-based genetically encoded calcium indicators

Förster resonance energy transfer (FRET) refers to a form of nonradiative energy transfer between two fluorophores where one acts as a donor fluorophore and the other as an acceptor fluorophore. In order for FRET to occur, the distance between the two fluorophores must be less than 10 nm. FRET based GECIs are, therefore, comprised of two spatially and spectrally separated fluorescent proteins: blue ECFP and yellow

VENUS. The linker connecting the two fluorophores is contains calmodulin and the M13 peptide. In the absence of calcium ions, the fluorophores are not within FRET-distance, and the emission is dominated by the blue ECFP fluorescence (480 nm) (Figure 2). Upon Ca^{2+} ions binding to calmodulin, intramolecular conformational changes bring the fluorophores closer together. When calcium is bound to calmodulin, blue ECFP acts as the donor fluorophore and excites the VENUS protein (acceptor fluorophore) via FRET which then emits photons of approximately 530 nm. The fluorescence from the blue ECFP decreases, and the yellow fluorescence from VENUS increases. Ultimately, the resulting change in calcium signal is expressed as a ratio between the VENUS and the ECFP fluorescence.[9–12]

Single fluorophore genetically encoded calcium indicators

The most prevalent and popular single-fluorophore GECIs are the GCaMP family of GECIs. These proteins are increasingly being used for calcium imaging in *in vivo* conditions. GCaMPs consist of a circularly permuted enhanced green fluorescent protein (EGFP). On one side of the fluorescent protein is the calmodulin protein sequence, and on the other is the calmodulin-binding M13 peptide sequence (Figure 3).

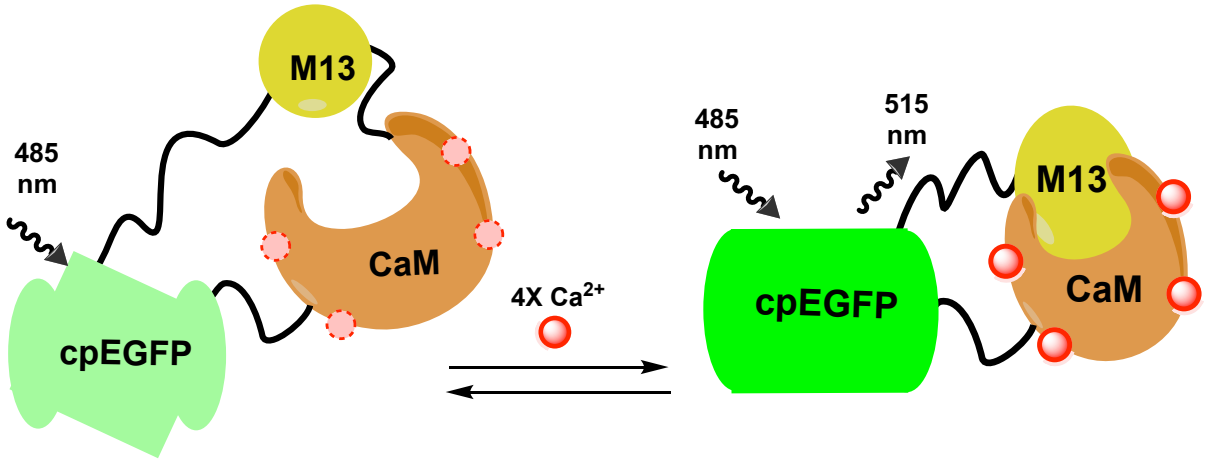

Figure 3. GCaMP Structure and mechanism of action of single-fluorophore genetically-encoded calcium Indicator (GECI): GCaMP. Calmodulin (CaM) binds four Ca^{2+} ions, and the M13 peptide binds to calmodulin.

In the absence of calcium, the EGFP displays decreased fluorescence due to the circular permutation that causes the fluorescent protein structure to have different connectivity than its correct fluorescing counterpart. However, upon the binding of calcium ions to calmodulin, the creation of the calmodulin and M13 complex elicits conformational changes in the fluorophore environment that lead to increased fluorescence. This increase in fluorescence is used to track calcium signaling.[3,13–22]

The primary advantage of using genetically-encoded calcium indicators can be genetically targeted to specific cell-types. The GECIs are assembled by the target cell's own genetic machinery and expressed within the cells. Thus, there is little to no membrane perturbation from delivering GECIs to cells of interest. However, the

expression of GECIs has to be empirically optimized in each target system. The proteins have to be translated by the cell's machinery, therefore expression levels, modes of expression, and regulation vary by cell type. These levels have to be optimized such that enough of the GECI is expressed to facilitate cellular activity experiments.

The efficacy of a calcium indicator is determined by the dynamic range, calcium binding affinity (K_d), selectivity, and response kinetics of the indicator. An efficient indicator displays large dynamic ranges and high affinity for calcium binding (low K_d), is selective for Ca^{2+} over other ions, has fast fluorescence response kinetics, and the change in fluorescence response is linear with changes in calcium concentration.[8] The most efficient GECIs have dynamic ranges that show greater than a 10-fold response upon the binding of Ca^{2+} ions. The binding affinities of GECIs vary greatly; the dissociation constants range from high (>300) nanomolar to low (<10) micromolar. Furthermore, the emission wavelengths of most effective GECIs fall in the green region of the visible spectrum (~514 nm).[8] New developments in protein engineering are bringing new innovations to genetically-encoded calcium indicators. However, low binding affinities, low signal-to-noise ratios, slow response kinetics, and non-linear fluorescence of GECIs limit the use of these indicators in more complex, tissue, multi-color, or multi-photon imaging experiment. Small-molecule or chemical calcium indicators address some of these disadvantages.

2.2 Chemical calcium Indicators

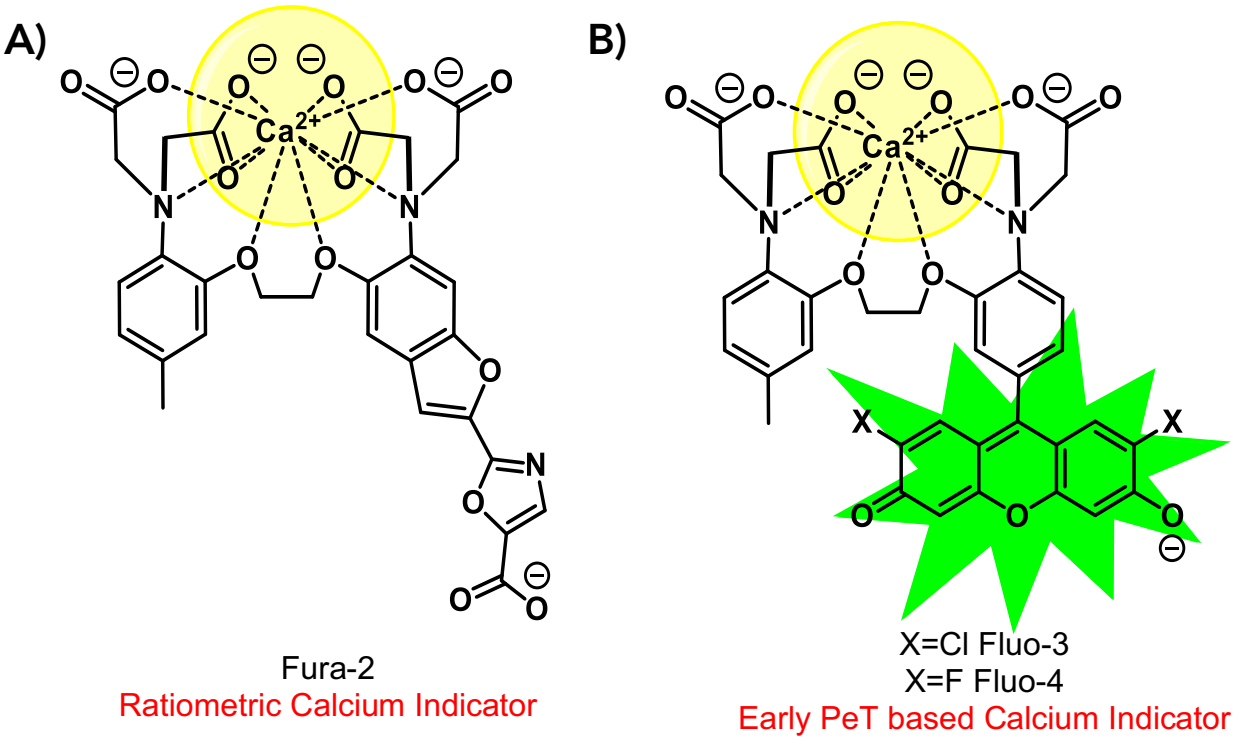

Figure 4. Chemical Calcium Indicators. Chemical calcium indicators are comprised of two parts: calcium chelating molecule (BAPTA) and a fluorophore. A) Structure of Fura-2, which is a ratio-metric calcium indicator. One of the first dyes of its kind to be introduced. B) Structure of Fluo family of calcium indicators. These are early versions of photoinduced electron transfer-based calcium indicators.

Chemical calcium indicators are comprised of two parts: a synthetic calcium chelator which is covalently linked to a fluorescent dye. The calcium chelator is BAPTA (1,2-bis(*o*-aminophenoxy)ethane-*N*,*N*,*N*′,*N*′-tetraacetic acid). The four acetic acid arms of the chelator bind calcium ions by donating electron density from the carboxylates and the lone pairs of nitrogen and oxygen atoms (Figure 4). The binding of Ca^{2+} ions is reversible and dependent on the amount of Ca^{2+} present in the cells at any given time. When Ca^{2+} ions flood the cell's cytoplasm immediately following an action potential, the excess Ca^{2+} binds to BAPTA, eliciting a response from the attached fluorophore. Once the [Ca^{2+}] of the cells returns to baseline amounts, the fluorescence change elicited from the Ca^{2+} binding decrease as fewer Ca^{2+} are bound to the chemical calcium indicator. Therefore, a Ca^{2+} transients can be tracked by calcium indicators. The dye can be single-wavelength fluorophores (ex. Fluo dyes, Figure 4B), or dual-wavelength – ratiometric – fluorophores (ex. Fura-2, Figure 4A).[23]

Ratiometric chemical calcium indicators

Ratiometric indicators are particularly useful for measurements of absolute concentrations. These indicators undergo a shift in their optimum absorption or emission wavelength intensities when binding to free Ca^{2+} ions. Fura-2 (Figure 4A) undergoes a shift in its absorption spectrum, therefore, it is a dual-excitation Ca^{2+} indicator. It exhibits two peak excitation wavelengths: when free of Ca^{2+} ions and when bound to Ca^{2+} ions. An increase in [Ca^{2+}] (Ca^{2+} concentration) initiates an increase in fluorescence emission intensity (Em. λ_{max}: 510 nm) when excited at the Ca^{2+}-bound excitation wavelength (335 nm), and a decrease in fluorescence emission intensity when excited at the Ca^{2+}-free wavelength (363 nm).[24] The ratios derived from the photometric data gathered elucidates the intracellular [Ca^{2+}]. These ratiometric indicators are advantageous as the effects of uneven dye loading, poor dye retention, and photobleaching are greatly reduced. However, these dual excitation dyes are not suitable for confocal microscopy to image tissues and more complex systems.[23–27]

Single-wavelength chemical calcium indicators

Single-wavelength calcium indicators, like the Fluo family of dyes, display a change in their fluorescence emission when Ca^{2+} signals occur (Figure 4B). There is not a shift in either the excitation and/or the emission wavelengths upon Ca^{2+} binding to allow ratiometric measurements. Variations in fluorescence intensity of single-wavelength calcium indicators may not reflect differences in [Ca^{2+}] between cells or between cellular locations. Uneven dye loading, poor dye retention, and photobleaching effect the fluorescence measurements of single-wavelength indicators.[28] For this reason, single-wavelength indicators are most useful for measuring relative changes in Ca^{2+} concentration. The fluorescence signal is usually reported relative to its starting signal to correct for uneven indicator concentration, and expressed as F/F_0 (or $\Delta F/F_0$ if the change in fluorescence is used) where F is the intensity of fluorescence emission recorded during the experiment and F_0 is the fluorescence intensity at the start of the experiment. This method of analysis normalizes differences of indicator concentration between cells, and provides a plausible method for comparing data between experiments. However, it does

not counteract changes in indicator concentration caused by bleaching, or compartmentalization that may occur during the experiment.[23,25,28,29]

The change in fluorescence of single-wavelength indicators occurs via photoinduced electron transfer (PeT). For single-wavelength indicators, calcium-free BAPTA acts as an electron donor to the excited state of the fluorophore (Figure 5A), thereby quenching its fluorescence.[29] Upon binding of Ca^{2+} to BAPTA, the HOMO

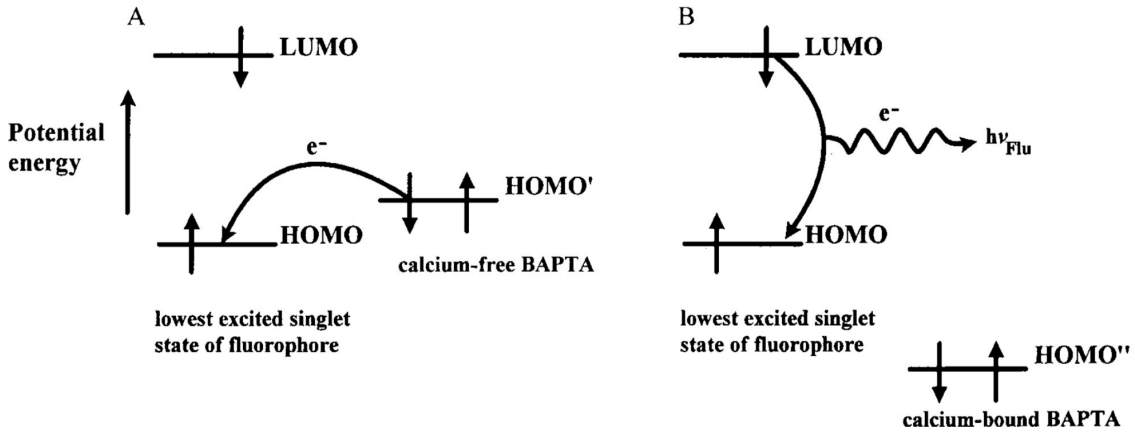

Figure 5. (Image from Tsien 1999). Energy level diagrams to explain why nonratiometric visible Ca^{2+} indicators increase their fluorescence upon Ca^{2+} binding. A) In the absence of Ca^{2+}, the BAPTA unit quenches the attached fluorophore by photoinduced electron transfer. B) When Ca^{2+} is bound, photoinduced electron transfer becomes energetically unfavorable.

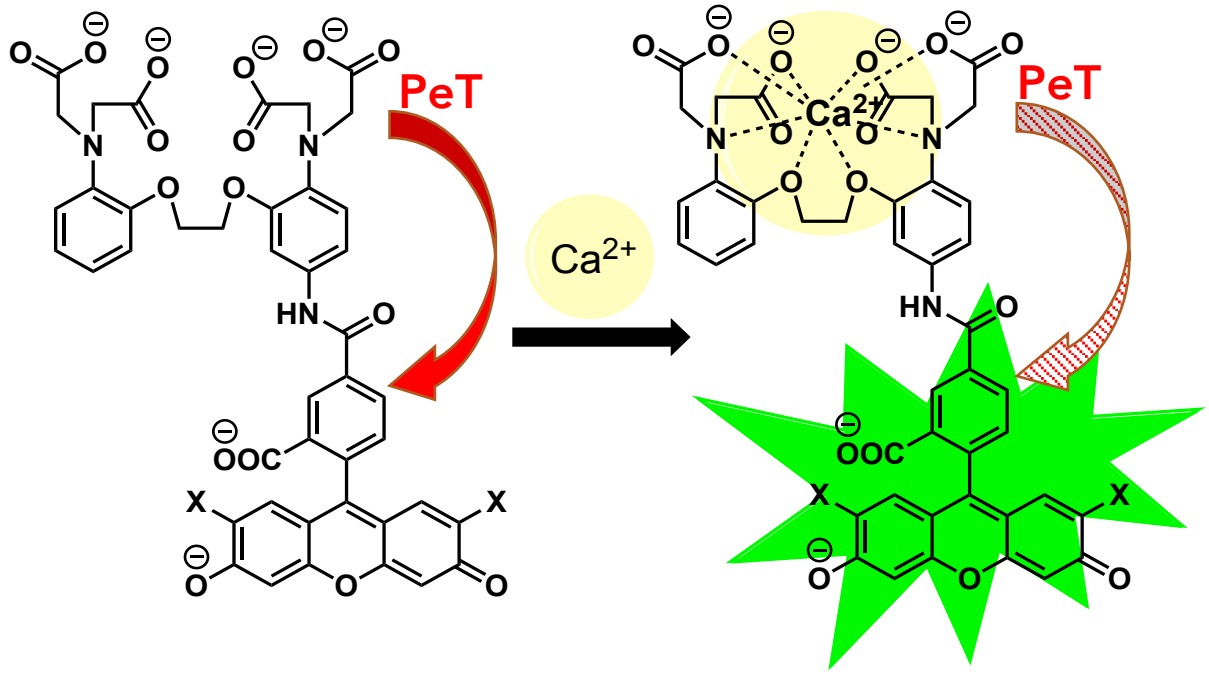

Figure 6. Structural visualization to explain why nonratiometric visible Ca^{2+} indicators increase their fluorescence upon Ca^{2+} binding. In the absence of calcium, the highly electro-negative Ca^{2+} chelator, BAPTA, donates electrons to the excited state of the fluorophore, thereby, quenching its fluorescence. This process of electron transfer is referred to as photoinduced electron transfer (PeT). Upon the binding of calcium, the BAPTA electrons are involved in chelating Ca^{2+} and can no longer quench fluorescence, thus, a fluorescence increase is recorded.

(Highest Occupied Molecular Orbital) of BAPTA drops in energy, and photoinduced electron transfer becomes energetically unfavorable (Figure 5B).[29] This unfavorable drop in energy disallows the BAPTA from acting as a donor for the excited state of the fluorophore, no longer quenching its fluorescence. Therefore, upon the binding of calcium to single-wavelength chemical calcium indicators, there is an increase in fluorescence. Figure 6 illustrates this mechanism.

Modular single-wavelength calcium indicators

Molecular Probes (Michael Kuhn) developed a modular form of PeT based calcium indicator via a general approach to synthesizing fluorophore-conjugated BAPTAs, whereby the fluorophore used could be changed with relative ease.[29] The fluorophores are separated from the BAPTA unit by an extra benzene ring and a variable linkage (amide, thiourea, sulfonamide, etc.). This approach has been exploited to produce a range of short to very long wavelength indicators for various biological applications. Using these conditions, Calcium Green-1, Calcium Orange, and Calcium Crimson were developed. These indicators calcium indicators are very similar in structure, as pictured in Figure 7, but their photophysical properties vary greatly.

The photophysical properties of the calcium indicator derive from the attached organic fluorophore. In the case of the calcium indicators depicted in Figure 7, the fluorophores attached to BAPTAs are fluorescein (Calcium Green-1), tetramethylrhodamine (Calcium Orange), and Texas red (Calcium Crimson). All of these fluorophores contain a xanthene core; xanthene dyes are widely-used, efficient fluorescent dyes for the development of a multitude of biological probes, sensors, or indicators. Xanthene dyes are mainly classified as cationic or anionic dyes. Fluoresceins are generally anionic and greener dyes (~500-530nm emission). Rhodamines are generally cationic and redder dyes (~560-620nm emission). Functional groups on the xanthene moiety control the dye's maximal emission wavelength – hydroxides give green dyes, while amines produce red dyes. Xanthene dyes have similar characteristics including large absorption and luminescence, excellent light resistance, low toxicity *in-vivo,* and relatively high solubility in aqueous solutions.

The modularity of single-wavelength calcium indicators has enabled the development of indicators with long wavelength emission (red-shifted emission) which allows imaging calcium signals in tissues and more complex systems, such as *in vivo* imaging in animals, as red-light penetrates deeper than green-light. As previously mentioned, in order to utilize calcium indicators for monitoring neuronal activity, the indicators must be cytosolically distributed. Red-shifted calcium indicators, such as Ca^{2+}-orange and Ca^{2+}-crimson (Figure 7), contain amine-functionalized xanthene-based fluorophores conjugated to BAPTA. The positive-charge on the amine nitrogen is delocalized over the xanthene. These dyes are often compartmentalized in membrane-bound internal organelles, ex. mitochondria and endoplasmic reticulum. Compartmentalization occurs due to the organelles' large negative membrane potential, which strongly accumulates delocalized cations. However, due to this compartmentalization, these red-shifted calcium indicators are unable to report cytoplasmic changes in Ca^{2+} concentration.[29]

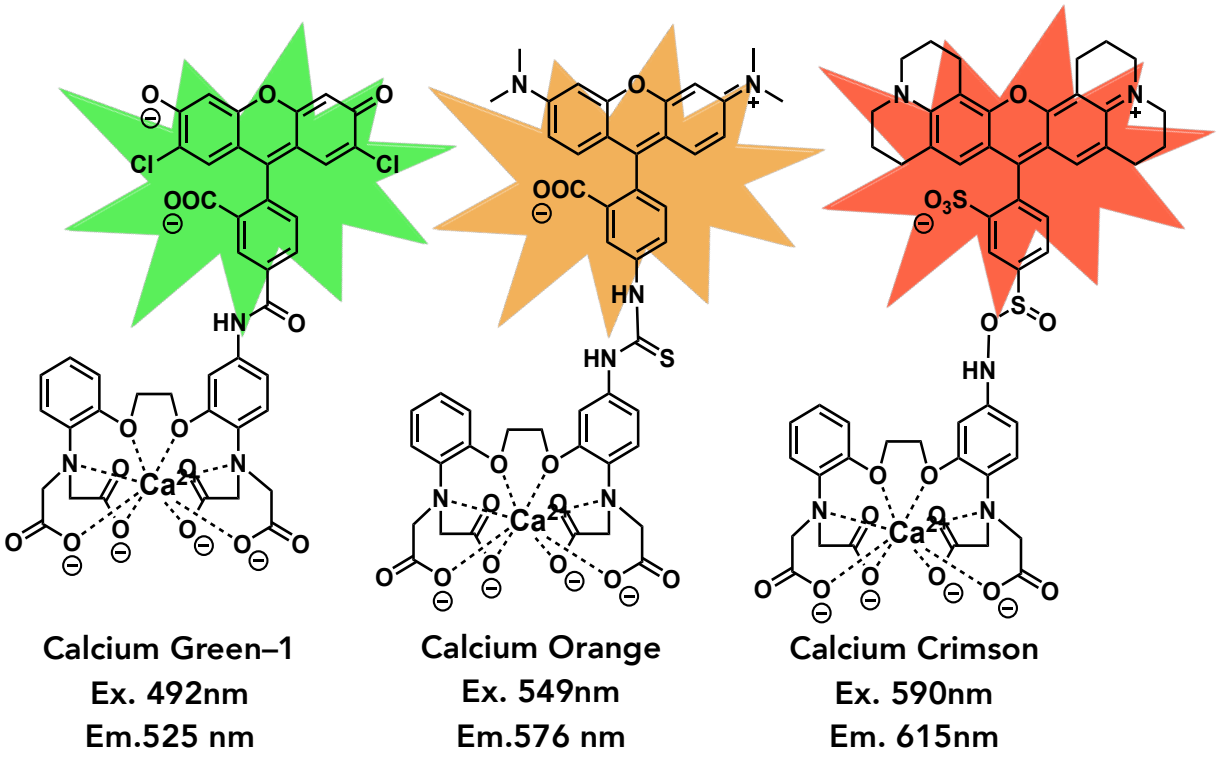

Figure 7. Structural changes of three variants of modular single-wavelength calcium indicators. The generalized approach developed by Molecular Probes facilitates the modularity of single-wavelength calcium indicators. The emission wavelength can be altered to suit the biological application. Changing the linkage of BAPTA to the fluorophore (shown here: amide, thiourea, and sulfonamide, respectively), affects the indicator's Ca^{2+}-binding capability. Modular single-wavelength calcium indicators enable the tuneability of both the emission wavelength and the Ca^{2+} affinity – with relative ease – as needed for biological applications.

Chemical calcium indicators are advantageous because these indicators display linear fluorescence response to increasing calcium concentration, and large dynamic range between the $Ca^{2=}$-free and the Ca^{2+}-bound state; they have high affinities for Ca^{2+} (~100s of nM);[23] they are synthetically tunable for emission wavelength and Ca^{2+} affinity; these indicators can be delivered to the cells at the start of the imaging experiment as they do not require the cell's machinery to assemble these dyes. Furthermore, the fluorescence response of small molecule chemical calcium indicators is not dependent on Ca^{2+}-dependent conformational changes. Thus, the response kinetics of chemical indicators is essentially instantaneous and dependent on the efficiency of PeT rather than conformational changes.

By themselves, chemical calcium indicators are cell-impermeant due to the negatively charged acetic acid arms that chelate Ca^{2+} ions, hence these charges are often capped with acetoxy methyl esters (AM esters) in order to increase permeability. These esters allow the indicator to pass through the cell membrane into the cytoplasm where intracellular esterase cleave the AM esters, freeing functional indicator which is now confined inside the cell (Figure 8). While the addition of AM esters enables the calcium indicators to passively diffuse through the hydrophobic core of cell membranes, they increase the hydrophobicity of the overall molecule, thereby decreasing their solubility in aqueous solutions. If the indicators are not soluble in aqueous extracellular medium, the

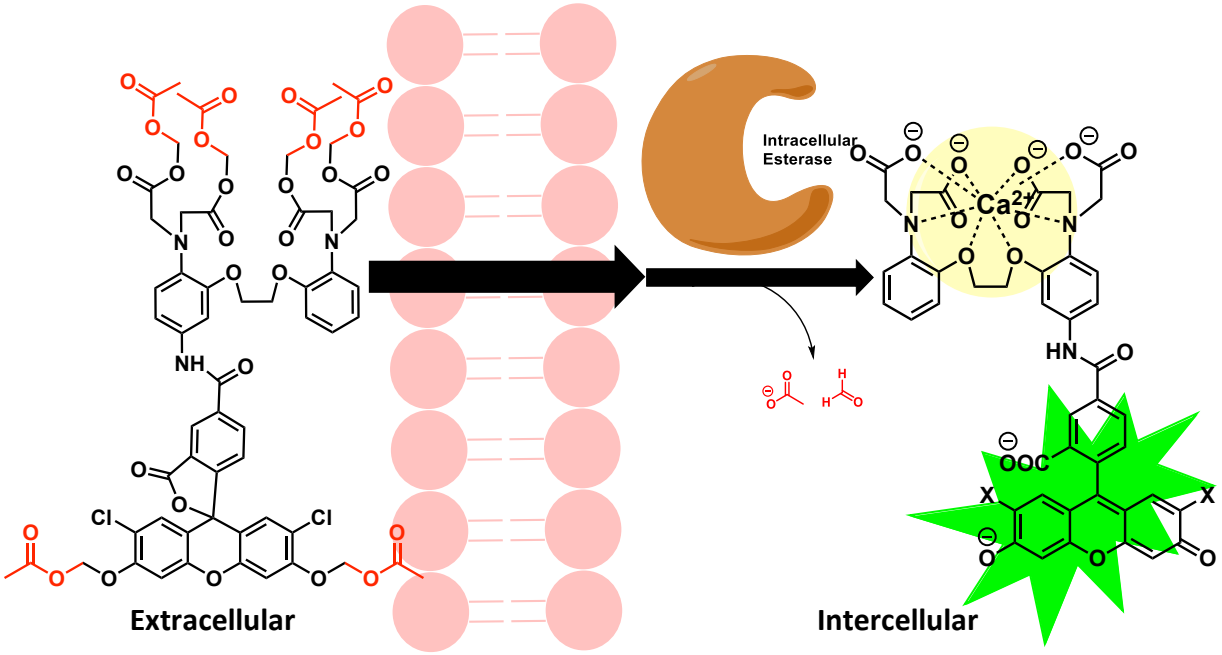

Figure 8. AM esters allow the indicators to be cell permeable. Once inside the cell, intracellular esterases work to cleave off the AM esters and release the fully functional calcium indicator. The structure of the AM ester is shown in red. These esters cap the negatively charged acetic acid arms on BAPTA that render the indicator cell-impermeant. The addition of AM esters effectively masks the hydrophilic indicator, and the indicators passively diffuse across the hydrophobic core of the cell membrane.

dye precipitates out of the imaging medium rather than loading into cells of interest. Therefore, additives such as DMSO and Pluronic-F127 are used to help disperse the AM-linked indicator dyes into the aqueous imaging media. These additives cause membrane perturbations because they act as detergents in order to deliver these dyes to the cells. However, as imaging apparatuses, and dye's photophysical properties have improved over time, a lower concentration of these additives is required to deliver chemical calcium indicators – low enough that the effects on the membranes is negligible.

3. Calcium Imaging Techniques

The instrumentation used to perform fluorescence imaging involves a microscope to which is attached a light-sensing device and a light source for the excitation of the calcium indicators. There are several forms of microscopy, but for calcium signaling the following are the most widely used and will be explored in this work: widefield microscopy, laser-scanning microscopy: confocal microscopy, and two-photon microscopy (Figure 9).[1]

3.1 Wide-field (WF) fluorescence microscopy

A fluorescence microscope irradiates a sample with a prescribed band of wavelengths, and specialized excitation, emission and dichromatic (dichroic) filters are used to separate the much weaker much weaker emitted fluorescence from the excitation light. Only the emission light should reach the eye or detector so that resulting fluorescent

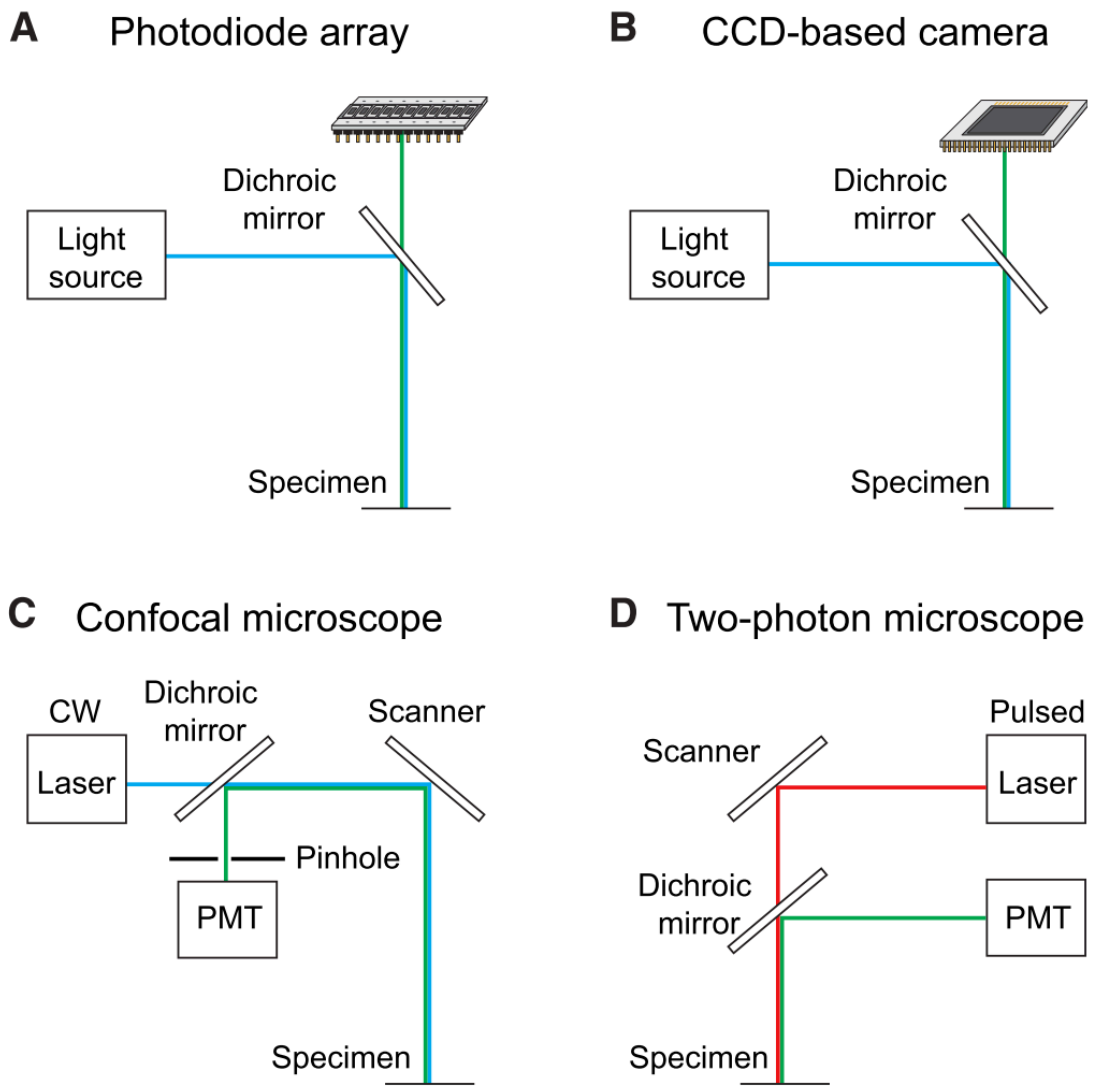

Figure 9. (Image from Grienberger 2012) Common Imaging Devices. (A and B) **Wide-field microcopy** using a photodiode array (A) or a charged coupled device (CCD)-based (B) detection unit. In both cases the light source can be a mercury or xenon lamp. Excitation and emission light are separated by a dichroic mirror. (C and D) **Laser scanning microscopy**. (C) Confocal microscopy using a continuous wave (CW) laser as light source. The excitation spot is steered across the specimen by a scanner. The emission light is descanned and reaches the photomultiplier tube (PMT) after passing a pinhole which is blocking out-of-focus fluorescence. Excitation and emission light are separated by a dichroic mirror. (D) Two-photon microscopy using a pulsed near-IR laser suitable for two-photon absorption. The excitation spot is steered across the specimen by a scanner. The emitted fluorescence is detected by a photo- multiplier tube (PMT).

structures are bright against a dark background. The signal-to-noise ratios are usually governed by the darkness of the background, and the excitation light is several hundred thousand to a million times brighter than the emitted fluorescence. However, many biological specimens exhibit autofluorescence (without the application of fluorophores) when they are irradiated. Therefore, the study of animal tissues is often complicated with either extremely faint or bright, nonspecific autofluorescence. This autofluorescence affects the darkness of the background and is reflected in the calcium indicators' signal-to-noise ratio.

The widefield epi-fluorescence microscope consists of a basic reflected light microscope – the wavelength of fluorescence is longer than that of the excitation. A vertical illuminator is attached to the setup with a light source position at one end and a filter cube turret at the other. Light of a specific wavelength (or defined band of wavelengths) – often in the UV, blue or green regions of the visible spectrum – is produced by passing multispectral light from an arc-discharge lamp or other source through a wavelength selective excitation filter. Wavelengths passed by the excitation filer reflect from the surface of a dichroic beamsplitter, through the microscope objective to bathe the specimen with intense light (Figure 9A and B).[1] If the sample fluoresces, the emitted light gathered by the objective passes back through the dichroic mirror and is, subsequently, filtered by a barrier (or emission) filter, which blocks the unwanted excitation wavelengths. The emitted light radiates spherically, regardless of the direction of the excitation light source. [30,31]

In widefield microscopy, the entire specimen is illuminated by light. Thus, regions above and below the focal plane will also fluoresce and be captured by a camera. Background fluorescence increases due to this out-of-focus fluorescence leading to an overall decrease in signal-to-noise ratio, and, therefore, a decrease in achievable resolution and contrast. The resolution of a microscope is the ability to distinguish detail in a specimen It is the minimum distance which two distinct points of a specimen can still be viewed as separate entities, and determined by the numerical aperture of objective and wavelength of light. The limit of resolution in light microscopy is around 200 nm. However, the resolution in the z-direction achieved by a WF microscope is exacerbated by the background fluorescence due to out-of-focus light. [30,31]

3.2 Laser-scanning microscopy (LSM)

Laser scanning microscopy is a form of optical microscopy in which a focused laser beam is scanned over the sample and the fluorescence generated from a local piece of tissue is displayed as a function of position to create a digital image of the sample. This method of scanning a focused laser beam allows the acquisition of digital images with very high resolution since the resolution is determined by the position and size of the laser beam. Laser scanning microscopy permits a wide range of qualitative and quantitative measurements that include topography mapping of a specimen and 3D visualization.

Confocal laser scanning microscopy

The key to confocal laser scanning microscopy is the use of spatial filtering to eliminate out-of-focus light in specimens that are thicker than the plane of focus. Using confocal microscopy offers advantages like controllable depth of field, the elimination of image degrading out-of-focus information, and the ability to collect serial optical sections from thick specimens. Therefore, this technique has gained popularity for those studying specimens that are thicker than 2 micrometers.

In a conventional widefield microscope, the entire specimen is bathed in light from a mercury or xenon source, and the image can be viewed directly by eye or projected directly on to a camera. In contrast, the method of image formation in confocal microscope is fundamentally different. One or more focused laser beams are scanned across the

specimen; these scans produce images referred to as optical sections. Confocal microscopy has facilitated the collection of three-dimensional data (z-series), and improved the images obtained of specimens using multiple labeling.

The configuration of modern confocal microscopes involves a laser which serves as the point source of excitation light. The point of light is focused by a dichroic mirror and a scanning unit the desired focal plane in the specimen, and the light that passes through it is focused by a second objective lens at a second pinhole which is in conjugate planes with the image plane. Any light that passes through the second pinhole strikes a photomultiplier, which generates a signal that is related to the brightness of the light from the specimen. The pinhole prevents light originating from above or below the plane of focus in the specimen from reaching the photomultiplier (Figure 9C).[1] This is spatial filtering and is key to the confocal approach. In order to build an image, the focused spot of light must be scanned across the specimen in some way. The image is then serially built up from the output of a photomultiplier tube or point detectors, directly processed in a computer imaging system, displayed on a high-resolution video monitor.

While the use of a pinhole excludes out-of-focus background fluorescence from detection, the excitation light generates fluorescence throughout the specimen, thereby producing photobleaching and phototoxicity throughout the specimen. Only signal generated within the plane of focus is collected, but the large excitation volume can cause significant photobleaching and phototoxicity problems, especially in live specimens. Furthermore, the penetration depth in confocal microscopy is limited by absorption of excitation energy throughout the beam path, and by specimen scattering of both the excitation and emission photons.

As the dyes used to add contrast to specimens have improved over time, advancements in modern technology has led to the growth and refinement of the confocal approach; this time of advancement is being dubbed a “Renaissance in Optical Microscopy.”[32] Among these are stable multiwavelength lasers for improved point light sources, improved dichromatic mirrors, sensitive low-noise photodetectors, fast microcomputers with image processing capabilities enhanced by availability of affordable large-capacity memory chips, sophisticated image analysis software packages, and high-resolution video displays and digital image printers.

Multiphoton Microscopy (Two-photon)

Multiphoton imaging is an alternative to confocal microscopy and also produces optical sections. This technique uses the same scanning system as the confocal microscope, but does not require the pinhole aperture at the detector. The pinhole is un-necessary because the laser excites the fluorophores in the specimen only at the point of focus, eliminating out-of-focus emission. Optical sectioning in multiphoton microscopy relies on the simultaneous absorption of two photons in a single quantized event. As the probability of absorption is greatest at the focal place where photon density is highest, the technique provides optical sectioning without excitation above and below the plane of focus. Multiphoton excitation is dependent on infrared which enables deeper specimen penetration than single photon excitation that is usually based on visible light. Consequently, this technique is often used for experiments that require deep penetration into living tissue or intact animal specimens. Multiphoton imaging excites the fluorophore

at longer wavelengths than widefield or confocal, and less light is absorbed since two photons have to excite the sample simultaneously, thereby, reducing photobleaching.[33]

The photophysics governing two-photon excitation vary greatly from that of conventional fluorescence excitation (Figure 10).[34] Two-photon excitation arises from the simultaneous absorption of two photons. Since the energy of a photon is inversely proportional to its wavelength, the two absorbed photons must have wavelength about twice that is required for one-photon excitation. Because two-photon excitation depends on simultaneous absorption, the resulting fluorescence emission varies with the square

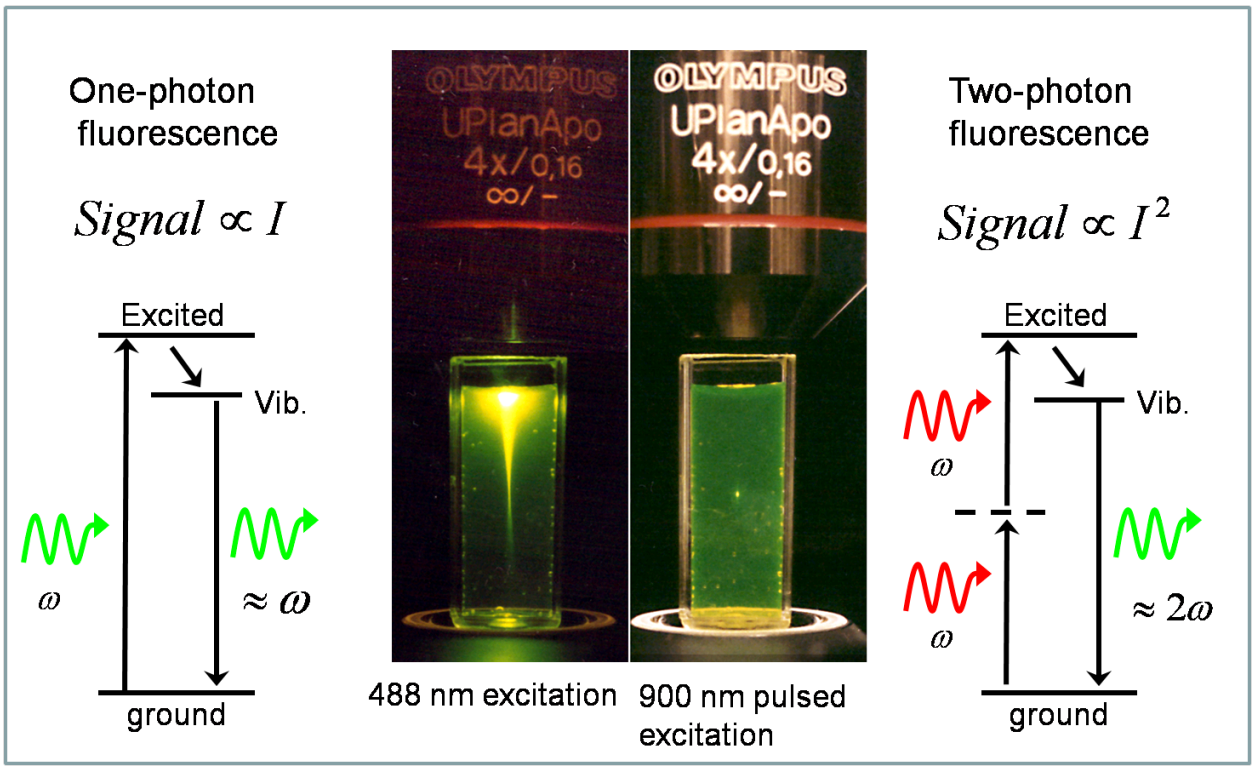

Figure 10. (Image from Webb Lab, Cornell University, Adapted by J. van Howe) Photophysics of one-photon fluorescence vs. two-photon fluorescence. The goal of MPM is to eliminate the scattering from background fluorescence outside of the focal plane (left). These photons are noise and do not contribute to meaningful information about the sample. Using two-photon fluorescence, however, one gets photons mainly near the focal plane and nowhere else, thereby significantly reducing the background fluorescence. This focused illumination allows scanning deep (~1 mm) through tissue. Reduction in scattering occurs because, in the two-photon configuration, the probability of a fluorescence event is much greater at the focus of the objective than anywhere else.

of the excitation intensity. In order to produce a significant number of two-photon absorption events, the photon density must be approximately one million times that required to generate the same number of one-photon absorption events. Consequently, extremely high laser power is required to generate significant two-photon-excited fluorescence. Mode-locked pulsed lasers, in which the power during the peak of the pulse is high enough to generate significant two-photon excitation, are focused on the sample, while the average laser power remains fairly low. The two-photon excited state from which emission occurs is the same singlet state that is populated when conventional fluorescence occurs. Thus, the fluorescent emission following two-photon excitation is exactly the same as emission generated in one-photon excitation (Figure 10).[33,34]

Two-photon excitation is generated by focusing a single pulsed laser through the microscope optics. As the laser beam is focused, the photons become more crowded (their spatial density increases), and the probability of two photons interacting simultaneously with a single fluorophore also increases. The laser focal point is the only location along the optical path where the photons are crowded enough to generate significant two-photon excitation. Above the focal point, the photon density is not sufficient for two photons to pass within the absorption cross-section of a single fluorophore at the same instant. At the focal point, however, the photons are so crowded that is possible for two to pass through within the absorption cross-section of a fluorophore simultaneously.[35,36]

4. Design of a new Rhodol-based Chemical Calcium Indicator

Thus far, the current advancement in calcium imaging probes and techniques have been discussed. As understanding the biological process governed by changes in Ca^{2+} concentration is the primary goal of calcium imaging, it is important that the calcium indicators used show fast, robust, and linear responses to calcium signaling without excessive photobleaching or photodamage. Furthermore, live cell imaging in tissues and complex systems requires that the calcium indicator be compatible with imaging techniques such as confocal and multiphoton microscopy.

Genetically-encoded calcium indicators require empirically optimized expression in cells and systems of interest. Furthermore, often these indicators display non-linear fluorescence response, slow response kinetics, and high signal-to-noise ratios due to lack of sensitive calcium binding. Red-shifted genetically-encoded calcium indicators that allow deep tissue calcium imaging have low affinities, and slow response kinetics. Determining the two-photon cross-section of fluorescent proteins is complicated by the cellular environment that these proteins are *in situ.* Furthermore, measuring the cross-section of the chromophore in solution provides unreliable results, as the chromophore of a fluorescent protein is buried in a complex, spatially organized protein environment that influences the optical properties of chromophore through electrostatic interactions. The two-photon cross-section is also sensitive to the electric field present in the protein beta-barrel. Thus, the two-photon absorption can be manipulated by changing the electrostatic environment of the chromophore.[37]

Chemical calcium indicators, on the other hand, have many versatile uses. These indicators display a large, robust linear response to calcium signaling. They are modular such that the emission wavelength and calcium binding capability is synthetically tunable. However, the most used chemical calcium indicators have green emission, and do not display a strong two-photon absorption cross-section. Two-photon absorption occurs when two photons simultaneously interact with the fluorophore, exciting it. The photons have the same energy, and arise from the same excitation beam of a laser. Determining the absorption cross-section allows the use of an appropriate wavelength that increases the probability of a two-photon excitation event occurring. Unlike fluorescent proteins, the two-photon absorption of a chemical calcium indicator is intrinsic to the fluorophore used. The larger the two-photon absorption, the greater the probability that a two-photon excitation event will occur at that excitation wavelength. Red-shifted fluorophores (ex. rhodamines) display larger two-photon cross-sections than their blue/green

counterparts.[38–43] However, the compartmentalization of rhodamine-based calcium indicators, like Calcium Orange and Calcium Crimson, limit the use of these indicators to track neuronal activity.

There is, therefore, a need for chemical calcium indicators with large and robust, linear calcium responses that have increased two-photon absorption – ones that are redder than OGB and CG-1, but do not localize to membrane-bound organelles.

We propose the use development of a novel rhodol-based calcium sensor. Rhodols are hybrid rhodamine/fluorescein fluorophores that are bright, photostable and have good two-photon absorption cross-sections (Figure 11).[44–47] The design, synthesis, and application of rhodol-based calcium sensors is presented in this work.

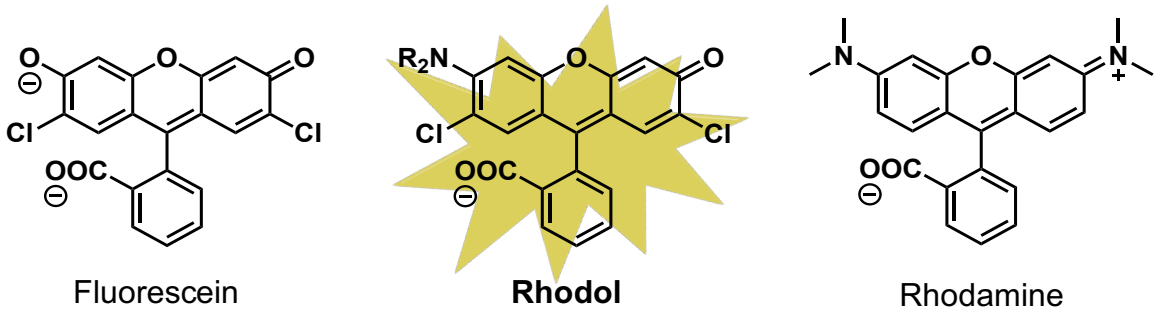

Figure 11. Rhodol fluorophore structure. Shown in the center panel is the basic structure of the fluorophore family dubbed Rhodols. These fluorophores are a hybrid of rhodamine and fluorescein fluorophores in that the xanthene moiety is functionalized with one hydroxide and one amine on each end rather than two hydroxides (fluorescein, left), or two amines (rhodamines, right). The amine functional moiety used is modular and controls the emission wavelength of the fluorophore.

As described previously, the emission wavelength of xanthene dyes is altered by changing the functional groups attached to the xanthene core. The replacement of one of the hydroxides with an amine shifts the excitation and emission profile of the fluorophore bathochromically. Rhodols have the same intrinsic characteristics of xanthene dyes: high extinction coefficients, high quantum yields, good photostability, and good water solubility. In other biological probes, rhodol-based sensors have shown increased two-photon absorption cross-sections.[47–51] Using these principles, we set out to design a family of rhodol calcium indicators we call Rhodol Calcium Sensors (RCSs). In chemical indicators, the calcium chelating group BAPTA is covalently attached to a fluorophore, thus, rhodol-based calcium sensor is comprised of a rhodol fluorophore covalently linked to BAPTA. Figure 12 shows a schematic representation of the design of RCSs. The fluorophore is covalently linked to the BAPTA calcium chelating domain by an amide linkage.

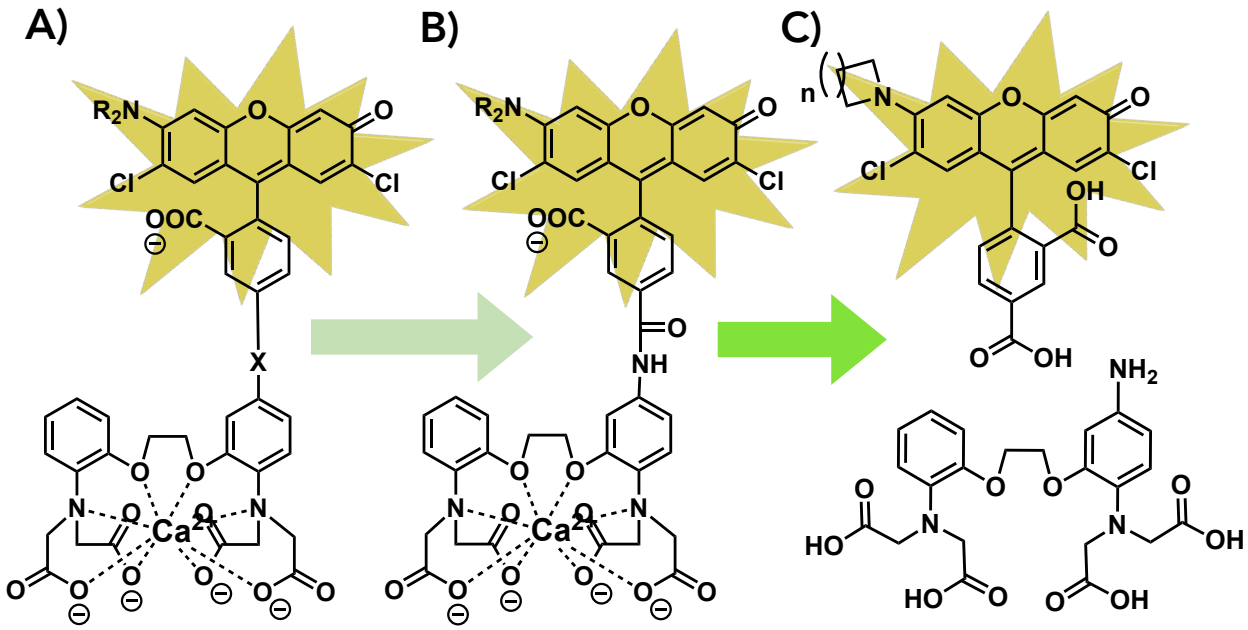

Figure 12. Schematic for the design of Rhodol Calcium Sensor. A) Shows that the rhodol fluorophore must be covalently attached to the calcium chelating BAPTA moiety. B) Shows that the covalent linkage chosen was an amide bond. C) Shows that synthesis needs to be broken down into two parts: the fluorophore and the calcium chelating group BAPTA.

Rhodol Calcium Sensor–1 (RCS-1) was synthesized using the synthetic scheme described above and reported in *ACS Biochemistry*.[52] RCS-1 is a chlorinated pyrrolidine-based rhodol calcium sensor. RCS-1 possesses a Ca^{2+} binding constant of 240 nM and a 10-fold turn on response to Ca^{2+} ion binding. RCS-1 effectively absorbs infrared light and has a σ_{TPA} of 76 GM at 840 nm, 3-fold greater than that of its fluorescein-based counterpart. The acetoxy-methyl ester of RCS-1 stains the cytosol of live cells, enabling observation of Ca^{2+} fluctuations and cultured neurons using both one- and two-photon illumination. Together, these results demonstrate the utility of rhodol-based scaffolds for Ca2+ sensing using two-photon illumination in neurons. Chapter 2 discusses RCS-1

Three other rhodol calcium sensors were designed; their syntheses and characterization are described in Chapter 3.

5. References

(1) Grienberger, C.; Konnerth, A. Imaging Calcium in Neurons. *Neuron* **2012**, *73* (5), 862–885.

(2) Clapham, D. E. Calcium Signaling. *Cell* **2007**, *131* (6), 1047–1058.

(3) Akerboom, J.; Carreras Calderón, N.; Tian, L.; Wabnig, S.; Prigge, M.; Tolö, J.; Gordus, A.; Orger, M. B.; Severi, K. E.; Macklin, J. J.; et al. Genetically Encoded Calcium Indicators for Multi-Color Neural Activity Imaging and Combination with Optogenetics. *Front. Mol. Neurosci.* **2013**, *6* (March), 2.

(4) Looger, L. L.; Griesbeck, O. Genetically Encoded Neural Activity Indicators. **2012**.

(5) Mank, M.; Griesbeck, O. Genetically Encoded Calcium Indicators. *Chem. Rev.* **2008**, *108* (5), 1550–1564.

(6) Tian, L.; Andrew Hires, S.; Looger, L. L. Imaging Neuronal Activity with Genetically Encoded Calcium Indicators. *Cold Spring Harb. Protoc.* **2012**, *7* (6), 647–656.

(7) Takahashi, a; Camacho, P.; Lechleiter, J. D.; Herman, B. Measurement of Intracellular Calcium. *Physiol. Rev.* **1999**, *79* (4), 1089–1125.

(8) Pérez Koldenkova, V.; Nagai, T. Genetically Encoded Ca2+indicators: Properties and Evaluation. *Biochim. Biophys. Acta - Mol. Cell Res.* **2013**, *1833* (7), 1787–1797.

(9) Miyawaki, a; Llopis, J.; Heim, R.; McCaffery, J. M.; Adams, J. a; Ikura, M.; Tsien, R. Y. Fluorescent Indicators for Ca2+ Based on Green Fluorescent Proteins and Calmodulin. *Nature* **1997**, *388* (6645), 882–887.

(10) Borst, J. W.; Laptenok, S. P.; Westphal, A. H.; Kühnemuth, R.; Hornen, H.; Visser, N. V.; Kalinin, S.; Aker, J.; Van Hoek, A.; Seidel, C. A. M.; et al. Structural Changes of Yellow Cameleon Domains Observed by Quantitative FRET Analysis and Polarized Fluorescence Correlation Spectroscopy. *Biophys. J.* **2008**, *95* (11), 5399–5411.

(11) Nagai, T.; Yamada, S.; Tominaga, T.; Ichikawa, M.; Miyawaki, A. Expanded Dynamic Range of Fluorescent Indicators for Ca2+ by Circularly Permuted Yellow Fluorescent Proteins. *Proc. Natl. Acad. Sci.* **2004**, *101* (29), 10554–10559.

(12) Krebs, M.; Held, K.; Binder, A.; Hashimoto, K.; Den Herder, G.; Parniske, M.; Kudla, J.; Schumacher, K. FRET-Based Genetically Encoded Sensors Allow High-Resolution Live Cell Imaging of Ca2+dynamics. *Plant J.* **2012**, *69* (1), 181–192.

(13) Nakai, J.; Ohkura, M.; Imoto, K. A High Signal-to-Noise Ca2+ Probe Composed of a Single Green Fluorescent Protein. *Nat. Biotechnol.* **2001**, *19* (2), 137–141.

(14) Tian, L.; Hires, S. A.; Mao, T.; Huber, D.; Chiappe, M. E.; Chalasani, S. H.; Petreanu, L.; Akerboom, J.; McKinney, S. A.; Schreiter, E. R.; et al. Imaging Neural Activity in Worms, Flies and Mice with Improved GCaMP Calcium Indicators. *Nat. Methods* **2009**, *6* (12), 875–881.

(15) Akerboom, J.; Rivera, J. D. V.; Rodríguez Guilbe, M. M.; Malavé, E. C. A.; Hernandez, H. H.; Tian, L.; Hires, S. A.; Marvin, J. S.; Looger, L. L.; Schreiter, E. R. Crystal Structures of the GCaMP Calcium Sensor Reveal the Mechanism of Fluorescence Signal Change and Aid Rational Design. *J. Biol. Chem.* **2009**, *284* (10), 6455–6464.

(16) Akerboom, J.; Chen, T.-W.; Wardill, T. J.; Tian, L.; Marvin, J. S.; Mutlu, S.; Calderon, N. C.; Esposti, F.; Borghuis, B. G.; Sun, X. R.; et al. Optimization of a GCaMP Calcium Indicator for Neural Activity Imaging. *J. Neurosci.* **2012**, *32* (40), 13819–13840.

(17) Chen, T.-W. W.; Wardill, T. J.; Sun, Y.; Pulver, S. R.; Renninger, S. L.; Baohan, A.; Schreiter, E. R.; Kerr, R. A.; Orger, M. B.; Jayaraman, V.; et al. Ultrasensitive Fluorescent Proteins for Imaging Neuronal Activity. *Nature* **2013**, *499* (7458), 295–300.
(18) Ding, J. J.; Luo, A. F.; Hu, L. Y.; Wang, D. C.; Shao, F. Structural Basis of the Ultrasensitive Calcium Indicator GCaMP6. *Sci. China Life Sci.* **2014**, *57* (3), 269–274.
(19) Rose, T.; Goltstein, P. M.; Portugues, R.; Griesbeck, O. Putting a Finishing Touch on GECIs. *Front. Mol. Neurosci.* **2014**, *7* (November), 1–15.
(20) Murakami, T.; Yoshida, T.; Matsui, T.; Ohki, K. Wide-Field Ca2+ Imaging Reveals Visually Evoked Activity in the Retrosplenial Area. *Front. Mol. Neurosci.* **2015**, *08* (June), 1–12.
(21) Niwa, F.; Sakuragi, S.; Kobayashi, A.; Takagi, S.; Oda, Y.; Bannai, H.; Mikoshiba, K. Dissection of Local Ca2+ Signals inside Cytosol by ER-Targeted Ca2+ Indicator. *Biochem. Biophys. Res. Commun.* **2016**, *479* (1), 67–73.
(22) Garcia, M. I.; Chen, J. J.; Boehning, D. Genetically Encoded Calcium Indicators for Studying Long-Term Calcium Dynamics during Apoptosis. *Cell Calcium* **2017**, *61*, 44–49.
(23) Paredes, R. M.; Etzler, J. C.; Watts, L. T.; Zheng, W.; Lechleiter, J. D. Chemical Calcium Indicators. *Methods* **2008**, *46* (3), 143–151.
(24) Tsien, R. Y. New Calcium Indicators and Buffers with High Selectivity Against Magnesium and Protons: Design, Synthesis, and Properties of Prototype Structures. *Biochemistry* **1980**, *19* (11), 2396–2404.
(25) Minta, A.; Kao, J. P.; Tsien, R. Y. Fluorescent Indicators for Cytosolic Calcium Based on Rhodamine and Fluorescein Chromophores. *J. Biol. Chem.* **1989**, *264* (14), 8171–8178.
(26) Yates, S. L.; Fluhler, E. N.; Lippiello, P. M. Advances in the Use of the Fluorescent Probe Fura-2 for the Estimation of Intrasynaptosomal Calcium. *J. Neurosci. Res.* **1992**, *32* (2), 255–260.
(27) Stosiek, C.; Garaschuk, O.; Holthoff, K.; Konnerth, A. In Vivo Two-Photon Calcium Imaging of Neuronal Networks. *Proc. Natl. Acad. Sci. U. S. A.* **2003**, *100* (12), 7319–7324.
(28) Bootman, M. D.; Rietdorf, K.; Collins, T.; Walker, S.; Sanderson, M. Ca2+-Sensitive Fluorescent Dyes and Intracellular Ca2+ Imaging. *Cold Spring Harb. Protoc.* **2013**, *8* (2), 83–99.
(29) Tsien, R. Y. Monitoring Cell Calcium. *Calcium as a Cellular Regulator*. 1999, pp 28–54.
(30) microscopyu. Introduction to Fluorescence Microscopy | MicroscopyU. 2016, pp 1–12.
(31) Wilson, M. Introduction to Widefield Microscopy. *Leica Microsystems*. 2017.
(32) Paddock, S. W. Introductory Confocal Concepts https://www.microscopyu.com/techniques/confocal/introductory-confocal-concepts.
(33) Piston, D. W.; Fellers, T. J.; Davidson, M. W. Multiphoton Microscopy | MicroscopyU. *Nikon Instruments Inc.* 2016.
(34) Jim. Jim's CLEO Blog_ Expo, Idea Generation, and Multiphoton Microscopy

http://cleoqels2010.blogspot.com/2010/05/expo-idea-generation-and-multiphoton.html.
(35) de Reguardati, S.; Pahapill, J.; Mikhailov, A.; Stepanenko, Y.; Rebane, A. High-Accuracy Reference Standards for Two-Photon Absorption in the 680–1050 Nm Wavelength Range. *Opt. Express* **2016**, *24* (8), 9053.
(36) Rumi, M.; Perry, J. W. Two-Photon Absorption: An Overview of Measurements and Principles. *Adv. Opt. Photonics* **2010**, *2* (4), 451.
(37) Drobizhev, M.; Makarov, N. S.; Tillo, S. E.; Hughes, T. E.; Rebane, A. Two-Photon Absorption Properties of Fluorescent Proteins. *Nat. Methods* **2011**, *8* (5), 393–399.
(38) Albota, M. A.; Xu, C.; Webb, W. W. Two-Photon Fluorescence Excitation Cross Sections of Biomolecular Probes from 690 to 960 Nm.
(39) Xu, C.; Williams, R. M.; Zipfel, W.; Webb, W. W. Multiphoton Excitation Cross-Sections of Molecular Fluorophores. *Bioimaging* **1996**, *4*, 198–207.
(40) Chandra Jha, P.; Wang, Y.; Ågren, H. Two-Photon Absorption Cross-Sections of Reference Dyes: A Critical Examination. *ChemPhysChem* **2008**, *9* (1), 111–116.
(41) Mütze, J.; Iyer, V.; MacKlin, J. J.; Colonell, J.; Karsh, B.; Petrášek, Z.; Schwille, P.; Looger, L. L.; Lavis, L. D.; Harris, T. D. Excitation Spectra and Brightness Optimization of Two-Photon Excited Probes. *Biophys. J.* **2012**, *102* (4), 934–944.
(42) Nag, A.; Goswami, D. Solvent Effect on Two-Photon Absorption and Fluorescence of Rhodamine Dyes. *J. Photochem. Photobiol. A Chem.* **2009**, *206* (2–3), 188–197.
(43) Kaatz, P.; Shelton, D. P. Two-Photon Fluorescence Cross-Section Measurements Calibrated with Hyper-Rayleigh Scattering. *J. Opt. Soc. Am. B-Optical Phys.* **1999**, *16* (6), 998–1006.
(44) Whitaker, J. E.; Haugland, R. P.; Ryan, D.; Hewitt, P. C.; Haugland, R. P.; Prendergast, F. G. Fluorescent Rhodol Derivatives: Versatile, Photostable Labels and Tracers. *Anal. Biochem.* **1992**, *207* (2), 267–279.
(45) Peng, T.; Yang, D. Construction of a Library of Rhodol Fluorophores for Developing New Fluorescent Probes. *Org. Lett.* **2010**, *12* (3), 496–499.
(46) Dickinson, B. C.; Huynh, C.; Chang, C. J. A Palette of Fluorescent Probes with Varying Emission Colors for Imaging Hydrogen Peroxide Signaling in Living Cells. *J. Am. Chem. Soc.* **2010**, *132* (16), 5906–5915.
(47) Kulkarni, R. U.; Kramer, D. J.; Pourmandi, N.; Karbasi, K.; Bateup, H. S.; Miller, E. W. Voltage-Sensitive Rhodol with Enhanced Two-Photon Brightness. *Proc. Natl. Acad. Sci.* **2017**, *114* (11), 2813–2818.
(48) Tomat, E.; Lippard, S. J. Ratiometric and Intensity-Based Zinc Sensors Built on Rhodol and Rhodamine Platforms. *Inorg. Chem.* **2010**, *49* (20), 9113–9115.
(49) Poronik, Y. M.; Bernaś, T.; Wrzosek, A.; Banasiewicz, M.; Szewczyk, A.; Gryko, D. T. One-Photon and Two-Photon Mitochondrial Fluorescent Probes Based on a Rhodol Chromophore. *Asian J. Org. Chem.* **2018**, *7* (2), 411–415.
(50) Gautam, S. G.; Perron, A.; Mutoh, H.; Knöpfel, T. Exploration of Fluorescent Protein Voltage Probes Based on Circularly Permuted Fluorescent Proteins. *Front. Neuroeng.* **2009**, *2* (October), 14.
(51) Kim, H. M.; Cho, B. R. Small-Molecule Two-Photon Probes for Bioimaging Applications. **2015**.
(52) Contractor, A. A.; Miller, E. W. Imaging Ca^{2+} with a Fluorescent Rhodol. *Biochemistry* **2017**, acs.biochem.7b01050.

Chapter Two: Imaging Ca^{2+} with a Fluorescent Rhodol

This work has been previously published in:
Contractor, A. A.; Miller, E. W. Imaging Ca $^{2+}$ with a Fluorescent Rhodol. *Biochemistry* 2017, acs.biochem.7b01050.

1. Abstract

Ca^{2+} ions mediate a host of biochemical and biophysical signaling processes in cells. The development of synthetic, Ca^{2+}-sensitive fluorophores has played an instrumental role in our understanding of the temporal and spatial dynamics of Ca^{2+} signaling. Coupling Ca^{2+}-selective ligands to fluorescent reporters has provided a wealth of excellent indicators that span the visible excitation and emission spectrum and possess Ca^{2+} affinities suited to a variety of cellular contexts. One underdeveloped area is the use of hybrid rhodamine/fluorescein fluorophores, or rhodols, in the context of Ca^{2+} sensing. Rhodols are bright and photostable and have good two-photon absorption cross sections (σ_{TPA}), making them excellent candidates for incorporation into Ca^{2+}-sensing scaffolds. Here, we present the design, synthesis, and application of rhodol Ca^{2+} sensor 1 (RCS-1), a chlorinated pyrrolidine-based rhodol. RCS-1 possesses a Ca^{2+} binding constant of 240 nM and a 10-fold turn-on response to Ca^{2+} ion binding. RCS-1 effectively absorbs infrared light and has a σ_{TPA} of 76 GM at 840 nm, 3-fold greater than that of its fluorescein-based counterpart. The acetoxy-methyl ester of RCS-1 stains the cytosol of live cells, enabling observation of Ca^{2+} fluctuations and cultured neurons using both one- and two-photon illumination. Together, these results demonstrate the utility of rhodol-based scaffolds for Ca^{2+} sensing using two-photon illumination in neurons.

2. Introduction

The development of synthetic fluorescent indicators for Ca^{2+} ions is one of the success stories of organic chemistry and molecular recognition. The majority of fluorescent Ca^{2+} indicators utilize BAPTA (1,2-bis(*o*-aminophenoxy)ethane-*N,N,N′,N′*-tetraacetic acid) as the key Ca^{2+}-recognizing domain and couple Ca^{2+} binding to changes in fluorescence intensity or wavelength.[1] First reported in 1980 by Roger Tsien,[2] BAPTA solved dual problems of slow Ca^{2+}-binding kinetics and pH dependence associated with the state of the art Ca^{2+}-selective chelator of the day, EGTA (ethyleneglycol-*N,N,N′,N′*-tetraacetic acid). Importantly BAPTA maintains selectivity for Ca^{2+} over Mg^{2+}, which is present in concentrations exceeding cytosolic Ca^{2+} by 4 to 5 orders of magnitude. Widely used Ca^{2+} indicators include fura-2,[3] which provides a ratiometric read-out of Ca^{2+} concentration using UV excitation; the fluo- and rhod-family of indicators that report on fluctuations in Ca^{2+} concentration via changes in fluorescence intensity at around 520 and 580 nm, respectively;[4] and Oregon Green-BAPTA (OGB)[5] and Calcium Green-BAPTA (CGB)[6] derivatives that employ fluorinated and chlorinated fluorescein as an optical reporter. More recently, the use of modern xanthene scaffolds has enabled access to Ca^{2+} sensing in the orange (Cal-590,[7] CaRuby-Nano[8]) to far-red (CaTM2[9] or Cal-630) region of the electromagnetic spectrum by employing halogenated carbofluorescein[10] or silicon-fluorescein, respectively.

Ca^{2+} indicators are widely used in neurobiology, where fluorescent indicators provide a convenient method to measure the relative activity of neurons. OGB, in particular, continues to be used for *in vivo* applications,[11] despite the recent emergence of excellent genetically-encoded Ca^{2+}-sensitive fluorescent proteins,[12] on account of its well-tuned K_d (170 nM) and fast Ca^{2+}-binding kinetics.[13] The use of fluorescent Ca^{2+} indicators, whether synthetically-derived or genetically-encoded, is frequently paired with two-photon microscopy, which allows greater tissue penetration on account of the use of high energy, pulsed lasers in the infrared regime. Despite the critical dependence on the use of two-photon illumination to image in thick tissues, most widely-used Ca^{2+} indicators show only modest ability to effectively absorb two-photon (2P) illumination.[14] CGB has a two photon excitation cross section of approximately 30 GM (when saturated with Ca^{2+}).[15] Alternatively, indicators based on rhodamines, with larger 2P cross sections in the 50 to 100 GM range (for example, Calcium Orange or Calcium Crimson),[15] often localize to cellular compartments rather than cytosol.[16] To surmount the problems of low 2P cross section while maintaining good Ca^{2+} affinity, sensitivity, and cellular localization, we hypothesized that rhodol-based fluorophores[17] would enable Ca^{2+} sensing under 2P illumination in live cells. Rhodols have intermediate to strong 2P cross sections, at around 120 GM,[18,19] and show good cellular localization.[20,21] Despite these promising characteristics, rhodols have never been combined with BAPTA to create a Ca^{2+} sensor. We here report the design, synthesis, characterization and application of rhodol Ca^{2+}-sensor 1, a fluorescent Ca^{2+} indicator with good 2P excitation cross section, sub-micromolar dissociation constants for Ca^{2+}, and the ability to report on [Ca^{2+}] fluxes in live cells and neurons under 2P illumination.

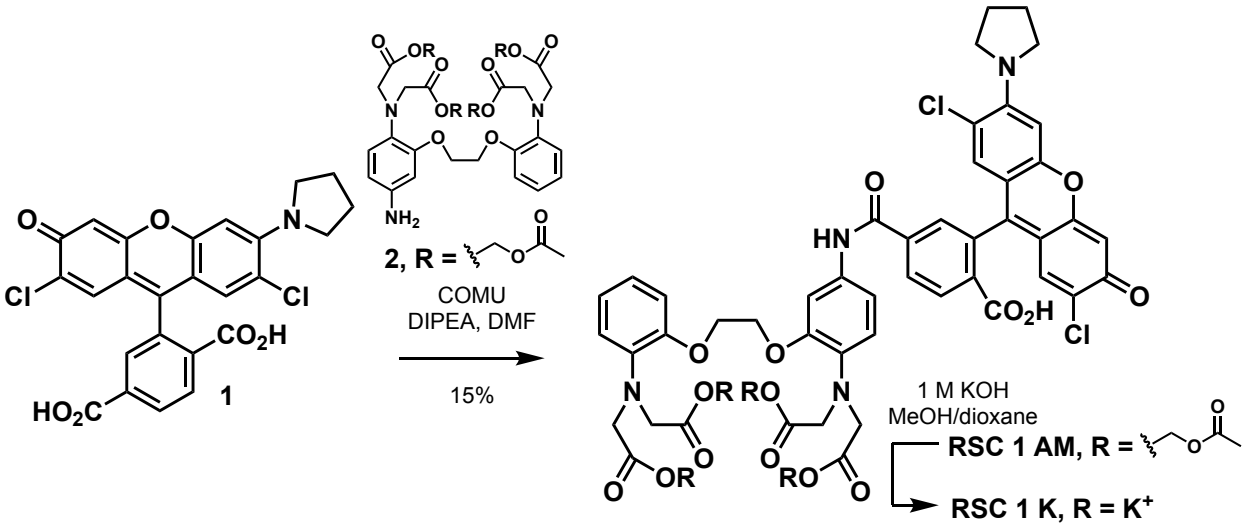

Scheme 1. Synthesis of rhodol Ca^{2+} sensor 1

Rhodol Ca^{2+} sensor 1 is synthesized in a single step from the corresponding 6'-carboxy-dichloropyrrolidylrhodol (1) and the AM-ester of 5-aminoBAPTA (2) (Scheme 1). Synthesis of 1 proceeds in 4 steps from carboxy-dichlorofluorescein. Construction of isomerically pure 6'-carboxy-dichlorofluorescein is achieved via recrystallization from acetic anhydride/pyridine to give the 6' isomer in gram quantities.[22] Protection of the pendant carboxylate as the *t*-butyl ester[23] enables selective protection of a single phenolic

oxygen as the methyoxymethyl (MOM) ether[24] and subsequent conversion of the remaining oxygen to the triflate. Conversion of the fluorescein to rhodol proceeds via Pd-catalyzed C-N bond formation with pyrrolidine followed by removal of the *t*-butyl ester to give compound 1 in 30% yield over two steps.[25] Formation of amide bond between rhodol 1 and the tetra-acetoxymethyl ester of 5'-amino-BAPTA 2[9] provided the acetoxy methyl ester[26] of rhodol Ca^{2+} sensor 1 (RCS-1 AM) in 15% overall yield following purification. Saponification of this material provided the hexapotassium salt of RCS (RCS-1 K) for *in vitro* spectroscopic characterization.

3. Synthesis

The synthesis of rhodol Ca^{2+} sensor 1 was carried out in two parallel streams: the synthesis of the rhodol fluorophore, and the synthesis of amino-BAPTA AM.

3.1 BAPTA-AM synthesis

The calcium chelating moiety, BAPTA, was synthesized as described from 2-nitrophenol. 5'-amino-BAPTA ethyl ester was synthesized over five steps.[9] The pendant amine was protected as a *t*-butyl carbamate, and the ethyl esters were hydrolyzed using low molarity potassium hydroxide to create the tetrapotassium salt. The acetate arms on the BAPTA group were alkylated with acetoxy methyl esters, the *t*-butyl carbamate was subsequently deprotected to give final 5'-amino-BAPTA tetra-acetoxymethyl ester (Scheme 2).[26]

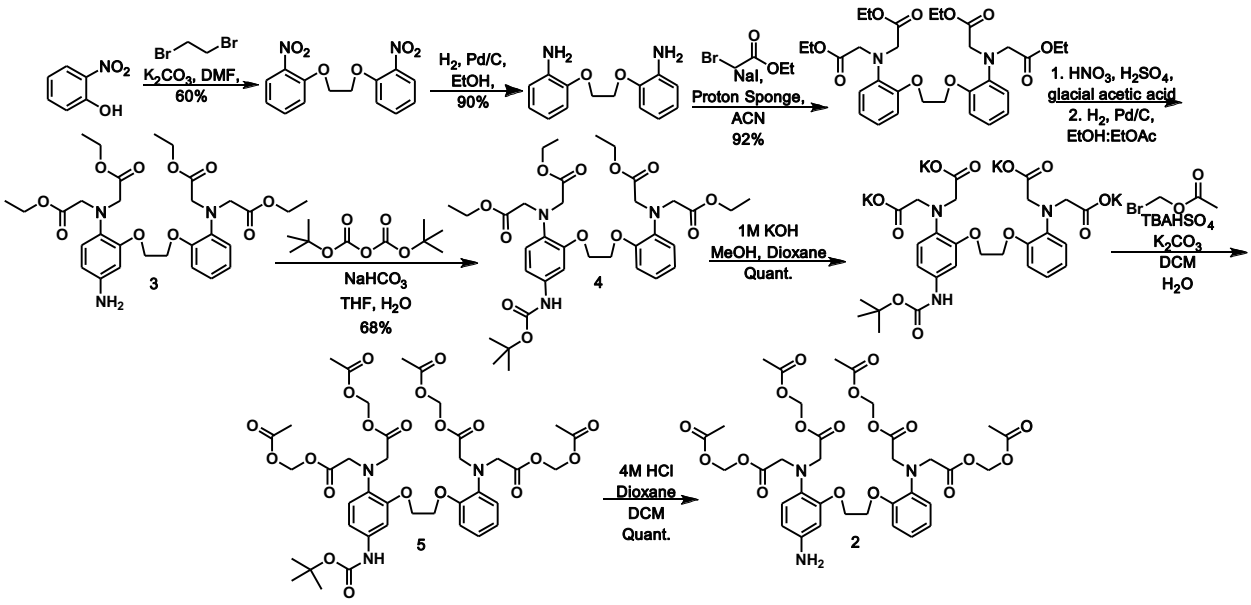

Scheme 2. Synthesis of tetra-acetoxymethyl ester of 5'-amino BAPTA (2).

Synthesis of 1,2-bis(2-nitrophenoxy)ethane:

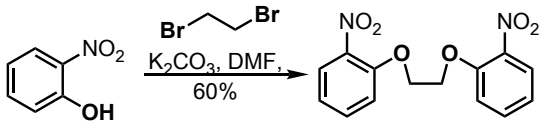

To a 250-mL round-bottom flask, 24.0g (0.173 mol, 2 equiv.) of 2-nitrophenol was added in 70 mL dimethylformamide. Once the 2-nitrophenol was dissolved, 7.46 mL (0.086 mol, 1 equiv.) of dibromoethane and 23.8g (0.173 mol, 2 equiv.) of potassium carbonate was added. The reaction mixture was then heated to 140 °C for 30 min, cooled slightly, then poured into 150 mL water. The precipitate was collected by vacuum filtration and then recrystallized from 350 mL boiling acetone, with the resulting suspension cooled to -20 °C in a freezer prior to collection by vacuum filtration, affording 22.09 g (86%) of 1,2-bis(2-nitrophenoxy)ethane as an off-white solid. ^{1}H NMR (400 MHz, $CDCl_3$) δ 7.83 (d, 2H), 7.65 – 7.35 (m, 2H), 7.29 – 7.21 (m, 2H), 7.07 – 7.02 (m, 2H), 4.52 (s, 4H). ESI-MS calculated for $C_{14}H_{12}N_2O_6$ [M+H]+ 305.28, found 305.0342. The ^{1}H NMR and ESI-MS agreed with reported literature values.[2]

Synthesis of 2,2'-(ethane-1,2-diylbis(oxy))dianiline:

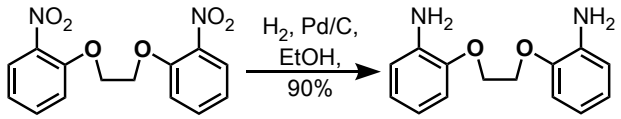

A solution of 5.00 g (16.4 mmol) of 1,2-bis(nitrophenoxy)ethane and 500 mg (0.1 equiv. by wt.) of 5% platinum on carbon in 100 mL of ethanol was evacuated and backfilled with nitrogen three times, then evacuated and backfilled with hydrogen three times. The reaction was left under 1 atm. of hydrogen (4 L) at room temperature for 24 h, at which point the reaction was judged to be complete by TLC. The reaction was charged with a further 5.00 g (16.4 mmol, 1.00 equiv.) of 1,2-bis(nitrophenoxy)ethane and four more liters of hydrogen and was stirred for a further 24 h. After completion of the reaction, 300 mL of dicholoromethane was added to the reaction mixture which was then filtered through a plug of diatomaceous earth. The combined organics were concentrated under reduced pressure and the resulting solid was triturated with 50% acetone in hexanes (20 mL), collecting the resulting solid by vacuum filtration. This process afforded 7.32 g (85%) of 2,2'-(ethane-1,2-diylbis(oxy))dianiline as a white solid. ^{1}H NMR (400 MHz, $CDCl_3$) δ 7.83 (d, 2H), 7.65 – 7.35 (m, 2H), 7.29 – 7.21 (m, 2H), 7.07 – 7.02 (m, 2H), 5.00 (br s, 4H), 4.32 (s, 4H). LCMS calculated for $C_{14}H_{16}N_2O_2$ [M+H]+ 245.128, found 245.234. The ^{1}H NMR and ESI-MS agreed with reported literature values.[2]

Synthesis of tetraethyl 2,2',2'',2'''-(((ethane-1,2-diylbis(oxy))bis(2,1-phenylene))bis(azanetriyl))tetraacetate:

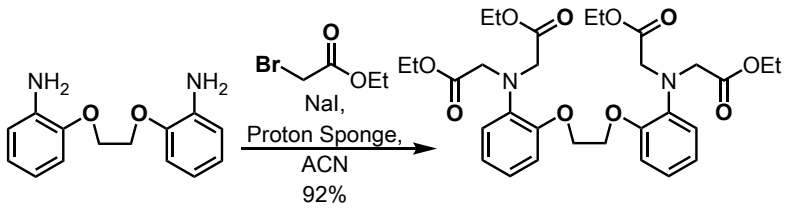

A solution of 2.25 g (9.3 mmol, 1.0 equiv.) of 7, 9.87 g (46.1 mmol, 5.0 equiv.) of proton sponge® and 1.80 g (12.0 mmol, 1.3 equiv.) sodium iodide was sparged with N_2 for 30

min, then 5.10 mL (46.1 mmol, 5.0 equiv.) of bromoethylacetate was added via syringe and the reaction mixture heated to reflux overnight. The reaction mixture was then cooled to room temperature and the organics concentrated under reduced pressure. To the remaining residue, 50 mL of toluene was added and the insoluble NaBr was removed by filtering through a thin pad of diatomaceous earth, rinsing with 50 mL more toluene. The combined organics were washed with pH 2 phosphate buffer until the aqueous fractions were colorless (3x 100 mL). The organic layer was dried with sodium sulfate and concentrated under reduced pressure. The remaining yellow oil was then triturated with 10% ethyl acetate in hexanes, with the precipitate collected by vacuum filtration. Washing with a further 50 mL of 10% ethyl acetate in hexanes afforded 5.02 g (92%) of tetraethyl 2,2',2'',2'''-(((ethane-1,2-diylbis(oxy))bis(2,1-phenylene))bis(azanetriyl))tetraacetate as a white solid. ^{1}H NMR (400 MHz, $CDCl_3$) δ 7.83 (d, 2H), 7.65 – 7.35 (m, 2H), 7.29 – 7.21 (m, 2H), 7.07 – 7.02 (m, 2H), 4.54 (s, 4H), 4.24 (q, *J* = 7.2, 8H), 3.83 (s, 8H), 1.30 (t, *J* = 7.1, 12H). ESI-MS calculated for $C_{30}H_{40}N_2O_{10}$ [M+H]+ 589.276 found 589.13. The ^{1}H NMR and LCMS agreed with reported literature values.[2]

*Synthesis of **3**:*

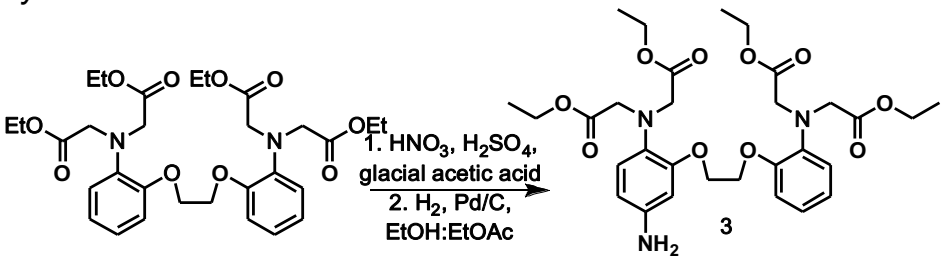

A 50-ml round-bottom flask was charged with 1.92 g (3.26 mmol, 1.0 equiv.) of tetraethyl 2,2',2'',2'''-(((ethane-1,2-diylbis(oxy))bis(2,1-phenylene))bis(azanetriyl))tetraacetate and 10 ml of glacial acetic acid. To the stirring mixture, 136 μL (3.26 mmol, 1.0 equiv.) of concentrated HNO_3 was added in 25 μL increments. The solution was allowed to stir for 10 minutes, after which time an additional 136 μL of HNO_3 was added. After the solution was stirred for an hour, it was poured slowly into sodium bicarbonate solution at 0 °C. The organics were extracted into ethyl acetate (3x 100 mL). The organic layer was dried with sodium sulfate and concentrated under reduced pressure. The brown oil was purified through a silica gel plug (20% EtOAc:Hexanes). The purified material was dissolved into 3:1 EtOH:EtOAc (50mL), and 192 mg of (0.1 equiv. by wt.) of 5% platinum on carbon was added. The solution was evacuated and backfilled with nitrogen three times, then evacuated and backfilled with hydrogen three times. The reaction was left under 1 atm. of hydrogen (4 L) at room temperature for 24 h, at which point the reaction was judged to be complete by TLC. After completion of the reaction, 300 mL of dicholoromethane was added to the reaction mixture which was then filtered through a thin pad of diatomaceous earth. The combined organics were concentrated under reduced pressure and the resulting solid was purified via silica gel chromatography (50–80% EtOAc/hexanes, linear gradient), yielding 953 mg (48%) of **3** as a brown oil. ^{1}H NMR (400 MHz, Chloroform-*d*) δ 7.83 (d, *J* = 8.1 Hz, 2H), 7.57 (t, *J* = 7.8, Hz, 2H), 7.23 (d, *J* = 1.6 Hz, 1H), 7.08 (t, *J* = 7.8 Hz, 2H), 4.54 (s, 4H), 4.24 (q, *J* = 7.2, 8H), 3.83 (s, 8H), 1.30 (t, *J* = 7.1, 12H). ESI-MS calculated for $C_{30}H_{40}N_3O_{10}$ [M+H]+ 604.28, found 604.1.

*Synthesis of **4:***

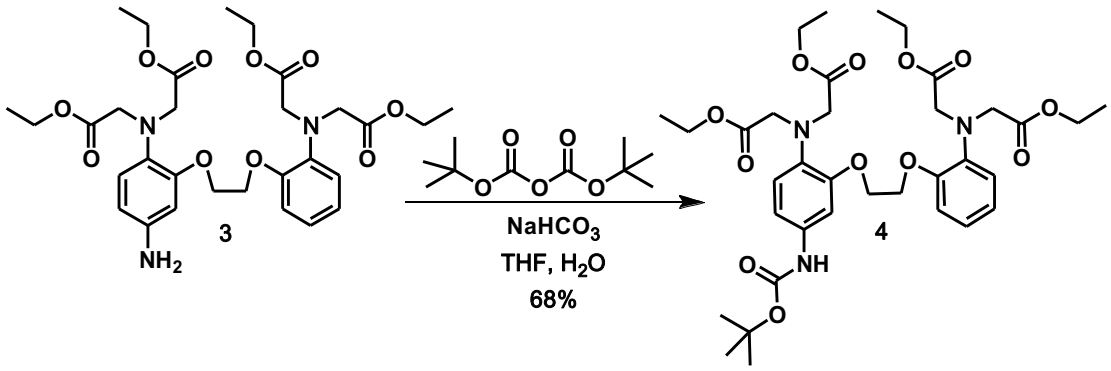

A solution of **3** (420 mg, 0.7 mmol, 1 equiv.) and $NaHCO_3$ (175 mg, 2.1 mmol, 3 equiv.) in 8 mL of 1:1 H_2O:THF was cooled to 0 °C, and 168 μL (0.73 mmol, 1.05 equiv.) boc-anhydride was added. After 30 min, the solution was stirred overnight at room temperature. The solution was extracted with EtOAc (2×200 mL). The aqueous layer was acidified to pH = 4-5 by careful addition of citric acid at 0 °C and then extracted with CH_2Cl_2 (3×200 mL). The combined organic phase was dried (Na_2SO_4), concentrated under reduced pressure, and the resulting solid was purified via silica gel chromatography (20–50% EtOAc/hexanes, linear gradient), yielding 390 mg (80%) of **4** as a brown oil. For long-term (>1 month) storage, the amino-BAPTA, **3**, was frozen as the boc-protected ester **4**. For short-term storage (1-4 weeks), the amino-BAPTA (**3**) was stored in the freezer as is. ^{1}H NMR (400 MHz, Chloroform-*d*) δ 7.83 (d, *J* = 8.1 Hz, 2H), 7.57 (t, *J* = 7.8 Hz, 2H), 7.23 (d, *J* = 1.2 Hz, 1H), 7.08 (t, *J* = 7.8 Hz, 2H), 4.54 (s, 4H), 4.24 (q, *J* = 7.2 Hz, 8H), 3.83 (s, 8H), 1.52 (s, 9H), 1.30 (t, *J* = 7.2 Hz, 12H).

*Synthesis of **5:***

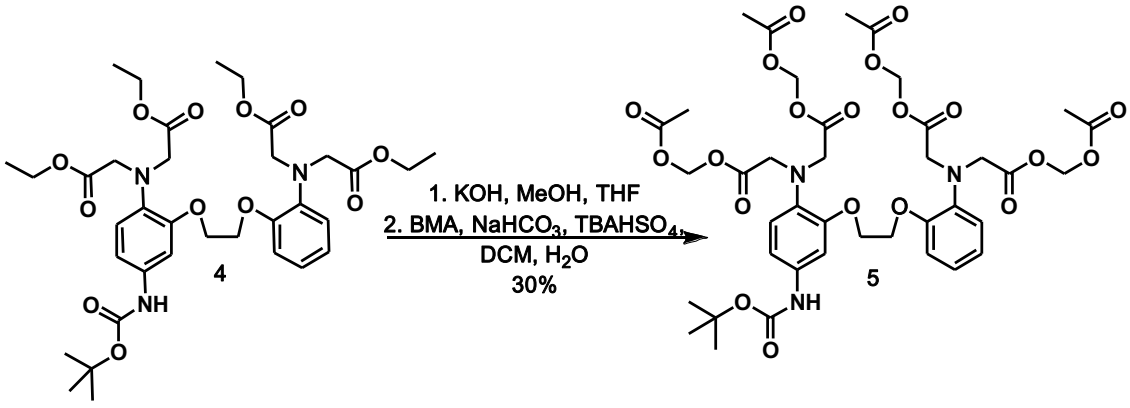

To a solution of **4** (390 mg, 0.55 mmol) in 1:1 THF/MeOH (20 mL) was added 1 M KOH (7.54 mL, 7.54 mmol, 16 equiv.). The solution was allowed to stir overnight. The solution was concentrated under reduced pressure, and re-dissolved in 10 mL of 1:1 DCM:H_2O. To this solution, bromomethyl acetate (BMA, 739 μL, 7.54 mmol, 16 equiv.), $TBAHSO_4$ (640 mg, 1.89 mmol, 4 equiv.), and $NaHCO_3$ (781 mg, 5.65 mmol, 12 equiv.) were added.

The reaction was stirred vigorously overnight. The organics were extracted into CH_2Cl_2 (3x 100 mL), dried over $NaSO_4$, and concentrated under reduced pressure. Silica gel column chromatography (0-30% EtOAc:Hexanes, linear gradient) yielded 146 mg (30%) of **5**. ^{1}H NMR (400 MHz, Chloroform-*d*) δ 7.83 (d, *J* = 8.1 Hz, 2H), 7.57 (t, *J* = 7.8 Hz, 2H), 7.23 (d, *J* = 1.2 Hz, 1H), 7.08 (t, *J* = 7.8 Hz, 2H), 5.79 (s, 8H), 4.54 (s, 4H), 3.83 (s, , 8H), 2.14 (s, 12H), 1.52 (s, 9H). ESI-MS calculated for $C_{39}H_{49}N_3O_{20}$ [M+H]+ 880.29, found 880.1

*Synthesis of **2:***

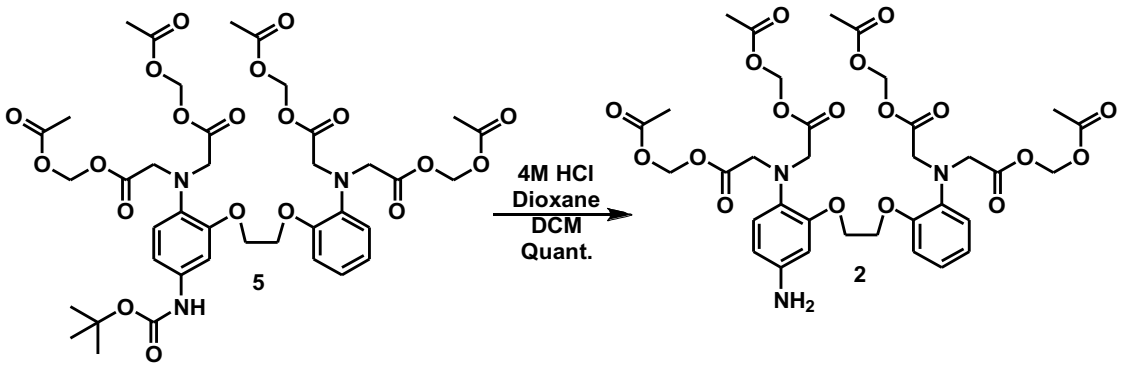

To a solution of **5** (146 mg, 0.166 mmol) in anhydrous dioxane, 4N HCl-dioxane (anhydrous, Sigma-Aldrich 345547) (200 μL) was added and stirred for 1 h at rt. Then excess reagent and solvent were removed under vacuum. The resulting white solid was stirred in anhydrous Et_2O (5 mL) for 2 h and the solid was collected by filtration. The reaction provides **2** in quantitative yield**.** ^{1}H NMR (400 MHz, Chloroform-*d*) δ 7.83 (d, *J* = 8.1 Hz, 2H), 7.57 (t, *J* = 7.8 Hz, 2H), 7.23 (d, *J* = 1.2 Hz, 1H), 7.08 (t, *J* = 7.8 Hz, 2H), 5.79 (s, 8H), 4.54 (s, 4H), 3.83 (s, 8H), 2.14 (s, 12H).

3.2 Rhodol fluorophore synthesis

The rhodol fluorophore was synthesized from isomerically pure acetylated 6'-carboxy-fluorescein. The pendant carboxylate is protected as an *t*-butyl ester to facilitate the selective protection of one phenolic oxygen on the xanthene core as the methoxymethyl (MOM) ether.[23,24] The remaining phenolic oxygen is converted to a trifluoromethanesulfonate (triflate). The triflated fluorescein is then converted to a rhodol via palladium-catalyzed carbon-nitrogen bond formation with a pyrrolidine.[25] The pyrrolidine was selected as previous syntheses of pyrrolidine-rhodol proceeded with high yields (>80%), and resulted large extinction coefficients, and good quantum yields.[24]

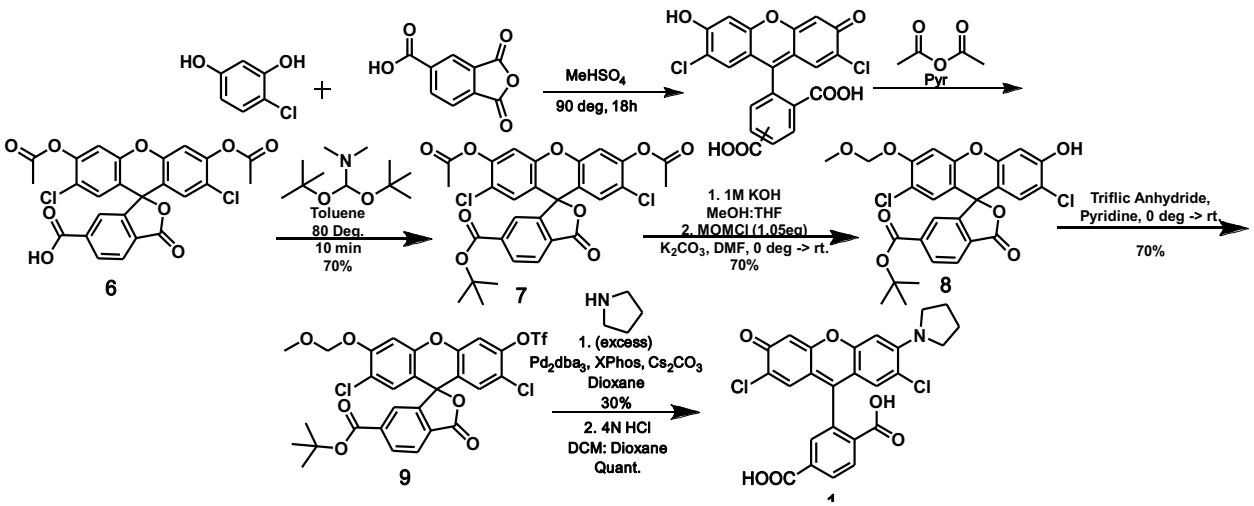

Scheme 3. Synthesis of 6'-carboxy-pyrrolidine rhodol (1).

Synthesis of ***7*****:**

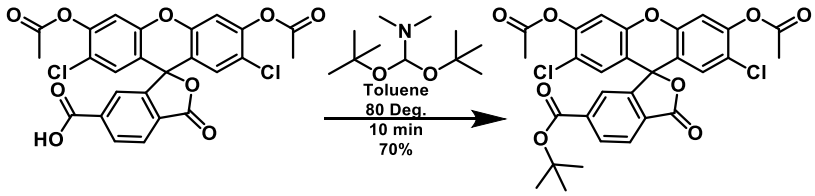

A suspension of **6** (synthesized according to the procedure reported here[22]; 1.73 g, 3.26 mmol) in toluene (6.5 mL) was heated to 80 °C, and N,N-dimethylformamide di-tert-butyl acetal (4.69 mL, 19.6 mmol, 6.0 equiv.) was added dropwise. The reaction was stirred at 80 °C for 10 min, during which time the colorless suspension became a red solution. After cooling the reaction to room temperature, it was diluted with saturated $NaHCO_3$ and extracted with CH_2Cl_2 (2× 100 mL). The combined organic extracts were dried (MgSO4), filtered, and evaporated. Flash chromatography (dry load with silica gel, 0–20% EtOAc/hexanes) provided **7** as a white solid (1.25 g, 66%). ^{1}H NMR (400 MHz, Methanol-d_4) δ 8.33 (d, J = 8.1 Hz, 1H), 8.18 – 8.01 (m, 1H), 7.79 (s, 1H), 6.85 (s, 2H), 6.67 (s, 2H), 2.18 (s, 6H), 1.49 (s, 9H). ESI-MS calculated for $C_{29}H_{22}Cl_2O_9$ [M+H]+ 585.071, found 585.1

Synthesis of ***9:***

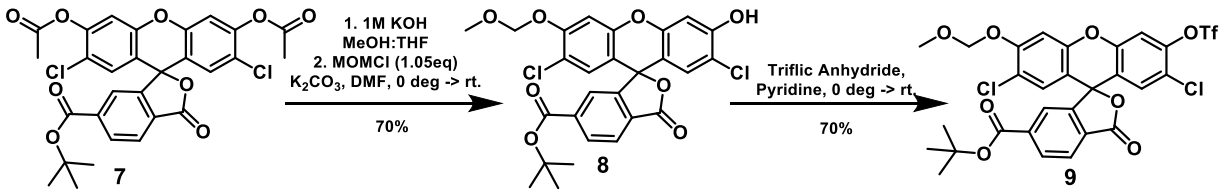

To a solution of **7** (2.10 g, 3.60 mmol) in 1:1 THF/MeOH (10 mL) was added 1 M KOH (8.64 mL, 8.64 mmol, 2.4 equiv.). The reaction was stirred at room temperature overnight.

The resulting orange suspension was concentrated in vacuo to provide a red solid. The solid was suspended in dimethylformamide (25 mL) and cooled to 0 °C. DIPEA (4.01 mL, 23 mmol, 6.5 equiv.) and chloromethyl methyl ether (1.89 mL, 3.96 mmol, 1.10 equiv., 2.1M std. solution in toluene, generated *in situ,* were added, and the ice bath was removed.[27] The reaction was stirred at room temperature for 5 h. It was subsequently diluted with saturated ammonium chloride solution and extracted with dichloromethane (2× 100 mL). The combined organic extracts were washed with brine, dried ($MgSO_4$), filtered, and evaporated. Silica gel chromatography (0–25% EtOAc/hexanes, linear gradient) yielded 1.48 g (70%) of **8** as a yellow solid. The compound was discovered to not be stable for more than 30 min. There was a distinct color change from yellow solid to red solid. Therefore, the product was carried directly on to the next step without characterization. A solution of **8** (1.48 g, 2.72 mmol) in dichloromethane (25 mL) was cooled to 0 °C. Pyridine (1.67 mL, 20.4 mmol, 7.5 equiv.) and trifluoromethanesulfonic anhydride (1.71 mL, 10.2 mmol, 3.75 equiv.) were added, and the ice bath was removed. The reaction was stirred at room temperature for 5 h. It was subsequently diluted with water and extracted with dichloromethane (2× 100 mL). The combined organic extracts were washed with brine, dried ($MgSO_4$), filtered, and evaporated. Silica gel chromatography (0–25% EtOAc/hexanes, linear gradient) yielded 1.29 g (70%) of **8** as a white solid. ^{1}H NMR (400 MHz, Methanol-d_4) δ 8.33 (d, J = 8.0 Hz, 1H), 8.10 (d, J = 8.1 Hz, 1H), 7.78 (s, 1H), 6.85 (s, 2H), 6.67 (s, 2H), 4.52 (s, 2H), 3.31 (s, 3H), 1.49 (s, 9H). ESI-MS calculated for $C_{28}H_{21}Cl_2F_3O_{10}S$ [M+H]+ 677.02, found 677.0.

*Synthesis of **10**:*

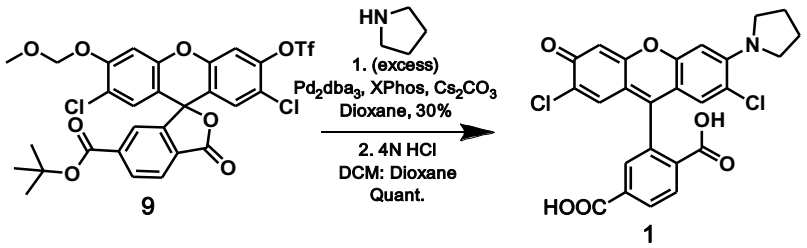

A vial was charged with **9** (189 mg, 0.278 mmol), $Pd_2(dba)_3$ (12.8 mg, 0.014 mmol, 0.05 equiv.), XPhos (20mg, 0.042 mmol, 0.15 equiv.), and Cs_2CO_3 (127 mg, 0.39 mmol, 1.4 equiv.). The vial was sealed and evacuated/backfilled with nitrogen (3×). Dioxane (0.435 mL) was added, and the reaction was flushed again with nitrogen (3×). Following the addition of pyrollidine (0.6M in dioxane) (2.322 mL, 1.39 mmol, 5 equiv.), the reaction was stirred at 80 °C for 4 h. It was then cooled to room temperature, deposited onto Celite, and concentrated to dryness. Purification by silica gel chromatography (0–35% EtOAc/hexanes, linear gradient; dry load with Celite) afforded the pyrrolidinyl rhodol with the MOM-ether and t-butyl-ester as an intermediate (64 mg, 45%) as an off-white solid. The intermediate (64 mg, 0.125 mmol) was taken up in DCM (1 mL), and 4N HCl in dioxane (50 µL, 2 mmol, 15 equiv.) was added. After stirring the reaction at room temperature for 6 h, the organics were washed with 9:1 DCM:Isopropanol (10 ml x 2), dried over Mg_2SO_4, and concentrated to dryness. The filmy solid was triturated in Et_2O to yield 42 mg (45%) of 20 as a bright orange solid. ^{1}H NMR (400 MHz, Methanol-d_4) δ 8.26

(d, *J* = 8.0 Hz, 1H), 8.06 (d, *J* = 8.0 Hz, 1H), 7.73 (s, 1H), 6.80 (s, 2H), 6.73 (s, 2H), 3.19 (s, 4H), 2.00 – 1.87 (m, 4H).

*Synthesis of **RSC-AM:***

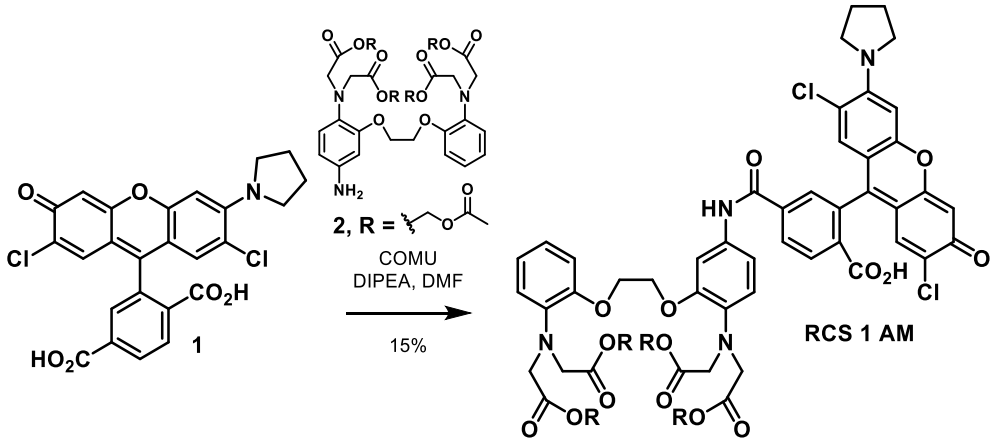

A 4-mL vial was charged with **1** (20 mg, 0.041 mmol, 1 equiv.), DIPEA (37 μL, 0.213 mmol, 5 equiv.), and 23 mg of **2** (0.038 mmol, 0.9 equiv.) in 1 mL DMF and cooled to 0ºC. COMU (0.45M in DMF, 473 μL, 0.213 mmol, 5 equiv.) was added at 0ºC, and the reaction was allowed to warm to room temperature overnight. The organics were concentrated under reduced pressure, dissolved in 1 mL MeOH, and deposited on a 1000 μm preparatory TLC plate (15% MeOH:DCM). After concentrating under reduced pressure, **RCS-1 AM** (7 mg, 15%) was isolated as a reddish powder. ^{1}H NMR (400 MHz, DMSO-d_6) δ 8.64 (s, 1H), 8.37 (d, *J* = 8.0 Hz, 1H), 7.63 (d, *J* = 8.1 Hz, 1H), 7.57 – 7.49 (m, 3H), 7.34 (d, *J* = 9.3 Hz, 1H), 7.03 (dd, *J* = 14.4, 9.0 Hz, 3H), 6.94 – 6.70 (m, 4H), 5.59 (d, *J* = 2.0 Hz, 8H), 4.18 (s, 8H), 2.36 (s, 6H), 2.03 (d, *J* = 5.9 Hz, 12H). ESI-MS calculated for $C_{59}H_{56}Cl_2N_4O_{23}$ [M^+] 1258.3, found 1258.2. High resolution ESI-MS calculated for 1258.2712, found: 1258.2977.

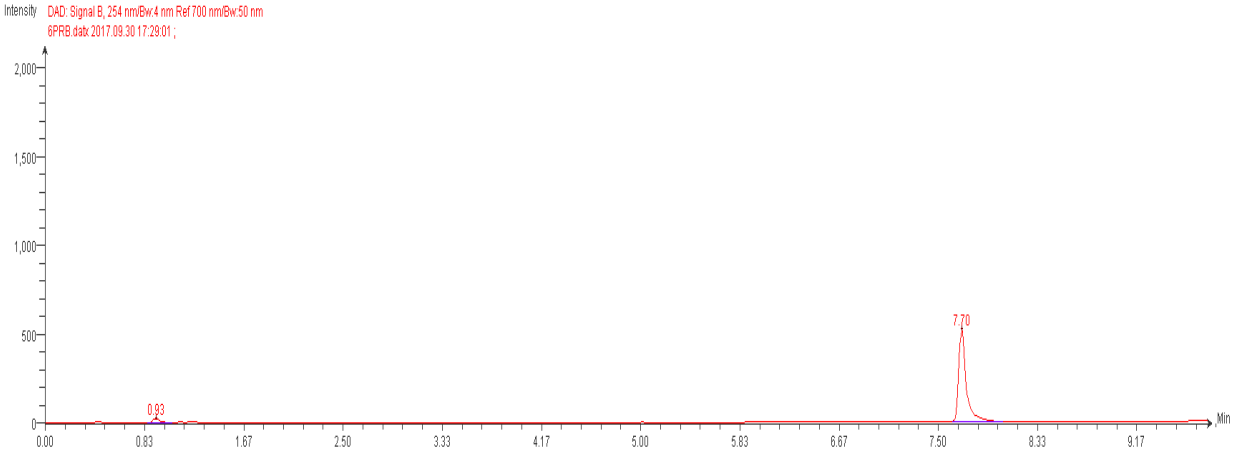

HPLC trace of RCS-1 AM.

4 Characterization

4.1 *In-vitro* characterization

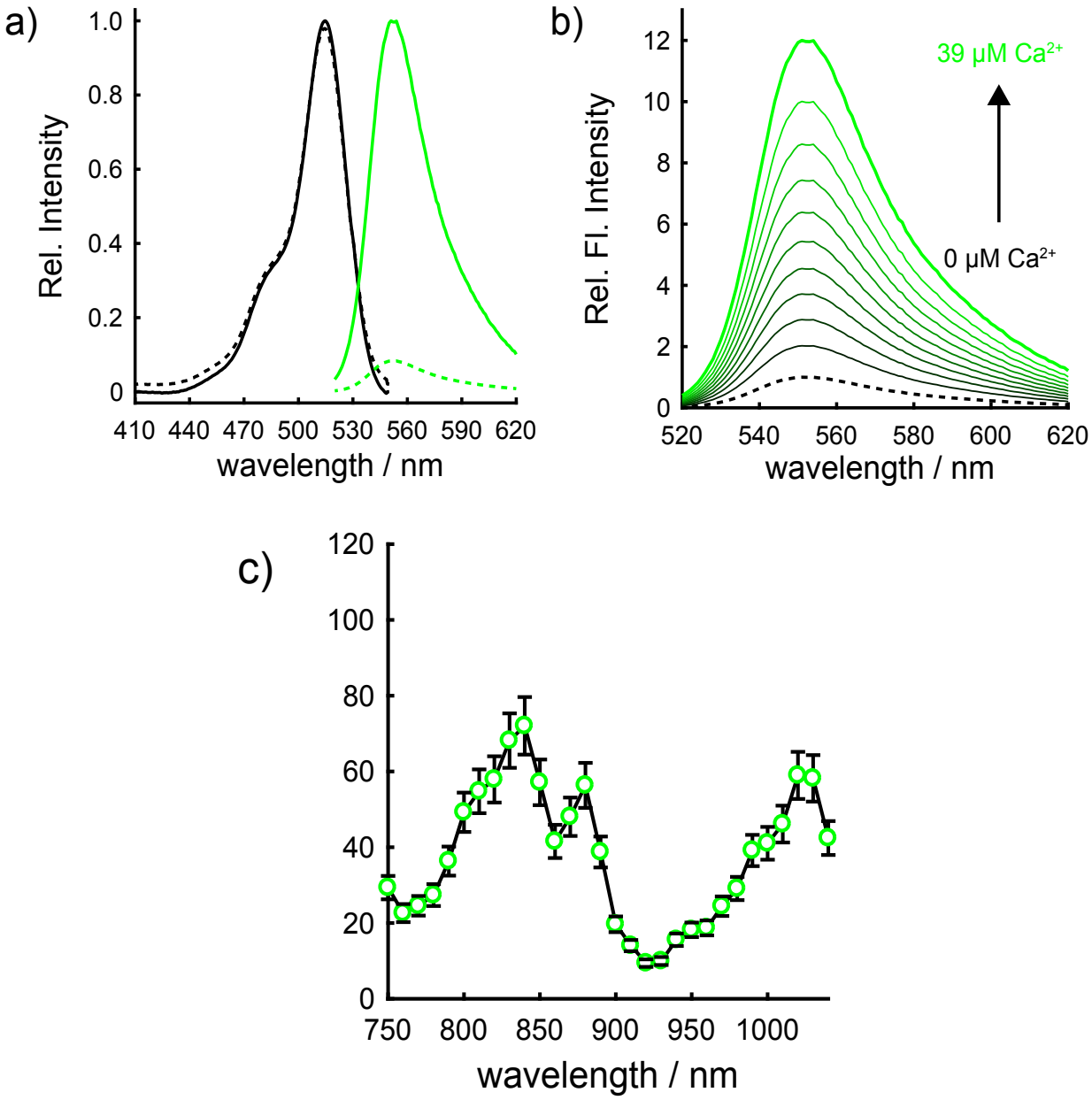

Figure 1. Spectroscopy characterization of rhodol Ca^{2+} sensor 1. a) Absorbance spectrum of rhodol Ca^{2+} sensor 1 (10 µM) in the absence (black dotted line) and presence (black solid line) of 39 µM Ca^{2+}. Fluorescence emission spectra of rhodol Ca^{2+} sensor 1 (10 µM) in the absence (green dotted line) and presence (green solid line) of 39 µM Ca^{2+}. b) Ca^{2+} titration of rhodol Ca^{2+} sensor 1. The fluorescence emission spectra of rhodol Ca^{2+} sensor 1 was recorded at increasing concentrations of Ca^{2+} from 0 µM to 39 µM, with intermediate concentrations of 17 nM, 38 nM, 65 nM, 100 nM, 150 nM, 225 nM, 351 nM, 602 nM, and 1.35 µM. c) Two-photon absorption spectra of rhodol Ca^{2+} sensor 1 with Ca^{2+} (39 µM). Error bars are ± standard deviation for n = 3 separate determinations.

RCS-1 shows excitation and emission profiles characteristic of substituted rhodols, with a λ_{max} absorption at 520 nm and emission maximum centered at 551 nm (Figure 1a). Addition of Ca^{2+} results in an increase in fluorescence intensity (Figure 1a). The quantum yield for RCS-1 is Ca^{2+}-dependent. In the absence of Ca^{2+}, Φ_{551} is 0.073; in the presence of saturating levels of Ca^{2+} (39 μM), Φ_{551} is 0.73. There is no Ca^{2+}-dependent change in absorption (Figure 1a). Titration with Ca^{2+} reveals a dissociation constant of 240 nM (±6 nM, S.E.M., *n* = 3 separate determinations), which is well-matched to the K_d reported for CGB-1 (190 nM) (Figure 1b).[6,13] In our hands, we determined a K_d of 180 nM for CGB-1 (±5 nM, S.E.M., *n* = 3 separate determinations), indicating a good match between RCS-1 and CGB-1. RCS-1 possesses a large dynamic range in response to Ca^{2+}, exhibiting a 10-fold increase (±1, S.E.M., *n* = 3) in fluorescence intensity upon Ca^{2+} binding (Figure 1b), again, well-matched to the dynamic range for CGB-1 (which we measured as a 13-fold increase).[6] We measured the two-photon excitation spectrum of RCS-1. Using rhodamine B as a standard, we determined the two-photon absorption cross-section (σ_{TPA}) of RCS-1.[15,19] RCS-1 displays a σ_{TPA} maximum at 840 nm, with a valu e of 72 GM. This is 3-fold larger than the 24 GM σ_{TPA} value we determined for CGB-1 (approximately 24 GM at 840 nm).[15]

4.2 Characterization in HeLa cells

The combination of large turn-on response to Ca^{2+} binding, nanomolar dissociation constant, and strong two-photon absorption cross-section suggests RCS-1 will be useful for monitoring Ca^{2+} transients in living cells. To investigate the ability of RCS-1 to report on Ca^{2+} fluxes in live cells, we utilized the tetra-AM ester version of RCS-1. Masking polar carboxylates with AM esters enable uptake anionic BAPTA-containing indicators into cells.[25] Cellular esterases remove the AM esters, liberating the Ca^{2+}-responsive fluorophore. Bath application of RCS-1 to HeLa cells (1.7 μM, with Pluronic F-127, 0.01%) resulted in bright intracellular fluorescence, as determined by laser scanning confocal microscopy (**Figure 2a**). Stimulation of RCS-1-loaded cells with histamine (5 μM) resulted in the induction of periodic Ca^{2+} oscillations that were readily observable with RCS-1 fluorescence (**Figure 2b**). Gratifyingly, Ca^{2+} transients could be monitored using infrared, two-photon microscopy, with excitation provided at 840 nm (**Figure 2c and d**).

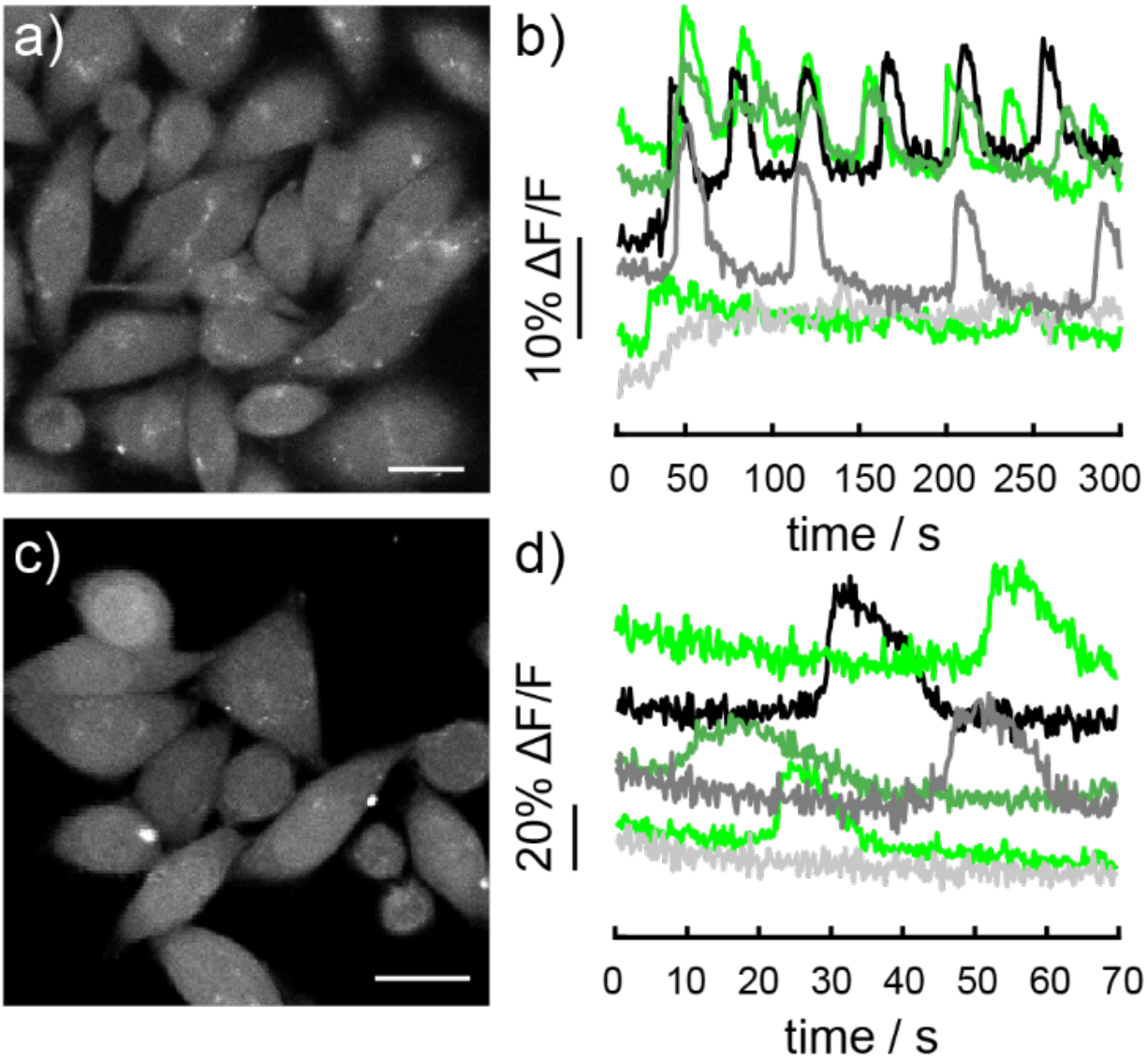

Figure 2. Live-cell imaging of histamine-evoked Ca^{2+} fluctuations with rhodol Ca^{2+} sensor 1. a) Confocal fluorescence microscopy images (one-photon) of HeLa cells incubated with rhodol Ca^{2+} sensor tetra-AM (1.7 μM). Scale bar is 20 μm. b) Quantification of intracellular [Ca^{2+}] fluctuations measured in response to stimulation with histamine (5 μM). c) Two photon laser scanning fluorescence microscopy images of HeLa cells incubated with rhodol Ca^{2+} sensor tetra-AM (1.7 μM). Scale bar is 20 μm. d) Quantification of intracellular [Ca^{2+}] fluctuations measured in response to stimulation with histamine (5 μM).

4.3 Characterization in Cultured Neurons

Building on these observations, we next determined whether RCS-1 could report on neuronal activity in cultured mammalian hippocampal neurons. Incubation of RCS-1 (1.7 μM, with Pluronic F-127, 0.01%) with cultured rat hippocampal neurons resulted in bright cellular fluorescence, as determined by widefield epifluorescence microscopy (**Figure 3a**). RCS-1 can report on spontaneous activity in hippocampal cultures (**Figure 3b**). Action potentials evoked by field stimulation give clear increases in fluorescence

(**Figure S1**). Importantly, RCS-1 can also report on spontaneous activity in cultured neurons when imaged under 2P illumination, using 840 nm excitation light (**Figure 3c and d**).

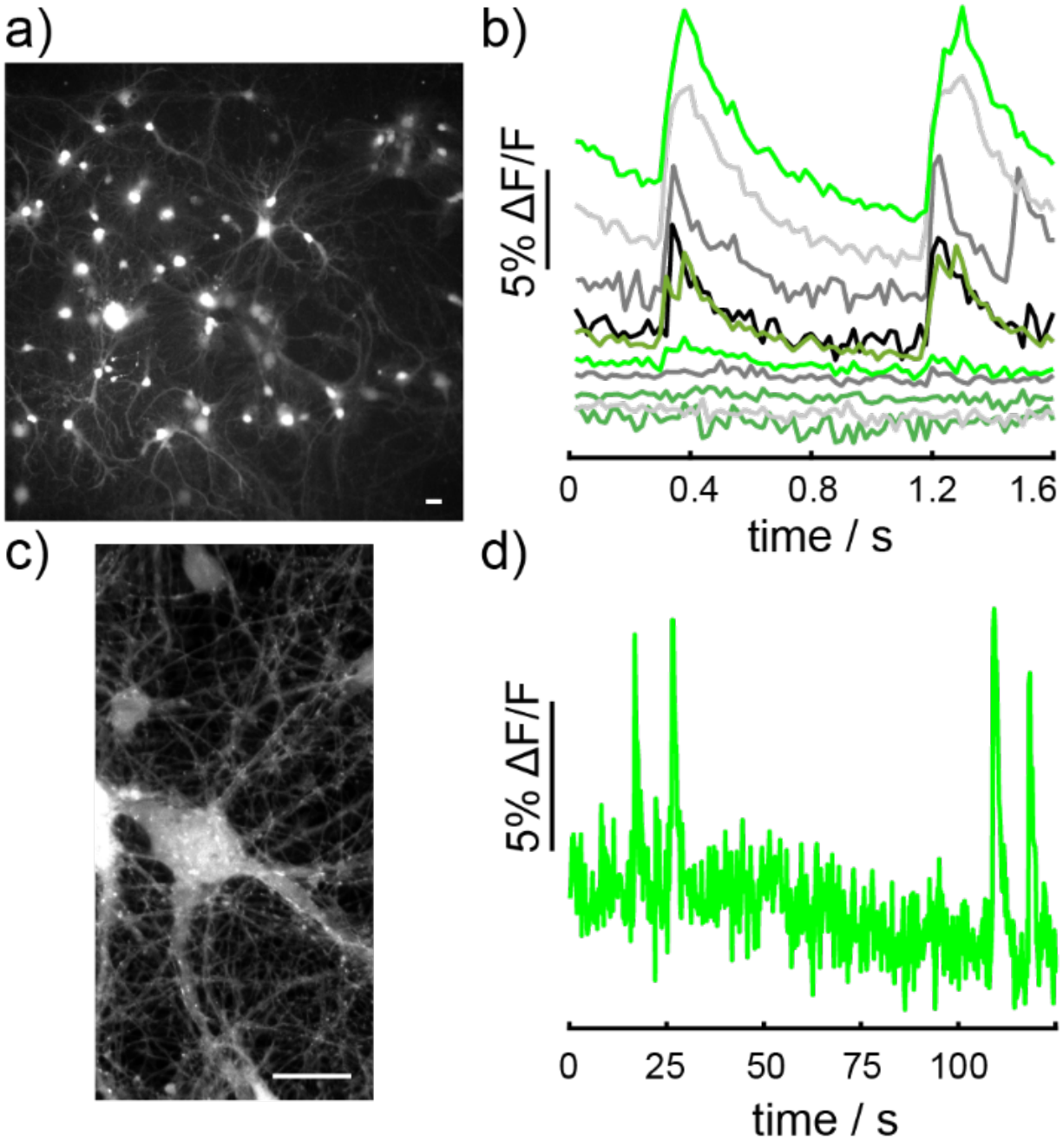

Figure 3. Visualization of Ca^{2+} transients in rat hippocampal neurons using rhodol Ca^{2+} sensor 1. a) Widefield fluorescence micrograph of cultured rat hippocampal neurons incubated with rhodol Ca^{2+} sensor 1 tetra AM ester (1.7 μM). Scale bar is 20 μm. b) Relative changes rhodol Ca^{2+} sensor 1 fluorescence vs. time for neurons in panel a. c) Two-photon laser scanning microscopy image of rat hippocampal neuron stained with rhodol Ca^{2+} sensor 1 tetra AM ester (1.7 μM). Scale bar is 20 μM. d) Intracellular Ca^{2+} transients recorded as relative changes in rhodol Ca^{2+} sensor 1 fluorescence vs. time for the neuron in panel c.

In summary, we present the design, synthesis, and application of RCS-1, a rhodol-based fluorescent indicator for Ca^{2+}. The large turn-on response to Ca^{2+}, high Ca^{2+} affinity, and good two-photon cross-section of RCS-1, coupled with the ability to monitor spontaneous activity in cultured neurons, make it a promising candidate for monitoring [Ca^{2+}] transients in the context of neurobiology and beyond.

5 Supplemental Information

5.1 General method for chemical synthesis and characterization

Chemical reagents and solvents (dry) were purchased from commercial suppliers and used without further purification. Thin layer chromatography (TLC) (Silicycle, F254, 250 μm) and preparative thin layer chromatography (PTLC) (Silicycle, F254, 1000 μm) was performed on glass backed plates pre-coated with silica gel and were visualized by fluorescence quenching under UV light. Flash column chromatography was performed on Silicycle Silica Flash F60 (230–400 Mesh) using a forced flow of air at 0.5–1.0 bar. NMR spectra were measured on Bruker AVB-400 MHz, 100 MHz, and AVQ-400 MHz, 100 MHz. Chemical shifts are expressed in parts per million (ppm) and are referenced to $CDCl_3$ (7.26 ppm), MeOD (3.31 ppm), or DMSO (2.50 ppm). Coupling constants are reported as Hertz (Hz). Splitting patterns are indicated as follows: s, singlet; d, doublet; t, triplet; q, quartet; dd, doublet of doublet; m, multiplet. High performance liquid chromatography (HPLC) and low resolution ESI Mass Spectrometry were performed on an Agilent Infinity 1200 analytical instrument coupled to an Advion CMS-L ESI mass spectrometer. The column used for the analytical HPLC was Phenomenex Luna 5 μm C18(2) (4.6 mm I.D. × 150 mm) with a flow rate of 1.0 mL/min. The mobile phases were MQ-H_2O with 0.05% formic acid (eluent A) and HPLC grade acetonitrile with 0.05% formic acid (eluent B). Signals were monitored at 254 nm and 490 nm over 12 min with a gradient of 10-100% eluent B. The column used for semi-preparative HPLC was Phenomenex Luna 5 μm C18(2) (10 mm I.D. x 150 mm) with a flow rate of 5.0 mL/min. The mobile phases were MQ-H_2O with 0.05% formic acid (eluent A) and HPLC grade acetonitrile with 0.05% formic acid (eluent B). Signals were monitored at 254 over 12 min with a gradient of 10-100% eluent B.

5.2 Spectroscopic studies

Stock solutions of RSC-AM were prepared in DMSO (1-5 mM) and diluted with PBS (10 mM KH_2PO_4, 30 mM $Na_2HPO_4 \cdot 7H_2O$, 1.55 M NaCl, pH 7.2). UV-Vis absorbance and fluorescence spectra were recorded using a Shimadzu 2501 Spectrophotometer (Shimadzu) and a Quantamaster Master 4 L-format scanning spectrofluorometer (Photon Technologies International). The fluorometer is equipped with an LPS-220B 75-W xenon lamp and power supply, A-1010B lamp housing with integrated igniter, switchable 814 photon-counting/analog photomultiplier detection unit, and MD5020 motor driver. Samples were measured in 1-cm path length quartz cuvettes (Starna. UV-Vis absorbance and fluorescence spectra were recorded using a Shimadzu 2501 Spectrophotometer (Shimadzu) and a Quantamaster Master 4 L-format scanning spectrofluorometer (Photon

Technologies International). The fluorometer is equipped with an LPS-220B 75-W xenon lamp and power supply, A-1010B lamp housing with integrated igniter, switchable 814 photon-counting/analog photomultiplier detection unit, and MD5020 motor driver. Samples were measured in 1-cm path length quartz cuvettes (Starna Cells).

Determining the dissociation constants (K_d) of RCS-1[28]

Using the spectrofluorometer, the dissociation constant (K_d) of RSC-1 was calculated from a plot generated by scanning the emission of the indicator in the presence of 11 different Ca^{2+} concentrations.

Stock solutions of 500 mL of 10 mM K_2EGTA and 500 mL of 10 mM CaEGTA were made. Both solutions contain 100 mM KCl and 30 mM MOPS, pH 7.2 and are prepared in deionized water. These stock solutions were used to prepare buffers with free Ca^{2+} concentrations ranging from 0 μM to 39 μM.

A stock solution of 1 mM RSC-1 (salt form) in DMSO was prepared. A 20 μL aliquot of stock RSC-1 solution was added to 2 mL of Zero Free Calcium Buffer (10 mM, K_2EGTA) to give a sensor concentration of 10 μM (zero Ca^{2+} sample). High Ca^{2+} sample was prepared by diluting 60 μL aliquot of stock RSC-1 solution into 6 mL of 39 μM Free Calcium buffer (10 mM CaEGTA).

Fluorescence spectrum of 2 mL of zero Ca^{2+} sample was recorded by exciting the sample at 515 nm and recording the emission from 520 nm to 620 nm. The next solution was prepared by removing 0.2 mL from the sample and replacing with an equal aliquot (0.2 mL) of the high Ca^{2+} sample. The new CaEGTA concentration was 1 mM and $[Ca^{2+}]_{free}$ to about 0.017 μM with no change in the concentration of the dye or of the total EGTA. The equation for determining the volume to remove and replace is:

$$Volume\ to\ replace = (Sample\ Volume)\left(\frac{b-a}{10-a}\right)$$ [Equation SI 1]

where a = current mM CaEGTA, b = desired mM CaEGTA, c = mM CaEGTA in high Ca^{2+} sample (10 mM CaEGTA). The spectrum was scanned again, and another aliquot (this time 0.22mL) was removed and replaced with 0.22 mL of the high Ca^{2+} sample. The new $[Ca^{2+}]_{free}$ was about 0.038 μM. RSC-1 solutions containing 3, 4, 5, 6, 7, 8, and 9 mM CaEGTA were prepared and the spectrum recorded in the same way, always starting with the solution used for the previous spectrum (Table 1). For the 10 mM CaEGTA spectrum, the previous measurement sample was discarded and replaced it with 2 mL from the high Ca2+ sample.

Table 1: Reciprocal dilutions used to arrive at the free [Ca^{2+}]

CaEGTA	$[CA^{2+}]_{free}$	Volume to remove/replace (2 mL sample)
0 mM	0 μM	zero Ca^{2+} sample
1 mM	0.017 μM	0.200 mL
2 mM	0.038 μM	0.222 mL
3 mM	0.065 μM	0.250 mL
4 mM	0.100 μM	0.286 mL
5 mM	0.150 μM	0.333 mL
6 mM	0.225 μM	0.400 mL
7 mM	0.351 μM	0.500 mL
8 mM	0.602 μM	0.667 mL
9 mM	1.35 μM	1.000 mL
10 mM	39 μM	high Ca^{2+} sample

After the spectra were recorded, the data from emission at a single wavelength (547 nm for RSC-1) is plotted as the log of the $[Ca^{2+}]_{free}$ (x-axis) versus the $\log\frac{(F-F_{\min})}{(F_{max}-F)}$ (y-axis). This double log plot gives an x-intercept that is the log of K_d of RSC-1 expressed in molarity. From this measurement, the K_d value for RSC-1 were determined on three separate occasions to be 240 ± 11 nM. An example plot is shown in Figure S1.

5.3 Cell culture

All animal procedures were approved by the UC Berkeley Animal Care and Use Committees and conformed to the NIH Guide for the Care and Use and Laboratory Animals and the Public Health Policy.
HeLa cells (75% confluent) were obtained from the UC Berkeley Tissue Culture Facility.
Hippocampi were dissected from embryonic day 18 Sprague Dawley rats (Charles River Laboratory) in cold sterile HBSS (zero Ca^{2+}, zero Mg^{2+}). All dissection products were supplied by Invitrogen, unless otherwise stated. Hippocampal tissue was treated with trypsin (2.5%) for 15 min at 37 °C. The tissue was triturated using fire polished Pasteur pipettes, in minimum essential media (MEM) supplemented with 5% fetal bovine serum (FBS; Thermo Scientific), 2% B-27, 2% 1M D-glucose (Fisher Scientific) and 1% glutamax. The dissociated cells were plated onto 12 mm diameter coverslips (Fisher Scientific) pre-treated with PDL (as above) at a density of 30-40,000 cells per coverslip in MEM supplemented media (as above). Neurons were maintained at 37 °C in a humidified incubator with 5 % CO_2. At 1 day in vitro (DIV) half of the MEM supplemented media was removed and replaced with Neurobasal media containing 2% B-27 supplement and 1% glutamax. Functional imaging was performed on mature neurons 12-20 DIV, except electrophysiological experiments which were performed on 12-18 DIV neurons.
Unless stated otherwise, for loading of hippocampal neurons, RSC-AM was diluted in DMSO to 1 mM, and then diluted 1:400 in HBSS. All imaging experiments were performed in HBSS.

5.4 Imaging parameters

Epifluorescence imaging was performed on an AxioExaminer Z-1 (Zeiss) equipped with a Spectra-X Light engine LED light (Lumencor), controlled with Slidebook (v6, Intelligent Imaging Innovations). Co-incident excitation with multiple LEDs was controlled by Lumencor software triggered through a Digidata 1332A digitizer and pCLAMP 10 software (Molecular Devices). Images were acquired with either a W-Plan-Apo 20x/1.0 water objective (20x; Zeiss). Images were focused onto either an OrcaFlash4.0 sCMOS camera (sCMOS; Hamamatsu) or an eVolve 128 EMCCD camera (EMCCD; Photometrix). More detailed imaging information for each experimental application is expanded below.

Histamine derived Calcium Oscillations in HeLa cells

HeLa cells were incubated with a HBSS solution (Gibco) containing RCS-AM (1.67 μM) or CGB-AM (1.67 μM) and 0.01% Pluronic F-127 at 37°C for 30 min prior to transfer to fresh HBSS (no dye) for imaging. Microscopic images were acquired with a W-Plan-Apo 20x/1.0 water objective (Zeiss) and OrcaFlash4.0 sCMOS camera (Hamamatsu). For RCS-AM and CGB-AM images, the excitation light was delivered from a LED (9.72 W/cm^2; 50 ms exposure time) at 475/34 (bandpass) nm and emission was collected with a quadruple emission filter (430/32, 508/14, 586/30, 708/98 nm; "QUAD") after passing through a quadruple dichroic mirror (432/38, 509/22, 586/40, 654 nm LP). Histamine was added as a 3x stock in a single 1 mL addition to the 2 mL of bath solution to give a final concentration of 5 μM. Images were acquired at a rate of 10 Hz over a five-minute period. Acquisition analysis settings were maintained through the course of the experiment. Timeseries were acquired for 300 time points, at 100 ms exposure, with 0 ms interval.

Evoked activity in neurons

Functional imaging of the RSC-AM and CGB-AM in neurons was performed using a 20x objective paired with image capture from the EMCCD camera at a sampling rate of 20 Hz. RSC-AM and CGB-AM were excited using the 475 nm LED with an intensity of 9.73 W/cm^2. Neurons were incubated with a HBSS solution (Gibco) containing RCS-AM (1.67 μM) or CGB-AM (1.67 μM) and 0.01% Pluronic F-127 at 37°C for 30 min prior to transfer to fresh HBSS (no dye) for imaging. For evoked activity, emission was collected with the QUAD filter and dichroic (see above). Neurons were stimulated by delivering 1-2 ms, 80 V voltage pulses at 20 Hz. Single, 2, 10, 15, and 20 pulse stimulations were delivered, with 50 ms of no stimulation delivered at the beginning of the time course of each experiment. 1 to 20 AP stimuli were pseudo-randomized. Timeseries were acquired for 80 frames, at 50 ms exposure, with 0 ms interval.

Imaging spontaneous activity of neurons

Imaging experiments looking at spontaneous activity from many (>5) neurons were performed without extracellular stimulation. RSC-AM was excited using the 475 nm LED with an intensity of 1.73-3.07 W/cm^2 and emission was collected with a QUAD filter and dichroic (see above). Images were binned 4x4 to allow sampling rates of 20 Hz. TTX was

added as a 3x stock in a single 1 mL addition to the 2 mL of bath solution to give a final concentration of 1 μM. Timeseries were acquired for 80 frames, at 50 ms exposure, with 0 ms interval.

Imaging with 2-Photon excitation

HeLa cells and neurons were incubated with a HBSS solution (Gibco) containing RCS-AM (1.67 μM) or CGB-AM (1.67 μM) and 0.01% Pluronic F-127 at 37°C for 30 min prior to transfer to fresh HBSS (no dye) for imaging. RSC-AM and CGB-AM were excited at 840 nm and the emission was collected from 493-603 nm.
Confocal imaging was performed with a Zeiss LSM 880 NLO AxioExaminer equipped with a Diode 405 nm laser line, Argon 458, 488, and 514 laser lines, and Coherent Chameleon 690-1040 nm (2-photon imaging). Images were acquired using a W-Plan-Apo 20x/1.0 DIC objective and a Zeiss Airyscan detector. Images acquired with a scan time of 200 ms.

Measurement of the 2-Photon cross-section

Two-photon absorbance cross section (σ_{TPA}) measurements were obtained by comparison to rhodamine b standards, according to the following equation, as previously reported.[15,19,29]

$$\sigma_{TPA_{RSC1}} = \frac{\eta_{2_{std}}\sigma_{TPA_{std}}}{\eta_{2_{RSC1}}}\left(\frac{F(t)_{new}}{F(t)_{std}}\right) \quad \text{[Equation SI 2]}$$

We used values of η_2 = 0.75 for CGB-1, η_2 = 0.73 for RSC-1, and the following table of values for rhodamine b.[15,30]

Table 2. Rhodamine b two photon cross section values.

Wavelength (nm)	Rhodamine B σ_{TPE} ($\sigma_{TPA} \times \eta_2$)	Wavelength (nm)	Rhodamine B σ_{TPE} ($\sigma_{TPA} \times \eta_2$)
700	280	**880**	38
710	176	**890**	22
720	109	**900**	11
730	78	**910**	8
740	48	**920**	6
750	55	**930**	6
760	68	**940**	10
770	92	**950**	12
780	108	**960**	13
790	136	**970**	16
800	153	**980**	19
810	164	**990**	26
820	177	**1000**	27
830	204	**1010**	31
840	195	**1020**	39
850	128	**1030**	36
860	66	**1040**	26
870	52	**1050**	20

5.5 Image analysis

Analysis of histamine driven calcium oscillations in Hela cells was performed using ImageJ (FIJI). Briefly, a region of interest (ROI) was drawn around the cell body and the fluorescence measured over 300 timepoints. For analysis of RSC-AM spontaneous activity in neurons, regions of interest encompassing cell bodies (all of approximately the same size) were drawn in ImageJ and the mean fluorescence intensity for each frame extracted. $\Delta F/F$ values were calculated by first subtracting a mean background value from all raw fluorescence frames. A baseline fluorescence value (F_{base}) is calculated either from the first several (10-20) frames of the experiment for evoked activity, and was subtracted from each timepoint of the trace to yield a ΔF trace. The ΔF was then divided by F_{base} to give $\Delta F/F$ traces.

Table 3. Selected Properties of CGB-1 and RCS-1.

Dye	λ_{max} Excitation	λ_{max} Emission	K_d	Φ High Ca^{2+}	Φ Low Ca^{2+}	2P cross section (GM) (at 840 nm)
CGB-1	492 nm	523 nm	190 nM	0.75	0.069	24
RCS-1	515 nm	551 nm	240 nM	0.73	0.073	72

6. Supplemental Figures

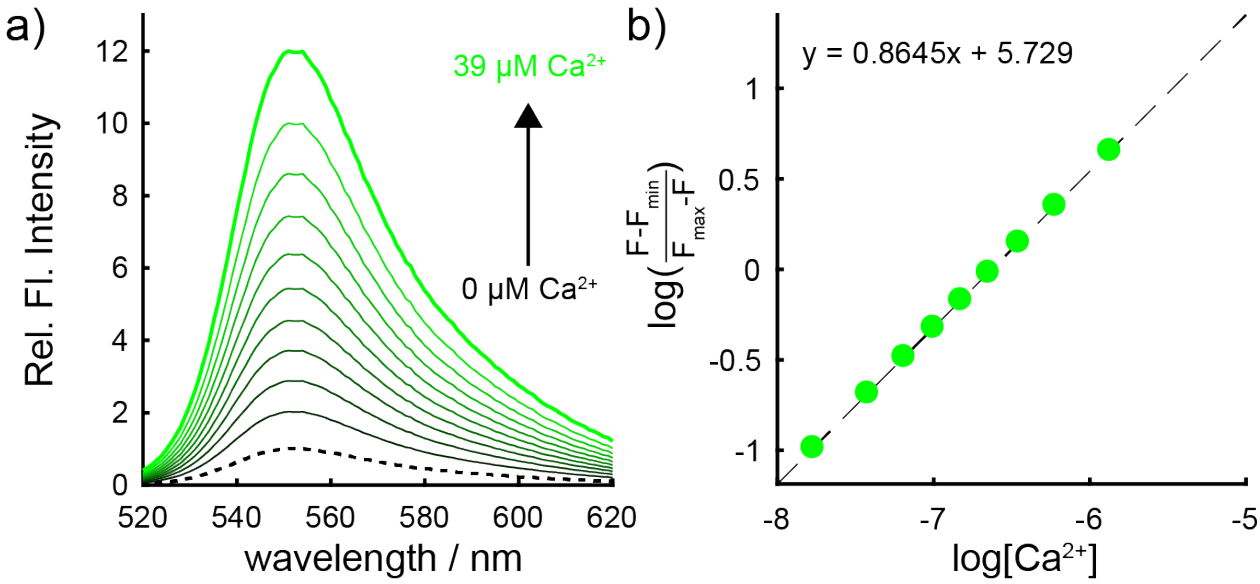

Figure S1. Determination of Ca^{2+} K_d for RCS-1. a) (From Figure 1b in main text) Ca^{2+} titration of rhodol Ca^{2+} sensor 1. The fluorescence emission spectra of rhodol Ca^{2+} sensor 1 was recorded at increasing concentrations of Ca^{2+} from 0 µM to 39 µM, with intermediate concentrations of 17 nM, 38 nM, 65 nM, 100 nM, 150 nM, 225 nM, 351 nM, 602 nM, and 1.35 µM. Excitation provided at 515 nm. b) Example of double-log plot to determine the Ca^{2+} K_d for RCS-1.

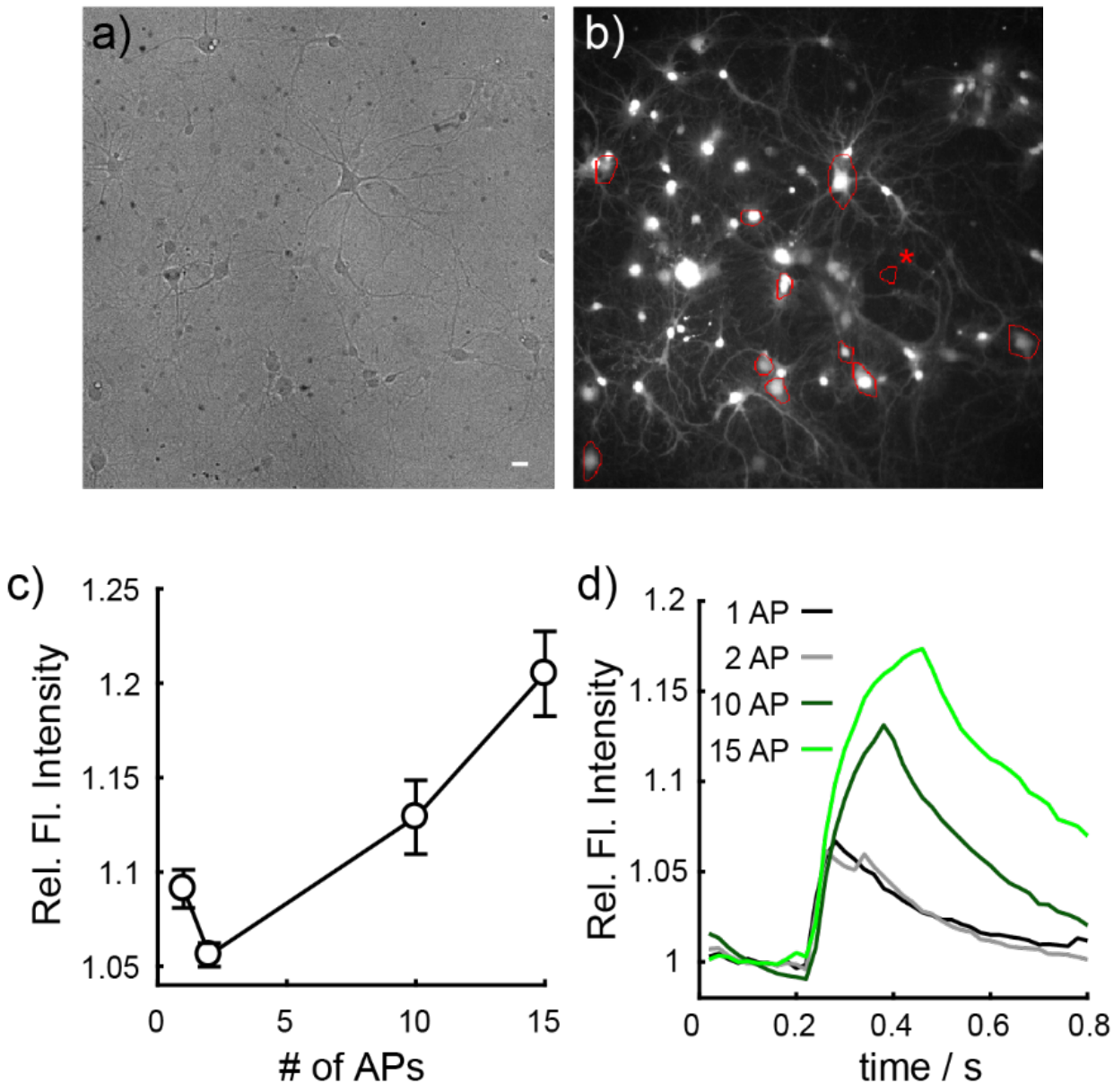

Figure S2. Visualization and quantification of Ca^{2+} transients in rat hippocampal neurons using rhodol Ca^{2+} sensor 1. a) Transmitted light image of cultured rat hippocampal neurons incubated with rhodol Ca^{2+} sensor 1 tetra AM ester (1.7 μM). b) Widefield fluorescence micrograph of cultured rat hippocampal neurons incubated with rhodol Ca^{2+} sensor 1 tetra AM ester (1.7 μM). Regions of interest (ROIs) for determining the plot in Figure 3b in the main text and action potential calibration are indicated in red. The ROI indicated by a red asterisk is the ROI used to determine background fluorescence. Scale bar is 20 μm. c) Quantification of the fluorescence response of RCS-1 to evoked action potentials in the indicated neurons in panel b. Relative changes in rhodol Ca^{2+}-indicator 1 fluorescence vs. time for neurons in panel a. d) Quantification of the response of RCS-1 fluorescence in 8 neurons to differing numbers of action potentials (black = 1, grey = 2, dark green = 10, green = 15 action potentials) vs. time.

7. References

(1) Adams, S. R. How Calcium Indicators Work. *Cold Spring Harb. Protoc.* **2010**, *2010* (3), pdb.top70.

(2) Tsien, R. Y. New Calcium Indicators and Buffers with High Selectivity Against Magnesium and Protons: Design, Synthesis, and Properties of Prototype Structures. *Biochemistry* **1980**, *19* (11), 2396–2404.

(3) Grynkiewicz, G.; Poenie, M.; Tsienb, R. Y. A New Generation of Ca2+ Indicators with Greatly Improved Fluorescence Properties*. *J. Biol. Chem. 260* (6), 1385.

(4) Minta, A.; Kao, J. P.; Tsien, R. Y. Fluorescent Indicators for Cytosolic Calcium Based on Rhodamine and Fluorescein Chromophores. *J. Biol. Chem.* **1989**, *264* (14), 8171–8178.

(5) Gee, K. R.; Poot, M.; Klaubert, D. H.; Sun, W. C.; Haugland, R. P. FLUORINATED XANTHENE DERIVATIVES. *J. Chem. Soc. Trans. 1* **1986**, *51*, 1658–1666.

(6) Michael A. Kuhn; Richard P. Haugland. REACTIVE DERIVATIVES OF BAPTAUSED TO MAKE ON-SELECTIVE CHELATORS, 1995.

(7) Diwu, Z.; Guo, H.; Peng, R.; Zhao, Q.; Liu, J.; Liao, J. Carbofluorescein Lactone Ion Indicators and Their Applications, August 4, 2014.

(8) Collot, M.; Wilms, C. D.; Bentkhayet, A.; Marcaggi, P.; Couchman, K.; Charpak, S.; Dieudonné, S.; Häusser, M.; Feltz, A.; Mallet, J.-M. CaRuby-Nano: A Novel High Affinity Calcium Probe for Dual Color Imaging. *Elife* **2015**, *4*, e05808.

(9) Egawa, T.; Hirabayashi, K.; Koide, Y.; Kobayashi, C.; Takahashi, N.; Mineno, T.; Terai, T.; Ueno, T.; Komatsu, T.; Ikegaya, Y.; et al. Red Fluorescent Probe for Monitoring the Dynamics of Cytoplasmic Calcium Ions. *Angew. Chem. Int. Ed. Engl.* **2013**, *52* (14), 3874–3877.

(10) Grimm, J. B.; Sung, A. J.; Legant, W. R.; Hulamm, P.; Matlosz, S. M.; Betzig, E.; Lavis, L. D. Carbofluoresceins and Carborhodamines as Scaffolds for High-Contrast Fluorogenic Probes. **2013**.

(11) Grienberger, C.; Konnerth, A. Imaging Calcium in Neurons. *Neuron* **2012**, *73* (5), 862–885.

(12) Chen, T.-W. W.; Wardill, T. J.; Sun, Y.; Pulver, S. R.; Renninger, S. L.; Baohan, A.; Schreiter, E. R.; Kerr, R. A.; Orger, M. B.; Jayaraman, V.; et al. Ultrasensitive Fluorescent Proteins for Imaging Neuronal Activity. *Nature* **2013**, *499* (7458), 295–300.

(13) Paredes, R. M.; Etzler, J. C.; Watts, L. T.; Zheng, W.; Lechleiter, J. D. Chemical Calcium Indicators. *Methods* **2008**, *46* (3), 143–151.

(14) Mütze, J.; Iyer, V.; MacKlin, J. J.; Colonell, J.; Karsh, B.; Petrášek, Z.; Schwille, P.; Looger, L. L.; Lavis, L. D.; Harris, T. D. Excitation Spectra and Brightness Optimization of Two-Photon Excited Probes. *Biophys. J.* **2012**, *102* (4), 934–944.

(15) Xu, C.; Williams, R. M.; Zipfel, W.; Webb, W. W. Multiphoton Excitation Cross-Sections of Molecular Fluorophores. *Bioimaging* **1996**, *4*, 198–207.

(16) Oheim, M.; van 't Hoff, M.; Feltz, A.; Zamaleeva, A.; Mallet, J.-M.; Collot, M. New Red-Fluorescent Calcium Indicators for Optogenetics, Photoactivation and Multi-Color Imaging. *Biochim. Biophys. Acta - Mol. Cell Res.* **2014**, *1843* (10), 2284–2306.

(17) Whitaker, J. E.; Haugland, R. P.; Ryan, D.; Hewitt, P. C.; Haugland, R. P.;

Prendergast, F. G. Fluorescent Rhodol Derivatives: Versatile, Photostable Labels and Tracers. *Anal. Biochem.* **1992**, *207* (2), 267–279.
(18) Poronik, Y. M.; Clermont, G.; Blanchard-Desce, M.; Gryko, D. T. Nonlinear Optical Chemosensor for Sodium Ion Based on Rhodol Chromophore. *J. Org. Chem* **2013**, *78*.
(19) Kulkarni, R. U.; Kramer, D. J.; Pourmandi, N.; Karbasi, K.; Bateup, H. S.; Miller, E. W. Voltage-Sensitive Rhodol with Enhanced Two-Photon Brightness. *Proc. Natl. Acad. Sci.* **2017**, *114* (11), 2813–2818.
(20) Dickinson, B. C.; Chang, C. J. A Targetable Fluorescent Probe for Imaging Hydrogen Peroxide in the Mitochondria of Living Cells. *J. AM. CHEM. SOC* **2008**, *130*, 46.
(21) Kathayat, R. S.; Elvira, P. D.; Dickinson, B. C. A Fluorescent Probe for Cysteine Depalmitoylation Reveals Dynamic APT Signaling. *Nat. Chem. Biol.* **2017**, *13* (2), 150–152.
(22) Woodroofe, C. C.; Lim, M. H.; Bu, W.; Lippard, S. J. Synthesis of Isomerically Pure Carboxylate- and Sulfonate-Substituted Xanthene Fluorophores. *Tetrahedron* **2005**, *61* (12), 3097–3105.
(23) Grimm, J. B.; English, B. P.; Chen, J.; Slaughter, J. P.; Zhang, Z.; Revyakin, A.; Patel, R.; Macklin, J. J.; Normanno, D.; Singer, R. H.; et al. A General Method to Improve Fluorophores for Live-Cell and Single-Molecule Microscopy. *Nat. Methods* **2015**, *12* (3), 244–250.
(24) Peng, T.; Yang, D. Construction of a Library of Rhodol Fluorophores for Developing New Fluorescent Probes. *Org. Lett.* **2010**, *12* (3), 496–499.
(25) Grimm, J. B.; Lavis, L. D. Synthesis of Rhodamines from Fluoresceins Using Pd-Catalyzed C – N Cross-Coupling S1 : Experimental Information. *Org. Lett.* **2011**, *13* (24), 6354–6357.
(26) Tsien, R. Y. A Non-Disruptive Technique for Loading Calcium Buffers and Indicators into Cells. *Nature* **1981**, *290* (5806), 527–528.
(27) Och, C.; Berliner, M.; Belecki Checked by William Paquette, K. D.; Wipf, P. SYNTHESIS OF ALPHA-HALO ETHERS FROM SYMMETRIC ACETALS AND in Situ METHOXYMETHYLATION OF AN ALCOHOL [1-Methoxymethoxy-1-Phenylethane] OH Solution of H 3 COCH 2 Cl in MeOAc/Toluene. *Org. Synth. Coll* **2007**, *84* (11), 102–110.
(28) Buffer, C. Calcium Calibration Buffer Kits. *Imaging* **2011**, No. C, 1–10.
(29) Albota, M. A.; Xu, C.; Webb, W. W. Two-Photon Fluorescence Excitation Cross Sections of Biomolecular Probes from 690 to 960 Nm.
(30) Fluorescent Ca2+ Indicators Excited with Visible Light—Section 19.3.

Chapter Four: Amino acid esters as capping moieties for delivery of negatively charged fluorescent probes

1. Introduction

Delivery of Chemical calcium indicators

Chemical calcium indicators are comprised of two parts: a calcium chelating moiety, BAPTA, and a fluorophore. The BAPTA moiety contains four carboxylate arms that chelate Ca^{2+} ions. In the absence of calcium, the electron density on the calcium-binding unit quenches the fluorescence of the attached fluorophore via photoinduced electron transfer (PeT). In the presence of calcium, the electron density is used to chelate the Ca^{2+} ion, thereby, reducing the rate of PeT and eliciting an increase in fluorescence of the fluorophore. This increase in fluorescence is tracked as a representation of calcium activity and used to study various biological phenomena.

Chemical calcium indicators are normally bath applied onto cells of interest. The chemical calcium indicators are bath applied to the cells in aqueous media, and passively diffuse into the cells through the cell membrane. However, negatively charged indicators cannot pass through the hydrophobic interior of core of the cell membrane. In order to deliver calcium indicators to cells, the negative charges are capped with protective esters

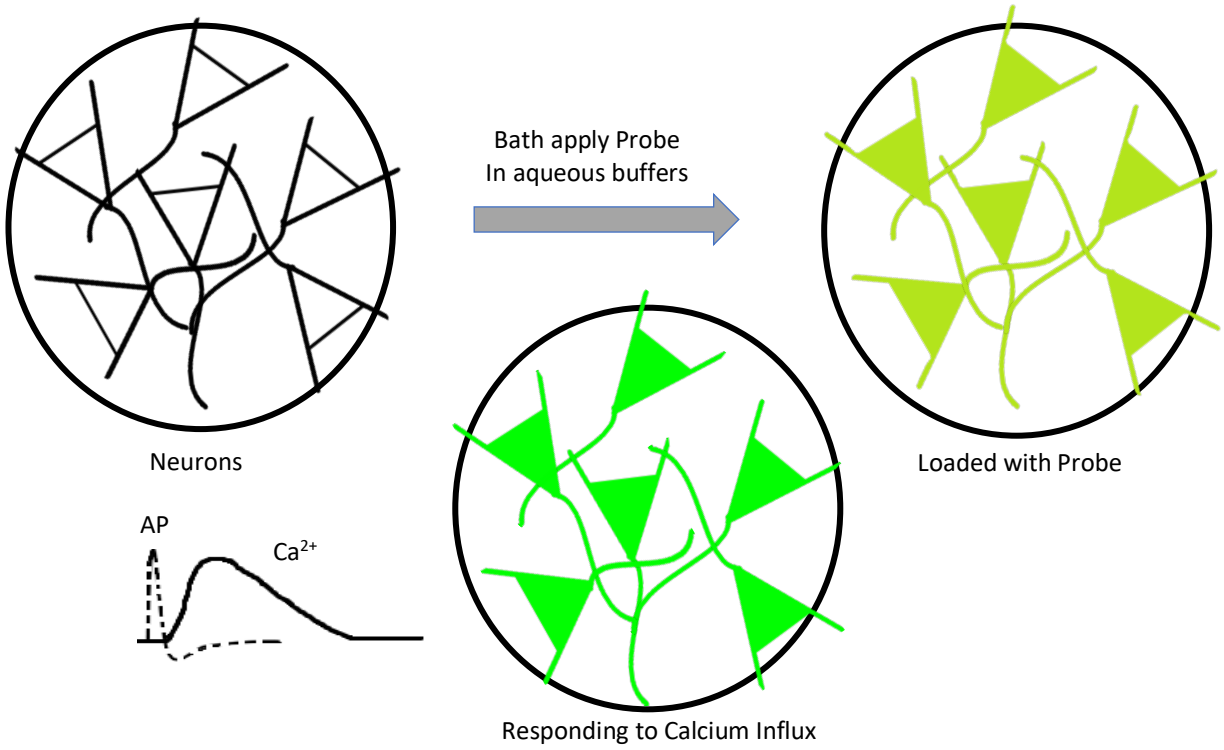

Figure 1. Schematic of calcium imaging in neurons. Calcium indicator is bath applied in aqueous buffer. The calcium indicator passively diffuses through the cell membrane into the cytoplasm of cells. Once inside the cells, the calcium indicators display an increase in fluorescence in response to neuronal activity. This change in fluorescence is recorded and used to study biological phenomena.

that can be cleaved by intracellular esterases. The most commonly used esters are acetoxymethyl esters. Once the negative charges are capped with AM esters, the indicator can pass through the core of the cell membrane. Inside the cell, esterases cleave the esters and release the functional, negatively charged probe, effectively trapping the probe inside the cells. While the AM esters render the probe cell permeable, they reduce the solubility of the overall probe in aqueous media. The hydrophobic dye crashes out of the aqueous solutions and does not interact with the cells enough to diffuse through the cell membrane. Therefore, solubilizing agents are needed to increase the interaction of the probe with the cells.

Further complications arise because solubilizing agents and other methods of delivery often perturb the membrane and membrane dynamics.[1,2] Methods such as detergents and electroporation are used to solubilize the calcium indicators in aqueous media (Figure 2). Detergents, like Pluronic F-127 – the most commonly used detergent, have hydrophobic cores and hydrophilic tails (Figure 2A). The hydrophobic core surrounds the capped dye, while the hydrophilic tails interact with water to solubilize the probe (Figure 2B). Pluronic© surfactant polymers have been shown to be biologically active with involvement in interruption of Ca^{2+} regulation pathways, neuronal apoptosis, and activity as an ionophore.[3–9] Surfactants perturb the membrane by altering the structure or behavior of the membrane. The other method, electroporation, involves the application of an electric field pulses across the cell (Figure 3C). Before the pulse, the probe is introduced to the cells; during the electric field stimulation, a voltage is induced across the cell membrane which results in the creation of pores that allow for the passage

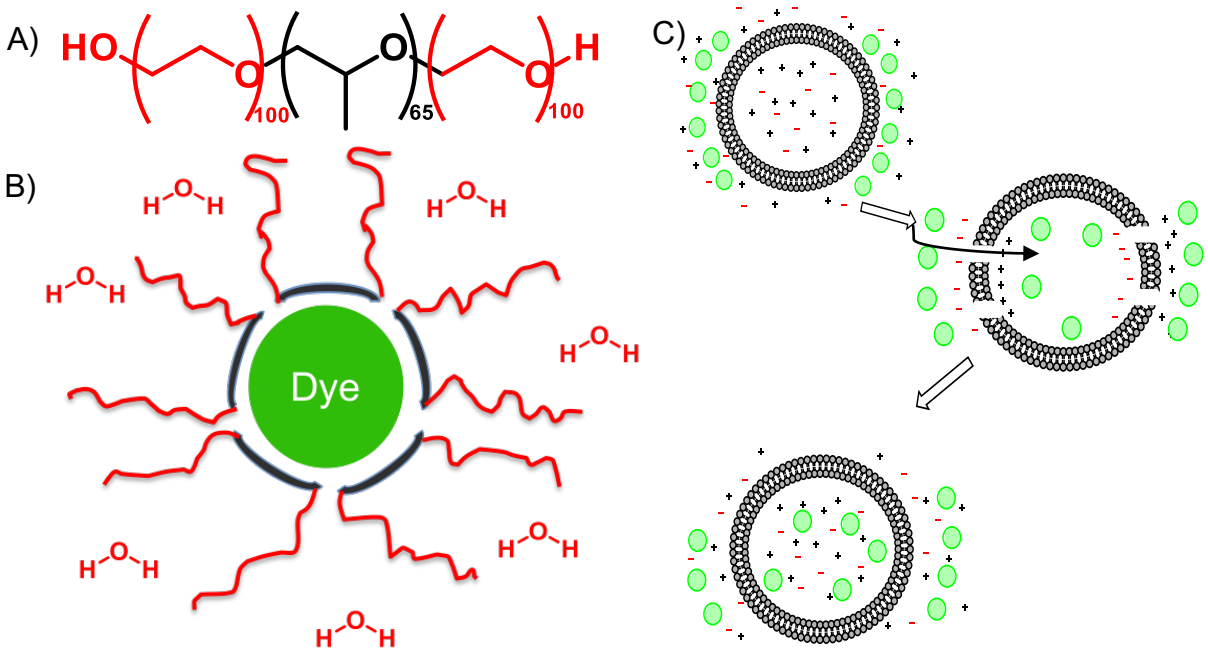

Figure 2. Methods of delivering AM ester protected calcium indicators to cells. A) Shows the structure of surfactant, Pluronic© F-127 B) The mechanism of detergents solubilizing the indicators: the hydrophobic core of the detergent surrounds the calcium indicator, while the hydrophilic tails interact with the aqueous solvent, effectively solubilizing the indicator. C) Electroporation is the method of delivering insoluble calcium indicators by applying an electric field across the cell which induces the creation of pores in the cell membrane which the indicators pass through. Following the stimulation, the cells are allowed to heal and seal up the pores, trapping the indicators inside the cells.

of probes across the cell membrane. Following the stimulation, the membranes are allowed to heal and the pores are closed with the indicators inside the cells. Electroporation ruptures membranes. The perturbation of the membranes complicates the data collected through calcium imaging. Therefore, methods of delivering calcium indicators that avoid the use of detergents or other invasive methods is desirable. The use of a capping moiety that masks the charges, is biocompatible, shows efficient unmasking in cells, preserves functionality of the indicator, while rendering the indicator water soluble would overcome the drawbacks of using AM esters.

In the pharmaceutical industry, water solubility of drugs is increased by developing prodrugs capped with amino acid esters. For example, the hydrophobic anesthetic Propofol is delivered as the salt form of the amino-acid ester.[10] The salt form is stable, water-soluble, and the biological activity is comparable to the commercial anesthetic. Using that example, we propose that use of amino acids as an alternative capping moiety will increase the solubility of calcium indicator while preserving the cell permeability of the indicator. We propose taking advantage of equilibrium between the salt form and the neutral form of the amino acids. The salt form increases the solubility in aqueous media, while the neutral form can permeate through the cell membrane. Once inside the esterases that work to cleave the acetoxymethyl (AM) esters will cleave the amino acid esters and deliver the functional calcium indicator that is now trapped within the cells (Figure 4). In order to test this hypothesis, we synthesized amino acid protected carboxyfluoresceins. The pendant carboxylate keeps the dye from becoming cell permeable, thereby making it an ideal test molecule to perform proof-of-principle

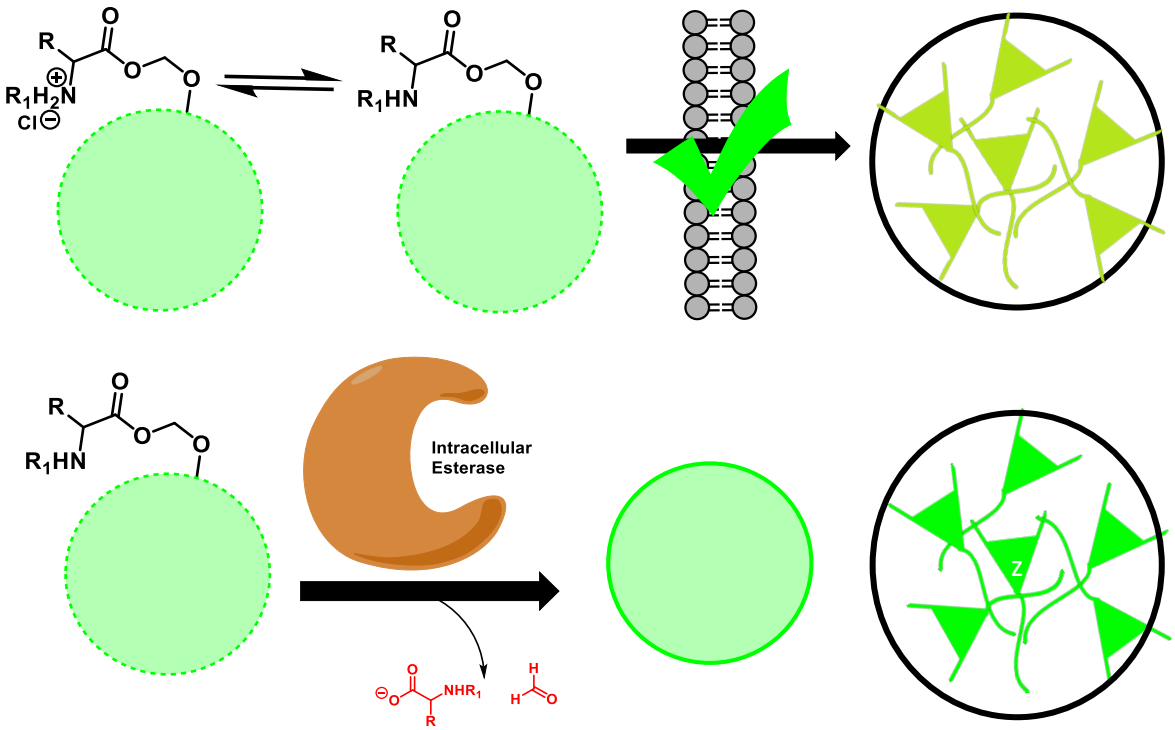

Figure 3. Mechanism of action of delivery of negatively charged probes using amino acid esters. There is an equilibrium between the salt form and the neutral form of the amino acid. The salt form facilitates solubility of the probe while the neutral form preserves cell permeability. Once inside the cell, intracellular esterases cleave the amino acid esters and release functional fluorescent probes inside the cell.

experiments. The carboxyfluorescein protected with amino acid esters will increase solubility and permeability of the fluorophore through the cell membrane. Once inside the cell, the esterases will cleave off the amino acid esters and trap the dye within the cell similar to the expected activity with negatively charged calcium indicators. The capped carboxyfluorescein was synthesized in a single step from the iodomethyl-amino acid and carboxyfluorescein; proline and beta-alanine were used as the amino acid esters. Starting from the boc-protected amino acid, the carboxylate was esterified to the chloromethyl ester, followed by a halogen exchange reaction to yield the iodomethyl ester of proline or beta-alanine.

2. Synthesis

Scheme 1

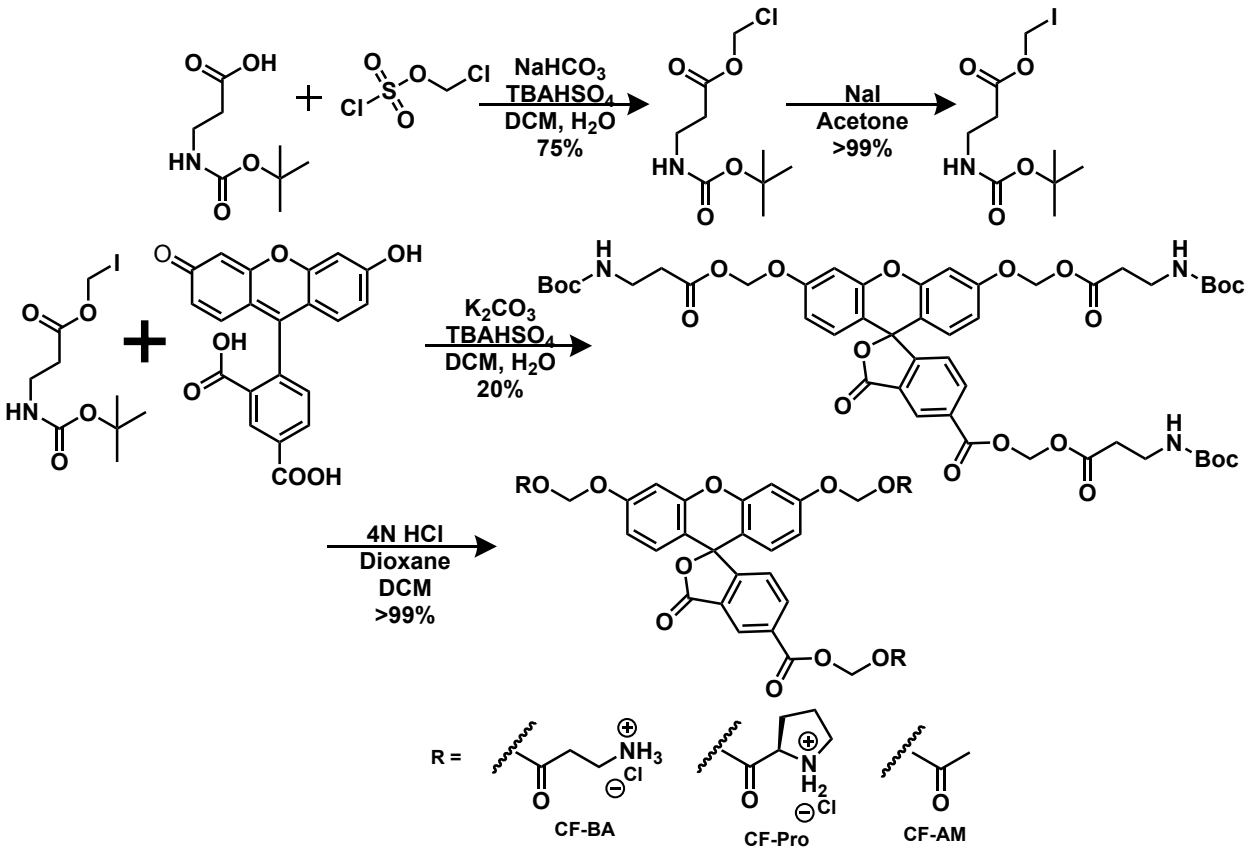

Scheme 1. Synthesis of CF-BA, CF-Pro, and CF-AM.

General procedure for the synthesis of chloromethyl boc-amino acid.

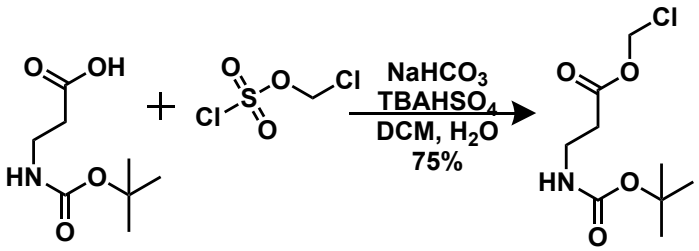

To a 25-mL round-bottom flask, 4 mmol (700 mg of Boc-β-Alanine, 1 eq.) of boc-amino acid, 6 mmol (602 µL, 1.5 eq.) chloromethyl chlorosulfate, 16 mmol (1.20g, 4 eq.) of sodium bicarbonate, and 0.4 mmol (136 mg, 0.1 eq.) of tetra-butylammonium bisulfate was added along with 5 mL of dichloromethane and 5 mL of water. The biphasic reaction mixture was stirred overnight. After completion of the reaction, 300 mL of dicholoromethane was added to the reaction mixture which was then filtered through a

plug of diatomaceous earth. The combined organics were concentrated under reduced pressure and the resulting solid was triturated with 50% acetone in hexanes (20 mL), collecting the resulting solid by vacuum filtration. This process afforded chloromethyl ester of amino acids in good yield:
768 mg (86% yield) of chloromethyl-boc-β-Alanine
960 mg (91% yield) of chloromethyl-boc-proline
as an off-white solid.

Chloromethyl-boc-β-Alanine – ^{1}H NMR (400 MHz, Chloroform-*d*) δ 5.71 (s, 2H), 3.42 (d, *J* = 6.1 Hz, 2H), 2.61 (t, *J* = 6.0 Hz, 2H), 1.43 (s, 9H).

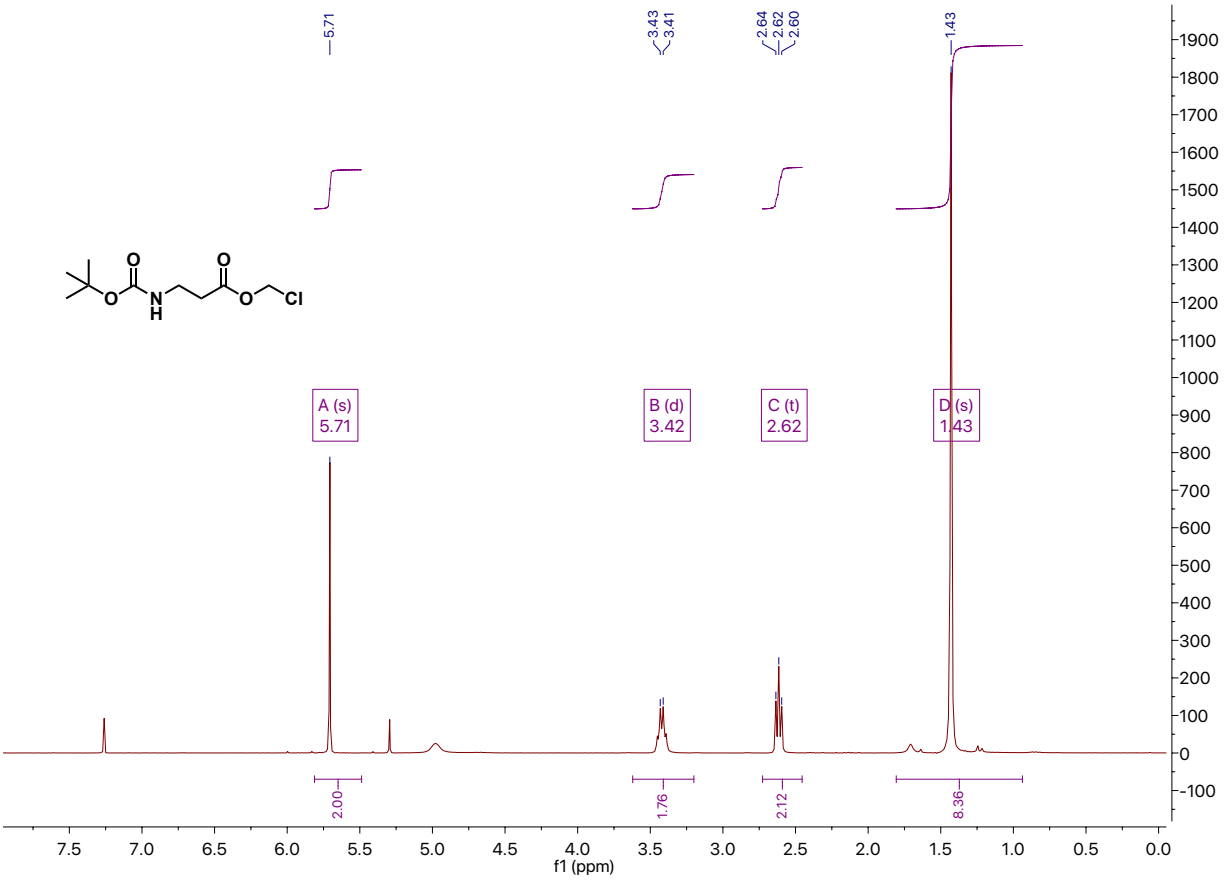

Chloromethyl-boc-Proline – ^{1}H NMR (400 MHz, Chloroform-*d*) δ 6.02 – 5.51 (m, 2H), 4.35 (ddd, *J* = 27.6, 8.8, 3.8 Hz, 1H), 3.76 – 3.27 (m, 2H), 2.43 – 2.17 (m, 1H), 1.99 (ddt, *J* = 32.7, 16.0, 5.5 Hz, 3H), 1.47 (d, *J* = 16.3 Hz, 9H).

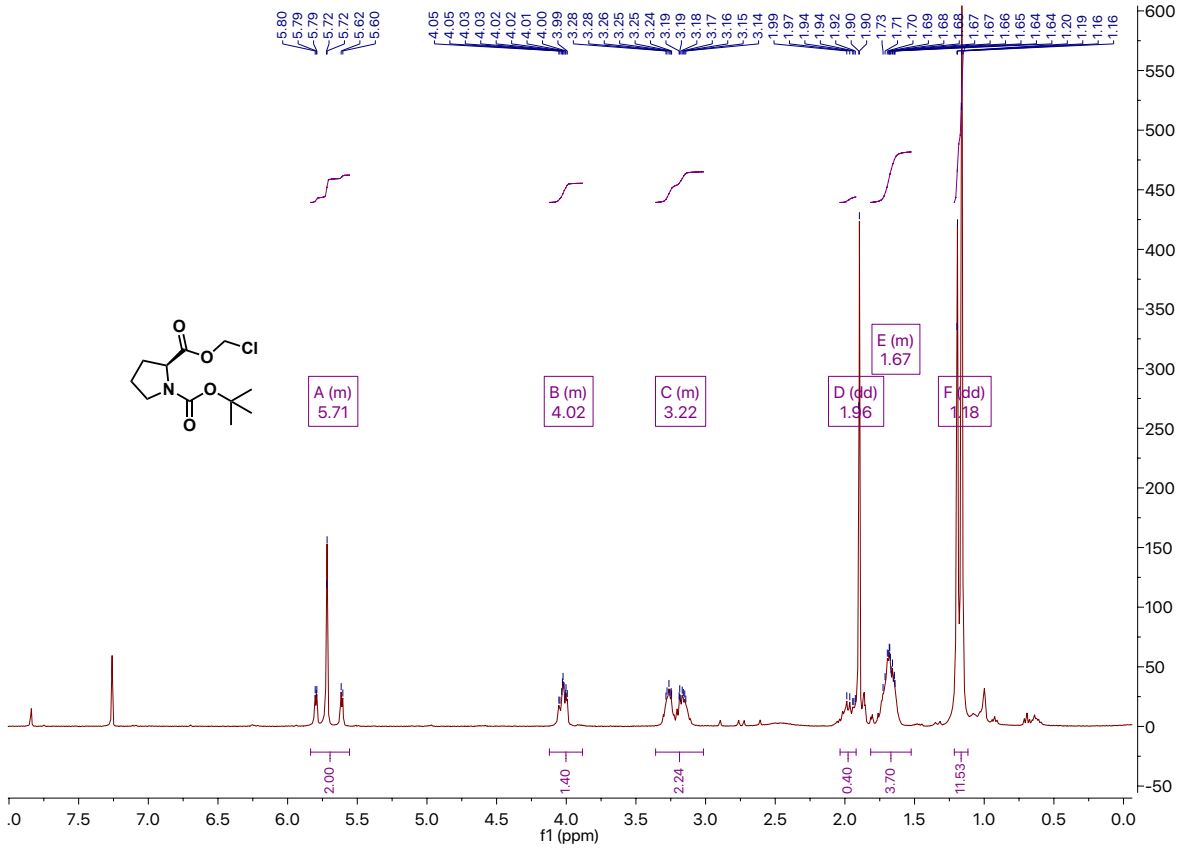

General procedure for the conversion of chloromethyl-boc-amino acids to iodomethyl-boc-amino acids

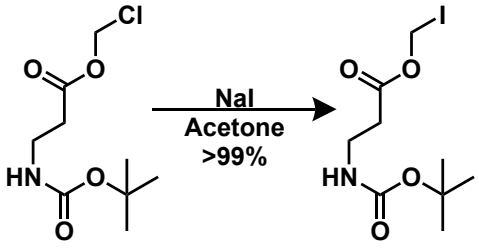

To a 10-mL round-bottom flask, the product from the previous reaction (~3.4 mmol, 1 eq.), and 3.4 mmol (510mg, 1 eq.) of sodium iodide were added along with 10 mL of acetone to dissolve the solids. The reaction was left to stir at room temperature overnight. Once the reaction was deemed complete via thin-layer chromatography, the sodium chloride by-product was removed via filtration, leaving a pale-yellow solution. The product was collected and concentrated in vacuo. This process afforded iodomethyl ester of amino acids – in very good yield (>99%) – as yellow solid.

Iodomethyl-boc-β-Alanine – ^{1}H NMR (300 MHz, Chloroform-*d*) δ 5.71 (s, 2H), 3.42 (d, *J* = 6.1 Hz, 2H), 2.62 (t, *J* = 6.0 Hz, 2H), 1.43 (s, 9H).
Iodomethyl-boc-Proline –^{1}H NMR (400 MHz, Chloroform-*d*) δ 5.84 – 5.56 (m, 2H), 4.12 – 3.88 (m, 1H), 3.36 – 3.02 (m, 2H), 1.96 (dd, *J* = 14.5, 5.9 Hz, 1H), 1.81 – 1.52 (m, 3H), 1.18 (dd, *J* = 12.9, 1.7 Hz, 9H).

General procedure for alkylating carboxyfluoresceins

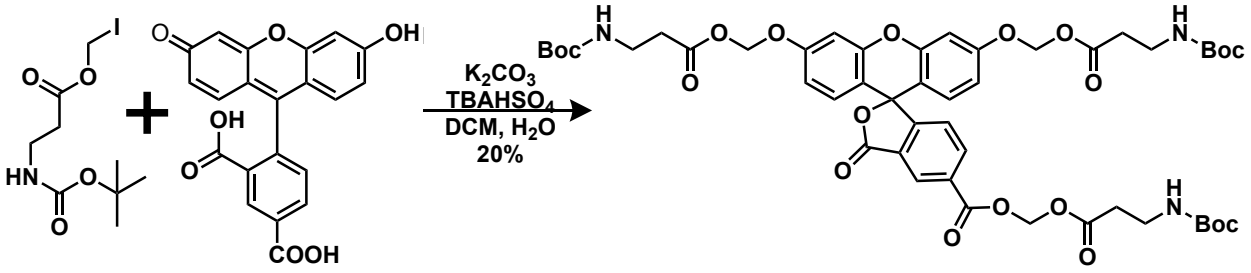

In a 25-mL round-bottom flask, 0.11 mmol (41.4 mg, 1 eq.) of 5(6)-carboxyfluorescein, 1.32 mmol (470 mg, 12 eq.) iodomethyl-amino acid, 91.3 mg (17 mmol, 6eq.) of potassium carbonate, and 75 mg (0.22 mmol, 2.0 eq.) were added together and dissolved in 5 mL dichloromethane and 5 mL of water. The bi-phasic reaction mixture was stirred vigorously overnight. The reaction progress was monitored via thin layer chromatography. When the reaction was complete, the product was extracted into 200 mL of DCM and washed with 100 of DCM each time. The organic layers were collected and concentrated in vacuo. The product was purified via silica gel chromatography (20-50% EtOAc:Hex), yielding ~10mg (10% yield) of product as a yellow oil.
CF-Boc-β-Alanine – ^{1}H NMR (400 MHz, Methanol-d_4) δ 8.65 (t, *J* = 1.0 Hz, 0.5H), 8.40 (dd, *J* = 18.5, 8.0 Hz, 1H), 8.18 (t, *J* = 8.0 Hz, 0.5H), 7.73 (d, *J* = 8.2 Hz, 0.5H), 7.37 (t, *J* = 7.6 Hz, 0.5H), 7.21 – 7.02 (m, 2H), 6.88 – 6.76 (m, 2H), 6.21 – 5.80 (m, 6H), 3.42 (d, *J* = 6.1 Hz, 6H), 2.62 (t, *J* = 6.0 Hz, 6H), 1.43 (s, 27H).

CF-Boc-Proline – ^{1}H NMR (400 MHz, Methanol-d_4) δ 8.65 (t, J = 1.0 Hz, 0.5H), 8.40 (dd, J = 18.5, 8.0 Hz, 1H), 8.18 (t, J = 8.0 Hz, 0.5H), 7.73 (d, J = 8.2 Hz, 0.5H), 7.37 (t, J = 7.6 Hz, 0.5H), 7.21 – 7.02 (m, 2H), 6.88 – 6.76 (m, 2H), 6.21 – 5.80 (m, 6H), 4.36 – 4.22 (m, 3H), 3.57 – 3.37 (m, 6H), 2.29 (td, J = 13.5, 13.1, 6.7 Hz, 3H), 1.91 (tq, J = 13.9, 6.3, 5.8 Hz, 6H), 1.50 – 1.29 (m, 27H).

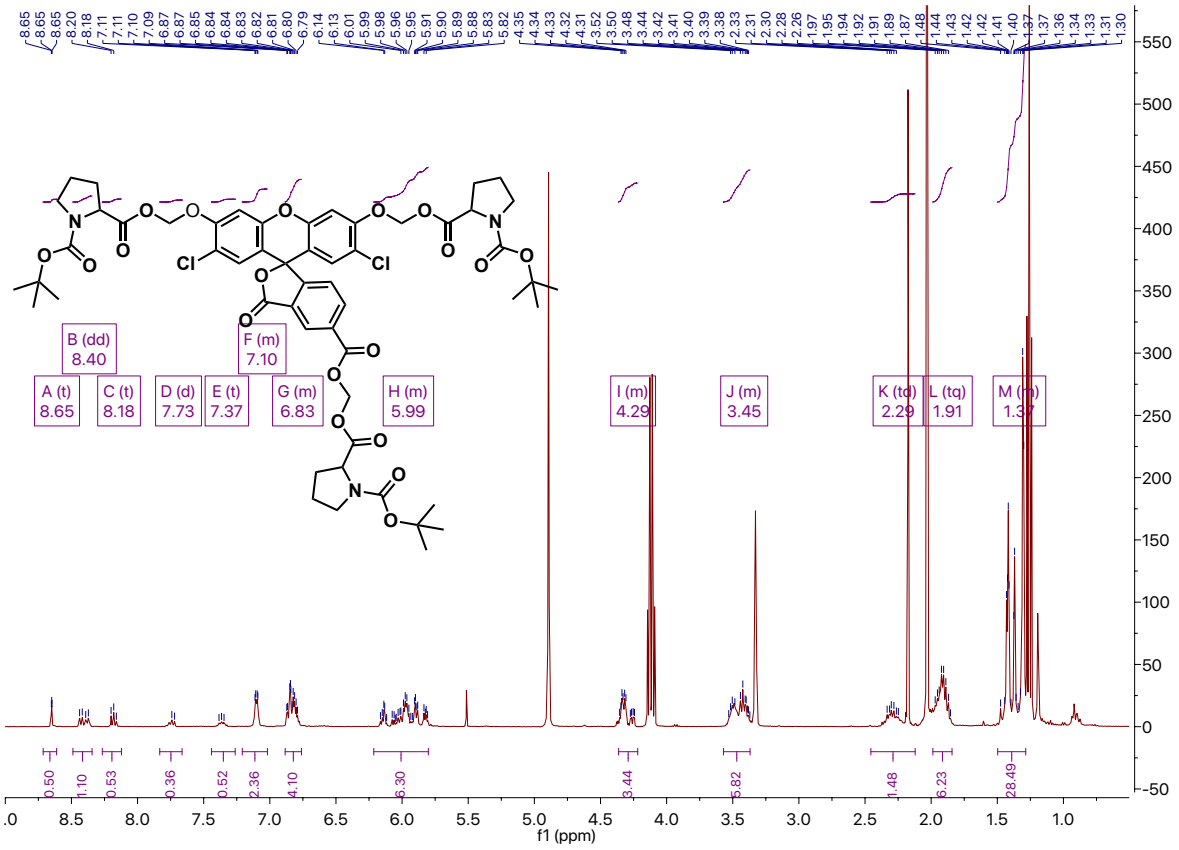

General procedure for the deprotection of boc-groups

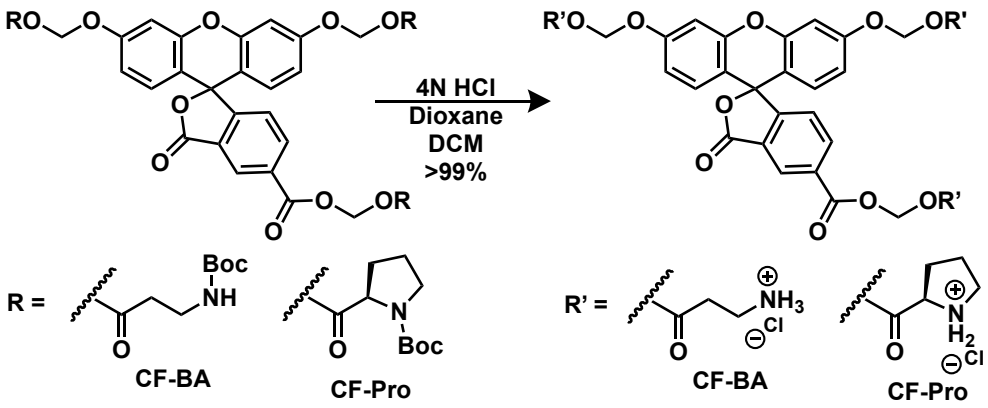

In a scintillation-vial the oil (10mg) from the previous reaction was dissolved in dioxane: methanol (3: 0.5 mL), and a 100 µL of 4N HCl in dioxane. The reaction was stirred for a couple hours. The solution was concentrated down and collected in vacuo. The solid was triturated in either and filtered via vacuum filtration. The yield was quantitative for both products.

Synthesis of CF-AM

AM Esters of carboxyfluorescein was synthesized according to literature procedure.[11]

3. Results and discussion

In-vitro solubility determination for CF-Pro, CF-βA, and CF-AM

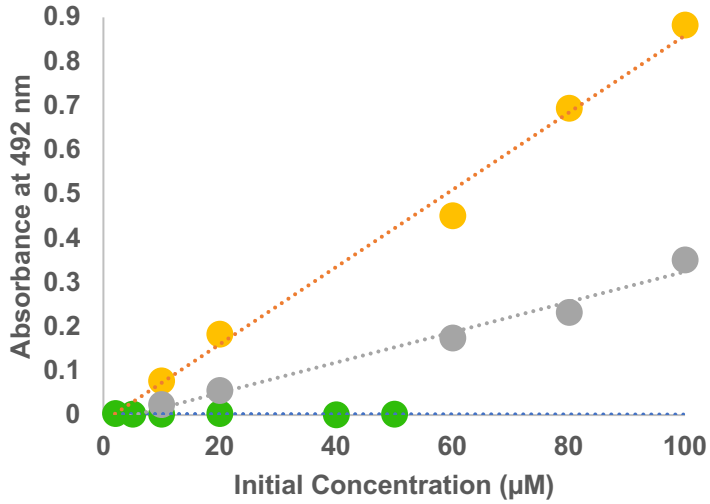

Figure 4. Base Catalyzed Hydrolysis: CF-AM, CF-βA, CF-Pro. The dots refer to the concentrations measured. Green: CF-AM; Grey: CF-BA; Yellow: CF-Pro. Lower concentrations of CF-AM were studied because at higher concentrations, the solution clogged the filter.

Various concentrations of the dye were dissolved in water, filtered through a 0.45 µm filter, and 1 mL of filtered solution was treated with 10 µL of 12M KOH to deprotect the amino acid esters. The deprotected dye's absorbance was measured in a 1:1 dilution in 1M KOH. CF-Pro showed a linear increase in absorption with increasing concentration, while CF-AM does not dissolve at all regardless of concentration. This experiment confirmed that the salt form of the amino acid ester increases the solubility of the probe in water.

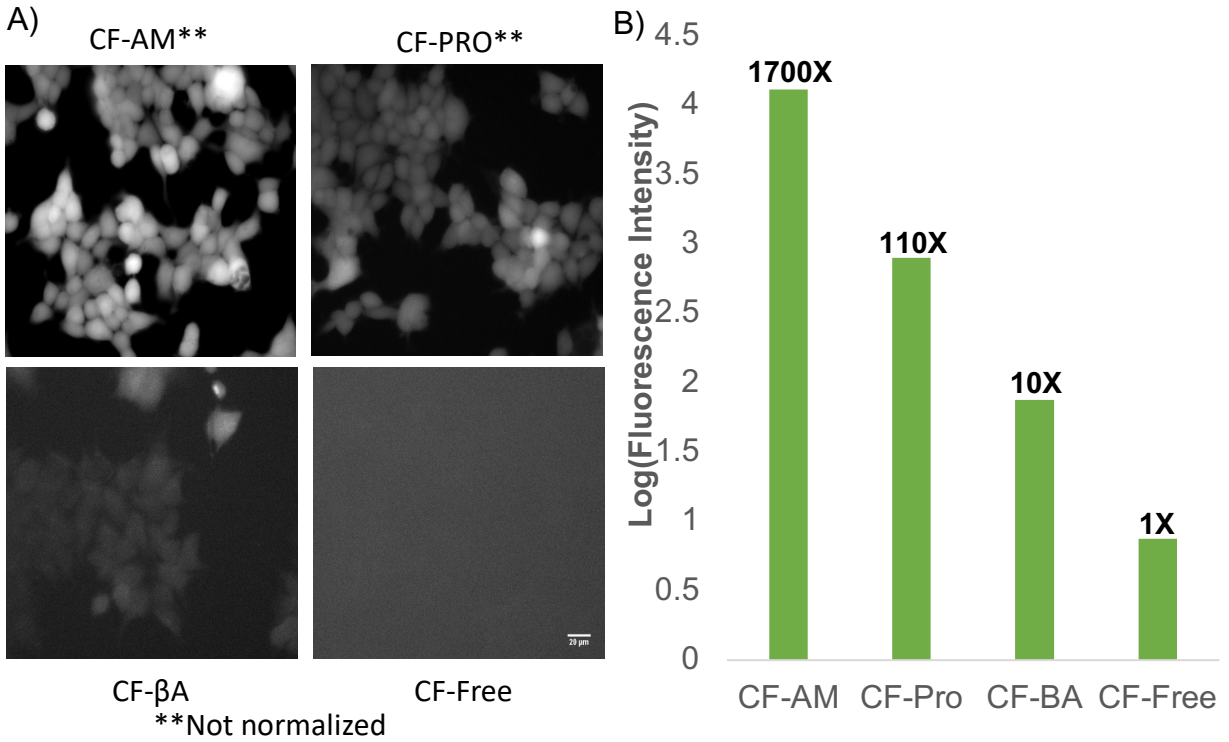

Figure 5. Dye delivered to HEK293T cells A) The dyes (5 µM) were bath applied to HEK293T cells, and incubated with the dye for 30 min before fluorescence images were acquired. The CF-AM esters were the most permeable and displayed the brightest staining. B) The carboxyfluorescein is not permeable and has lowest brightness value. CF-BA shows 10 times brighter fluorescence in HEK cells; CF-Pro shows 110 times brighter staining; CF-AM shows the brightest (1700 times) staining of HEK293T cells.

With that result, we wanted to ascertain cell permeability in HEK 293T cells. The amino acid protected dye (5 μM) was dissolved in HBSS and bath applied to the cultured HEK 293T cells (Figure 6A). The acetoxymethyl ester protected carboxyfluorescein showed the brightest staining in cells (1700 times brighter than unprotected carboxyfluorescein), however, Pluronic© F-127 was added to the media to facilitate solubility of CF-AM. CF-Pro delivered cellular staining that was ~110 times brighter than free, unprotected carboxyfluorescein. CF-BA delivered cellular staining that was 10 times brighter than CF-Free (Figure 6B).

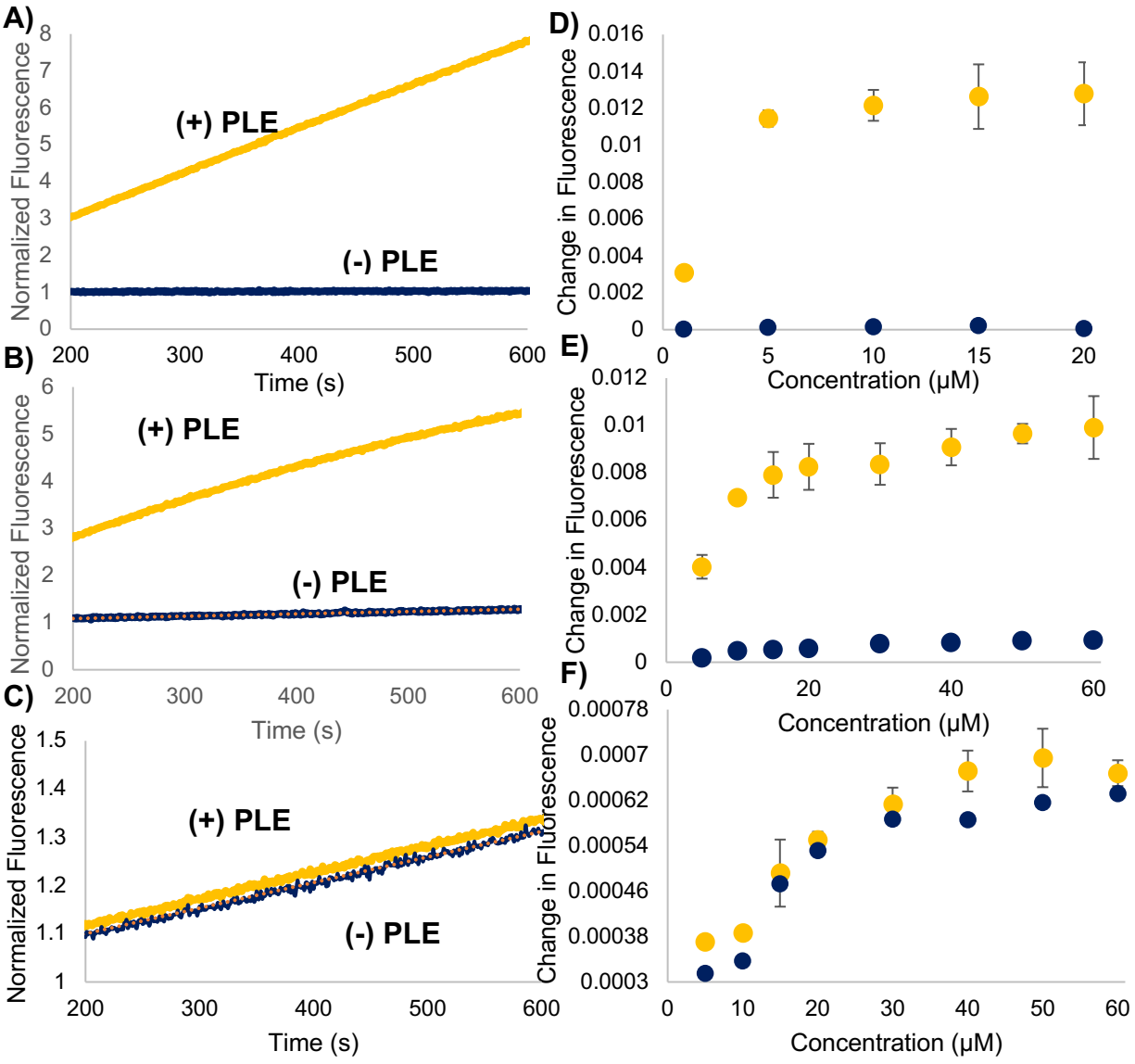

Figure 6. Stability assay and treatment with Porcine Liver Esterase (PLE). Yellow is the presence of PLE; Blue is the absence of PLE A) CF-AM fluorescence recorded in the presence and absence of Porcine Liver Esterase (PLE) B) CF-BA fluorescence recorded in the presence and absence of PLE C) CF-Pro fluorescence recorded in the presence and absence of PLE. D) Quantification of the change in fluorescence at various concentrations of CF-AM in (+)/(-) PLE E) Quantification of the change in fluorescence at various concentrations of CF-BA in (+)/(-) PLE F) Quantification of the change in fluorescence at various concentrations of CF-Pro in (+)/(-) PLE

In order to determine if the poor cellular uptake of CF-Pro and CF-BA was a result of cellular esterases not cleaving the amino acid esters or a result of hydrolysis prior to cellular uptake, a stability assay was performed. Fluorescence intensity was recorded in presence and absence of porcine liver esterase for approximately 10 min *in vitro*. The treatment of prolyl-esters of carboxyfluorescein (CF-Pro), beta-alanyl-esters of carboxyfluorescein (CF-BA), and acetoxymethyl esters of carboxyfluorescein (CF-AM) with porcine liver esterase (PLE) also enables the determination of whether these esters are substrates for intracellular esterases (Figure 7). The acetoxymethyl esters are substrates of porcine liver esterase, additionally, the acetoxymethyl esters are very stable in the absence of PLE – the fluorescence does not change over time in the absence of PLE, suggesting that the esters are not hydrolyzed in the absence of PLE (Figure 7A). The beta-alanyl esters of carboxyfluorescein is also a good substrate of PLE as the fluorescence increases over time when in presence of PLE. The baseline fluorescence increases slightly over time in the absence of the PLE suggesting that the esters hydrolyze slightly in aqueous solutions (Figure 7B). The prolyl-esters of carboxyfluorescein are not substrates for PLE. Furthermore, prolyl-esters were the least stable in aqueous solutions, the fluorescence increases rapidly when dissolved in aqueous solutions (Figure 7C). The stability assay was performed at different concentrations in order to arrive at Michealis-Menton type kinetic curves for CF-AM and CF-BA with porcine liver esterase (Figure 7D-F). The data was used to find the K_M which is the substrate concentration at which the rate of activity is ½ of V_{max} – the fastest rate at which the esterase hydrolyzes the esters (Table 1). The acetoxymethyl esters are better substrates for PLE than the beta-alalinyl esters.

Table 1: Determination of Michaelis-Menton Kinetics

Probe	K_M (μM)	K_{cat}/K_M (M^{-1} s^{-1})	Enzyme Concentration
F-AM**	3.2	$6.8x10^5$	8.30 ng/mL
CF-AM	4.85	$2.68x10^8$	830 ng/mL
CF-βA	12.9	$1.86x10^7$	830 ng/mL
CF-Pro	Not a substrate for PLE		

While preliminary results showed some promise – the amino acid esters were more soluble in aqueous solutions than AM ester counterparts and were fairly cell permeable, we were unable to alkylate calcium indicators with amino acid esters. After many attempts detailed in Table 2, the correct conditions for the synthesis for the synthesis of Calcium Green BAPTA were determined to be the addition of the fluorophore (1 eq), the ethyl-ester of 5-amino BAPTA (0.9 eq), DIPEA (5 eq) to 1 mL of dry dimethylformamide, followed by cooling the reaction solution to 0 ºC before the addition of 0.45M HATU (5 eq) in dry DMF. The reaction was allowed to warm to room temperature while stirring overnight. The product collected via preparatory thin-layer chromatography.

Table 2: Varied conditions attempted for amide coupling of carboxyfluorescein (CF) and 5-amino BAPTA.

Starting Material	Coupling Reagent	Base	Solvent	Product	Yield
Acetylated-CF	EDC (1.1eq) NHS (1.1eq)	DIPEA	MeCN	No	-
Ac-CF	HATU (1.55 eq)	DIPEA (2eq)	MeCN	No	-
AC-CF	Mixed anhydride (Isobutylacid Chloride)	TEA	DCM	No	-
Ac-CF	PS-IIDQ	-	MeCN	No	-
Ac-CF	IIDQ	-	MeCN	No	-
Ac-CF	HATU (5eq)	DIPEA (5eq)	DMF	1/2 Times	10%
CF	IIDQ	-	MeCN	No	-
CF	PS-IIDQ	-	MeCN	No	-
CF	0.45M HATU/HOBt (DMF) (1.2 eq)	DIPEA (3.0 eq)	DMF	2/5 Times	35%
CF	0.45M HATU (5eq)	DIPEA (5eq)	DMF	Yes	50%

Once the synthesis of the calcium indicator was complete, the same reaction conditions used to alkylate carboxyfluorescein were attempted with no success. Attempts at alkylating in more concentrated reaction mixture in DMF – not biphasic as previous attempts – were also unsuccessful (summarized in Table 3).

Table 3: Conditions for Alkylation of CGB

Starting Material	Iodo-amino acid	Base	Solvent	Product	Yield
CGB-K^+ salt	Proline	$TBAHSO_4$ K_2CO_3	DCM: H_2O	No	-
CGB-K^+ salt	Beta-Alanine	$TBAHSO_4$ K_2CO_3	DCM: H_2O	No	-
CGB-K^+ salt	Proline	DIPEA	DMF	No	-
CGB-K^+ salt	Beta-Alanine	DIPEA	DMF	No	-

Next, we hoped by breaking up the molecule such that the amino-BAPTA portion would be differentially esterified with acetoxymethyl esters while the carboxyfluorescein would be selectively esterified with the amino acyl esters (Figure 8). Attempts to synthesize acetoxymethyl esters of 5-aminoBAPTA were successful, and later used to synthesize rhodol calcium sensors. However, efforts to selectively esterify carboxyfluorescein with amino acyl esters proved futile. We had hoped that by protecting the pendant carboxylic acid with a benzyl ether protecting group (para-methoxybenzyl, PMB) would facilitate selective esterification of the xanthene hydroxides but we were unable to determine the correct reaction conditions required to enable that esterification.

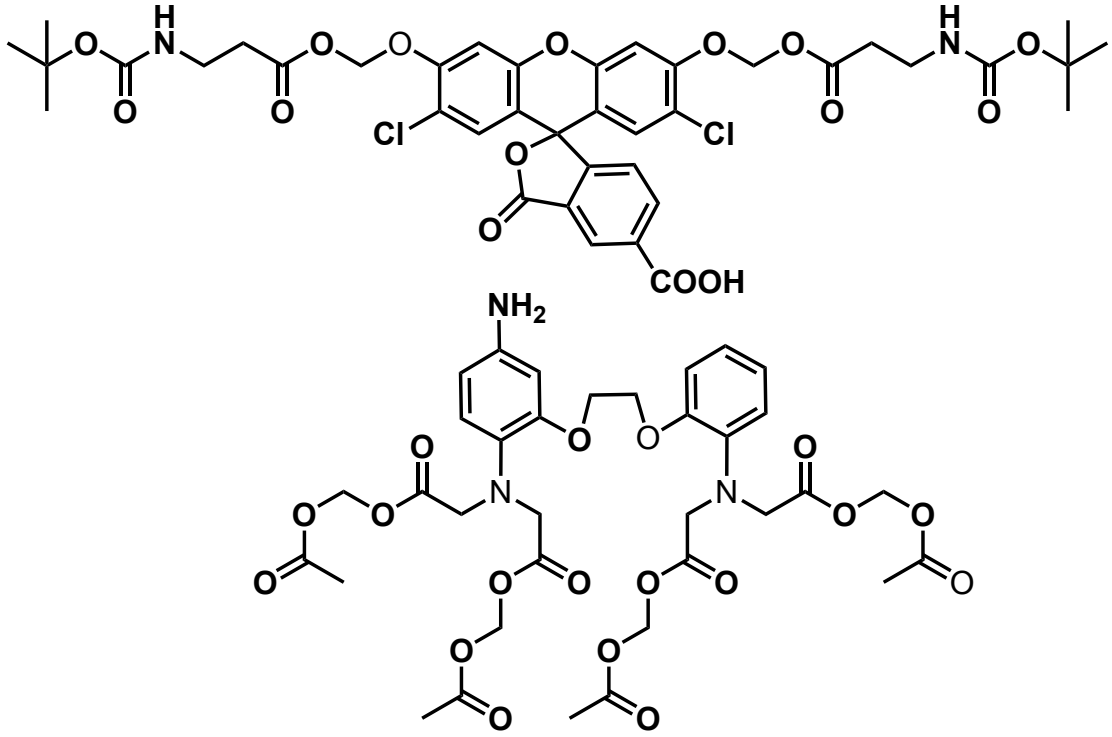

Figure 7. Structures of selectively esterified pieces of the final calcium indicator attempted in this chapter. We hoped that differential esterification of the calcium indicator would still provide beneficial characteristics such as greater solubility. However, we were unable to access the diamino-acyl esters of carboxyfluorescein.

4. References

(1) Sutachan, J.-J.; Montoya, J. V; Xu, F.; Chen, D.; Blanck, T. J. J.; Recio-Pinto, E. Pluronic F-127 Affects the Regulation of Cytoplasmic Ca 2+ in Neuronal Cells. **2006**.

(2) Bardi, G.; Tognini, P.; Ciofani, G.; Raffa, V.; Costa, M.; Pizzorusso, T. Pluronic-Coated Carbon Nanotubes Do Not Induce Degeneration of Cortical Neurons in Vivo and in Vitro. **2009**.

(3) Krylova, O. O.; Pohl, P. Ionophoric Activity of Pluronic Block Copolymers. *Biochemistry* **2004**, *43* (12), 3696–3703.

(4) Chandaroy, P.; Sen, A.; Alexandridis, P.; Hui, S. W. Utilizing Temperature-Sensitive Association of Pluronic F-127 with Lipid Bilayers to Control Liposome-Cell Adhesion. *Biochim. Biophys. Acta - Biomembr.* **2002**, *1559* (1), 32–42.

(5) Hong, W.; Shi, H.; Qiao, M.; Zhang, Z.; Yang, W.; Dong, L.; Xie, F.; Zhao, C.; Kang, L. PH-Sensitive Micelles for the Intracellular Co-Delivery of Curcumin and Pluronic L61 Unimers for Synergistic Reversal Effect of Multidrug Resistance. **2017**.

(6) Chowdhury, P.; Nagesh, P. K. B.; Kumar, S.; Jaggi, M.; Chauhan, S. C.; Yallapu, M. M.; Chowdhury, P.; Nagesh, Á. P. K. B.; Kumar, Á. S.; Jaggi, Á. M.; et al. Pluronic Nanotechnology for Overcoming Drug Resistance. *Nanomedicine and Nanotoxicology*.

(7) Kabanov, A. V.; Batrakova, E. V.; Alakhov, V. Y. An Essential Relationship between ATP Depletion and Chemosensitizing Activity of Pluronic?? Block Copolymers. *J. Control. Release* **2003**, *91* (1–2), 75–83.

(8) Kabanov, A.; Zhu, J.; Alakhov, V. Pluronic Block Copolymers for Gene Delivery. *Adv. Genet.* **2005**, *53* (05), 231–261.

(9) Bromberg, L.; Alakhov, V. Effects of Polyether-Modified Poly(Acrylic Acid) Microgels on Doxorubicin Transport in Human Intestinal Epithelial Caco-2 Cell Layers. *J. Control. Release* **2003**, *88* (1), 11–22.

(10) Merisko-Liversidge, E.; Liversidge, G. G.; Cooper, E. R. *N Anosizing: A Formulation Approach for Poorly-Water-Soluble Compounds*; 2003; Vol. 18.

(11) Lavis, L. D.; Chao, T.; Raines, R. T. Synthesis and Utility of Fluorogenic Acetoxymethyl Ethers. *Chem. Sci.* **2011**, *2* (3), 521.